Analysis and simulation of multimodal cardiac images to study the heart function

Adityo Prakosa

UNIVERSITY OF NICE - SOPHIA ANTIPOLIS

GRADUATE SCHOOL STIC

INFORMATION AND COMMUNICATION TECHNOLOGIES AND SCIENCES

THESIS

to fulfill the requirements for the degree of

Doctor of Philosophy - Ph.D.

of the University of Nice - Sophia Antipolis

Specialized in: CONTROL, SIGNAL AND IMAGE PROCESSING

presented and defended by

Adityo PRAKOSA

Analysis and Simulation of Multimodal Cardiac Images to Study the Heart Function

Thesis supervised by

Hervé DELINGETTE, Maxime SERMESANT and Nicholas AYACHE

prepared at Inria Sophia Antipolis, ASCLEPIOS Project-Team

defended on January 21^{st}, 2013

Jury :

Reviewers:	Patrick CLARYSSE	-	CREATIS
	Elsa ANGELINI	-	Telecom ParisTech
Supervisor:	Hervé DELINGETTE	-	Inria (Asclepios)
Co-Supervisor:	Nicholas AYACHE	-	Inria (Asclepios)
Examiners:	Shérif MAKRAM-EBEID	-	Philips Healthcare (Medisys)
	Pascal ALLAIN	-	Philips Healthcare (Medisys)
	Eric SALOUX	-	CHU Caen
	Maxime SERMESANT	-	Inria (Asclepios).

UNIVERSITÉ DE NICE - SOPHIA ANTIPOLIS

ÉCOLE DOCTORALE STIC

SCIENCES ET TECHNOLGIES DE L'INFORMATION ET DE LA COMMUNICATION

THÈSE

pour obtenir le titre de

Docteur en Sciences

de l'Université Nice - Sophia Antipolis

Mention : AUTOMATIQUE, TRAITEMENT DU SIGNAL ET DES IMAGES

presenté et soutenue par

Adityo PRAKOSA

Analyse et Simulation des Images Multimodales du Coeur pour l'Etude de la Fonction Cardiaque

Thèse dirigée par

Hervé DELINGETTE, Maxime SERMESANT and Nicholas AYACHE

préparée á l'Inria Sophia Antipolis, Asclepios Équipe-Projet

soutenue le 21 janvier 2013

Jury :

Rapporteurs :	Patrick CLARYSSE	-	CREATIS
	Elsa ANGELINI	-	Telecom ParisTech
Directeur :	Hervé DELINGETTE	-	Inria (Asclepios)
Co-Directeur :	Nicholas AYACHE	-	Inria (Asclepios)
Examinateurs :	Shérif MAKRAM-EBEID	-	Philips Healthcare (Medisys)
	Pascal ALLAIN	-	Philips Healthcare (Medisys)
	Eric SALOUX	-	CHU Caen
	Maxime SERMESANT	-	Inria (Asclepios).

Analysis and Simulation of Multimodal Cardiac Images to Study the Heart Function

Abstract: This thesis focuses on the analysis of the cardiac electrical and kinematic function for heart failure patients. An expected outcome is a set of computational tools that may help a clinician in understanding, diagnosing and treating patients suffering from cardiac motion asynchrony, a specific aspect of heart failure.

Understanding the inverse electro-kinematic coupling relationship is the main task of this study. With this knowledge, the widely available cardiac image sequences acquired non-invasively at clinics could be used to estimate the cardiac electrophysiology (EP) without having to perform the invasive cardiac EP mapping procedures.

To this end, we use real clinical cardiac sequence and a cardiac electromechanical model to create controlled synthetic sequence so as to produce a training set in an attempt to learn the cardiac electro-kinematic relationship. Creating patient-specific database of synthetic sequences allows us to study this relationship using a machine learning approach.

A first contribution of this work is a non-linear registration method applied and evaluated on cardiac sequences to estimate the cardiac motion. Second, a new approach in the generation of the synthetic but virtually realistic cardiac sequence which combines a biophysical model and clinical images is developed. Finally, we present the cardiac electrophysiological activation time estimation from medical images using a patient-specific database of synthetic image sequences.

Keywords: Cardiac motion tracking, synthetic cardiac sequences, cardiac inverse electro-kinematic learning

Analyse et Simulation des Images Multimodales du Coeur pour l'Etude de la Fonction Cardiaque

Resumé : Le travail de thèse porte sur l'analyse de la fonction électrique et mécanique du coeur afin d'étudier les effets de l'insuffisance cardiaque. Il débouche sur un ensemble d'outils qui peuvent aider le clinicien à mieux comprendre et traiter l'asynchronisme cardiaque, un des aspects de l'insuffisance cardiaque.

Il a pour principal objectif de résoudre le problème inverse du couplage électro-cinématique : estimer l'électrophysiologie cardiaque sans avoir à effectuer des procédures invasives de cartographie cardiaque. Les séquences cardiaques acquises de manière non-invasive sont déjà largement utilisées dans les centres cliniques et pourraient permettre de caractériser l'électrophysiologie cardiaque sans procédure invasive.

La première contribution de ce travail est l'évaluation d'une méthode de recalage non-linéaire appliquée sur des séquences cardiaques pour l'estimation du mouvement. La deuxième est une nouvelle approche de simulation de séquences synthétiques d'images cardiaque. Nous utilisons des séquences réelles et un modèle électromécanique du coeur pour créer des séquences synthétiques contrôlées. Le réalisme des séquences générées repose sur l'utilisation conjointe d'un modèle biophysique et d'images réelles lors de la simulation. Enfin, la troisième contribution concerne une méthode d'estimation de la carte d'activation électrique du coeur à partir d'images médicales. Pour ce faire, nous utilisons une base de données d'images synthétiques cardiaques personnalisée à chaque patient. Ces images et les cartes d'activation électrique utilisées lors de la simulation fournissent une base d'entrainement pour apprendre la relation électro-cinématique du coeur.

Mots clés : Suivi de mouvement cardiaque, simulation de séquences synthétiques d'images cardiaque, problème inverse du couplage électro-cinématique

Acknowledgments

First of all I would like to thank my thesis advisors Hervé Delingette, Nicholas Ayache and Maxime Sermesant. I am grateful to have the opportunity to works in Asclepios Research Project under their supervision. Their advice, support and availability are truly valuable for me during my learning process to become a research scientist. I would also like to thank Xavier Pennec for the precious discussion during this work.

Second, I would like to thank the reviewers of this manuscript, Patrick Clarysse and Elsa Angelini for their precious time spent to review this work. Their sharp comments and encouraging compliments are very valuable. I would also like to thank Sherif Makram-Ebeid, Pascal Allain and Eric Saloux for also accepting to be members of jury. It is an honor for me to have them in my jury.

I would like to thank Nicolas Villain for the research stay opportunity in Medisys Research Lab of Philips Healthcare Suresnes. I would also like to thank Pascal Cathier and Patrick Etyngier who had supervised me during my stay. Your advice and support are truly valuable.

I would also like to acknowledge the support of the MedYMA advanced grant funded by the European Research Council and also the support of the EuHeart funding.

I thank my friends and colleagues from the Asclepios Research Project of Inria Antipolis who have given great atmosphere during my stay. Special thanks to Ezequiel Geremia for the time spent and the support in our office. I would like to also thank Isabelle Strobant for all the administrative helps.

At last but not least, I thank my family for their continuous support; my wife Cheria Jelita who always there for me and my daughter Anaïs Sophia who has just joined our adventure, my parents Sutanto Hadisupadmo and Dewi Sawitri who always encourage me. Most gratitude to Allah SWT for all that is given to me.

Thank you.

Contents

Chapter 1

Introduction

Contents

To better describe the clinical context of this thesis, we present a brief introduction to cardiac imaging and then present the objectives as well as the motivation of this thesis.

1.1 Brief Introduction to Cardiac Imaging

The recent advances in medical image processing and also the wide availability of medical imaging modalities at clinics makes it feasible for clinicians to obtain detailed information about the cardiac function in order to understand, to diagnose and also to treat the patient better. Cardiologists analyse a patient's cardiac function from the time series of cardiac images. For example echocardiography is one of the non-invasive imaging modality widely used by cardiologists. Based on the analysis of these images, a cardiologist could diagnose and also plan a treatment for the patient. For instance, for a patient diagnosed with heart failure and cardiac motion asynchrony, the cardiac resynchronization therapy (CRT) is a treatment which could improve the life quality of the patient.

1.1.1 Cardiac Function

The heart is an organ which has an important role in the blood circulation (cf. Fig. 1.1). It is composed of involuntary cardiac muscle (myocardium) and consists of four chambers, the two superior atria (left and right) and also the two inferior ventricles (left and right).

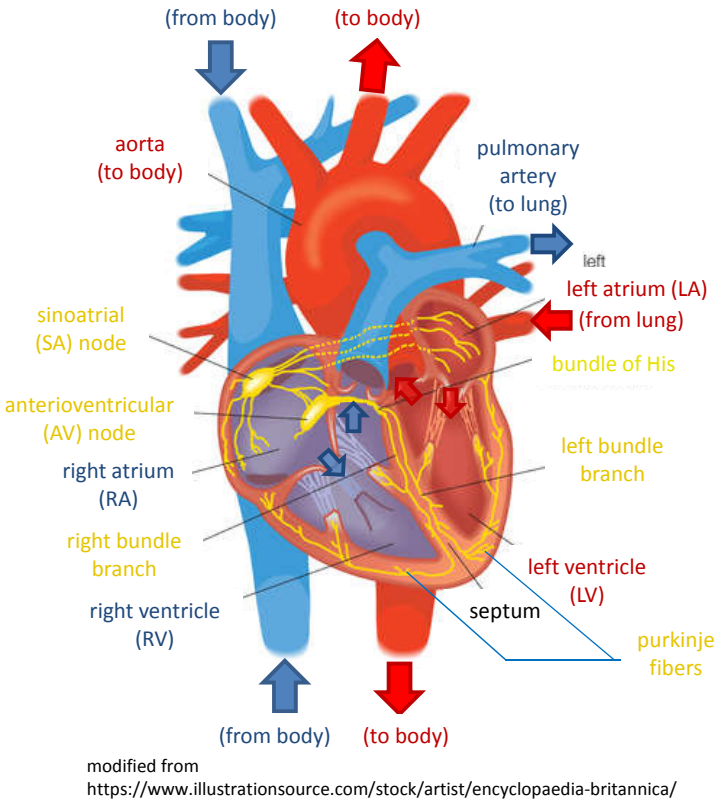

Figure 1.1: The cardiac conduction system (yellow path) allows the electrical impulse from the SA node to be transmitted to the AV node and the atria, causing the atria contraction. The impulse is then conducted through the bundle of His to the bundle branches (left and right), to the Purkinje fibers and finally to the ventricular muscles, causing the ventricular myocardium contraction. The blue color shows the de-oxygenated part of the heart while the red color shows the oxygenated part.

Different cardiac events are described in the Wiggers Diagram (cf. Fig. 1.2). The atria collect the blood to the ventricles which pump it during each heartbeat. The heart is able to beat automatically since it has a natural pacemaker which is called the sinoatrial (SA) node which generates electrical impulses. It also has a conduction system which allows the action potential from the SA node to be transmitted to the atrioventricular (AV) node and to the right and left atria, causing the atria to contract during the atrial systolic phase or during the end of ventricular diastolic phase. This is shown as the P wave on the electrocardiogram (ECG). The electric stimulus is then conducted through the bundle of His to the bundle branches (left and right) where it rapidly spreads using the Purkinje fibers to the ventricular muscles, causing them to contract during the ventricular diastolic phase. This is shown as the QRS complex on the ECG. The right side of the heart deals with the de-oxygenated blood where the right atrium collects the de-oxygenated blood from

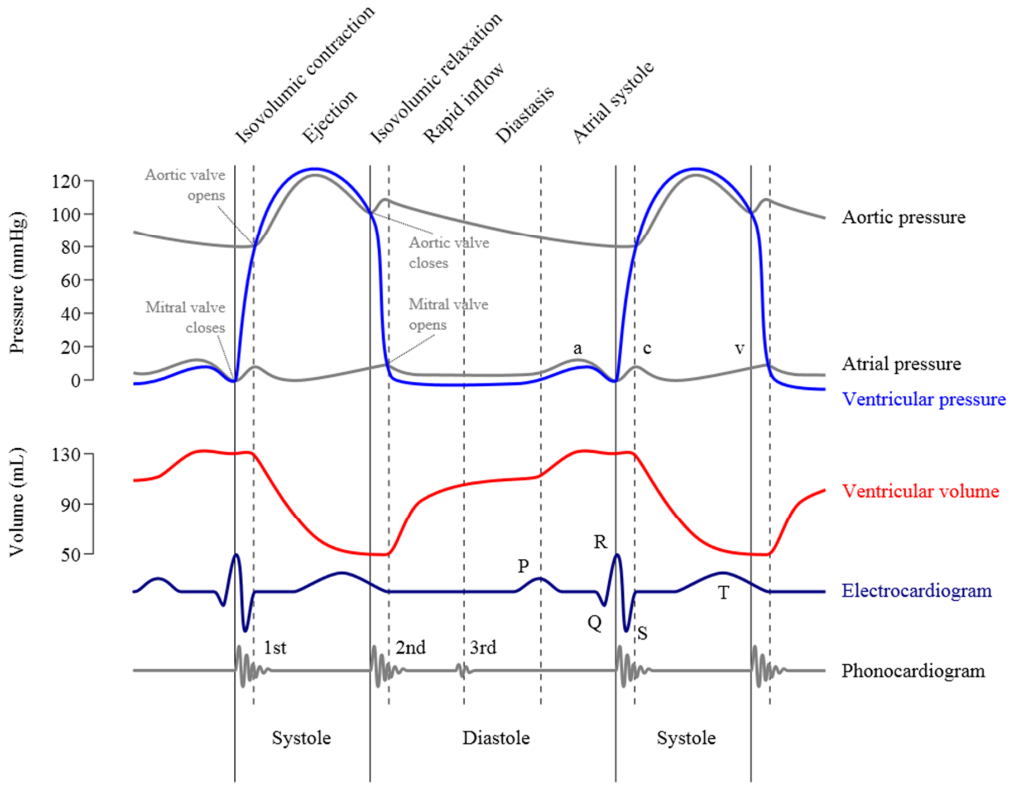

Figure 1.2: The Wiggers diagram describes the different events in the cardiac cycle.

the body and the right ventricle pumps it to the lungs. The left side of the heart deals with the oxygenated blood where the left atrium collects the oxygenated blood from the lungs and the left ventricle pumps it to the body.

1.1.2 Heart Failure and Cardiac Motion Asynchrony

Cardiovascular diseases (CVDs) are the number one cause of death globally [WHO 2012] with an estimation of 17.3 million people died from CVDs in 2008. This represents 30 % of all global deaths. Heart failure is an event of CVD and is described by the inability of the heart to pump sufficient amount of blood required by the body. Cardiac motion asynchrony, a specific aspect of heart failure, is caused by the conduction disturbances, most commonly by the left bundle branch block (LBBB) [Kuijpers 2011, Leclercq 2004]. In LBBB, the cardiac electrical impulse is not well transmitted to the left ventricle through the left bundle branch. As a result, left ventricle activation is delayed and it contracts later than the right ventricle. This impairs the systolic function and reduces the volume of blood being pumped by the heart (the cardiac output). Cardiac resynchronization therapy is a treatment which

could improve the hemodynamic in patient by increasing cardiac output. Electrical resynchronization improves mechanical synchrony between and within the right and left ventricles. In CRT, an artificial pacemaker is placed under the skin in the upper chest (cf. Fig. 1.3). Its leads are implanted through the subclavian vein into the

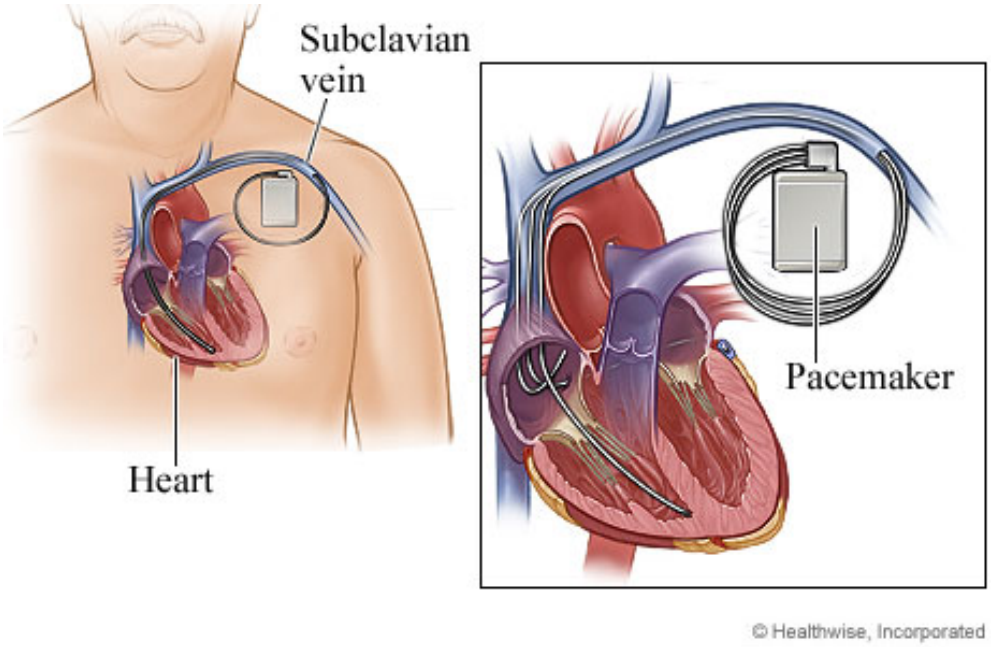

Figure 1.3: Biventricular pacemaker in cardiac resynchronisation therapy

right ventricle and into the coronary sinus vein to pace the left ventricle. Another lead is usually implanted into the right atrium. Small electrical impulses are sent through the leads which maintain the right and left ventricles pumping together.

1.1.3 Analyzing Cardiac Image Sequences

During this study, we first processed 4D echocardiography (US) data acquired by Dr. Eric Saloux. A 3D segmentation of the endocardium is also provided. This dataset contained images from patients receiving CRT with different pacemaker activation modes (e.g. sinus rhythm, left ventricular pacing, right ventricular pacing, and bi-ventricular pacing). Concerning the purpose of this study, it is expected that analysis of the images from this modality could provide a hint for the placement of pacemaker leads in patients being treated with CRT since currently, 30% of the patients with pacemaker show no benefit from this therapy. Therefore, the idea is to find the relationship between kinematic descriptors obtained from images analysis, which is widely available, and the electrical activation time. By understanding this inverse electro-kinematic coupling, we could predict the cardiac electrical activation time from 4D US image analysis. This prediction is important in order to see the

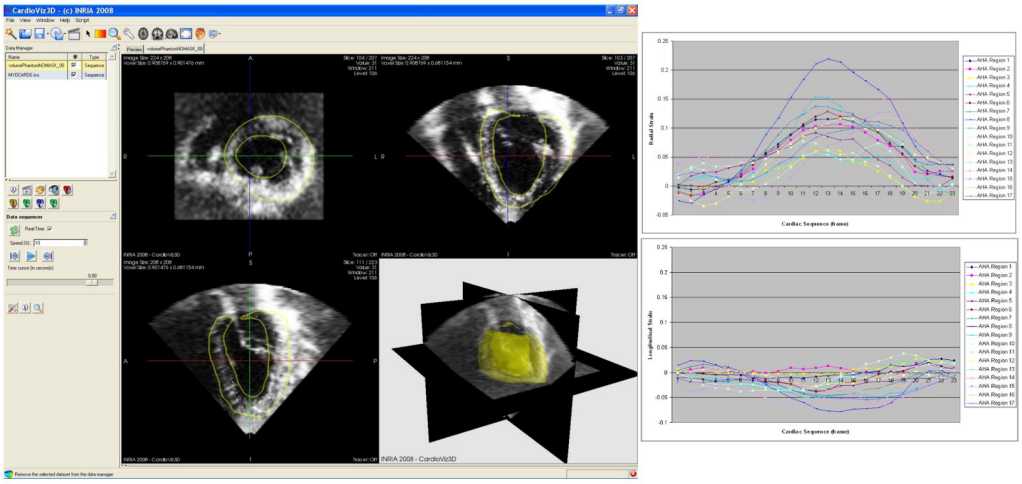

Figure 1.4: Non-linear registration result is shown as the tracking of the myocardium (left) and the radial (upper right) and longitudinal strain (lower right)

effect of the CRT. To this end, we evaluated the strain based on the incompressible diffeomorphic demons algorithm (iLogDemons) [Mansi 2011]. Different approaches for the tracking the cardiac motion using a template cardiac model are also developed in [Schaerer 2010]. With iLogDemons, we track the myocardium and obtain strain curves (radial, longitudinal and circumferential). The best registration parameter is estimated by computing the difference between the provided segmentation and the deformed initial segmentation. Tools developed within the Asclepios group are used for this need. The first observation of the 3D strains obtained by this method shows encouraging results (cf. Fig. 1.4). A further evaluation of the iLogDemons registration algorithm was done in [McLeod 2012, Prakosa 2012a]. Currently, the evaluation of image analysis methods is still challenging since there is lack of ground truth. However, recent study [Lebenberg 2012] has developed a statistical method to find a consensus between different cardiac segmentation and motion tracking method in order to estimate the left ventricle ejection fraction.

1.1.4 Cardiac Electrical Mapping

The cardiac electrical mapping has an important role as the reference in understanding the inverse electro-kinematic coupling relationship. However, acquisition of the cardiac electrical mapping is an invasive procedure since it requires the insertion of a catheter in order to reach the heart chamber (catheterisation).

A first acquisition on cardiac electrical mapping from a patient using EnSite system has started at the University Hospital of Caen and an EnSite dataset has been sent to be visualized (cf. Fig. 1.5). A surface mesh along with the potential isochrones mapping was visualized. However, the corresponding 4D echocardiogra-

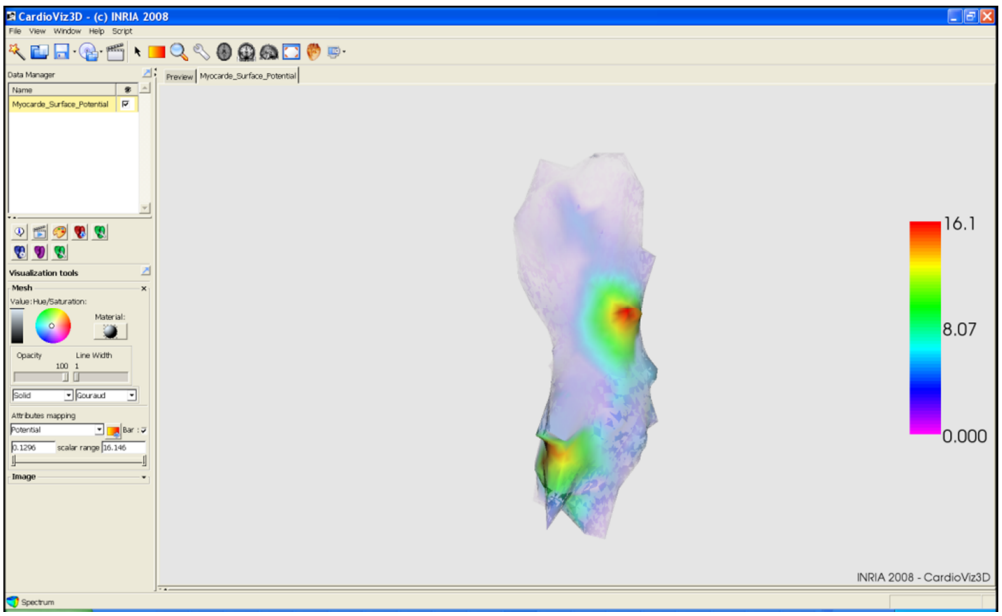

Figure 1.5: EnSite cardiac electrical potential mapping visualization

phy acquisition from the same patient is not of sufficient quality in order to apply a motion tracking algorithm. This is due to the use of contrast agent during the acquisition for this particular study. Therefore, we cannot use the pair of cardiac electrical mapping and 4D echocardiography as a ground truth for the validation of the inverse electro-kinematic learning algorithm.

Nonetheless, we have processed the provided dataset by first registering the EnSite mesh to a 3D echocardiography image sequence. From the 3D US image, the endocardium is manually delineated and a tridimensional surface is reconstructed. The EnSite mesh is registered to the endocardial surface, by first aligning their long axis and then selecting a feature point on both surfaces. The activation times and the infarct mapping information contained in the EnSite mesh are then projected to the endocardium surface (cf. Fig. 1.6).

1.1.5 Cardiac Simulation

The development of the computational cardiac electromechanical models allows us to simulate various cardiac cases [Smith 2000, Belik 2004, Sainte-Marie 2006, Sermesant 2012, Chapelle 2012]. These models are built based on the biophysical properties of the heart and the knowledge of pathologies. It enables the creation of virtual hearts. Using personalisation method [Sermesant 2012, Marchesseau 2012a], the cardiac model can produce similar behavior than the one clinically observed. The availability of this personalised biophysical model helps the clinicians in the study of the patient's cardiac function. This is helpful for example for diagnosing

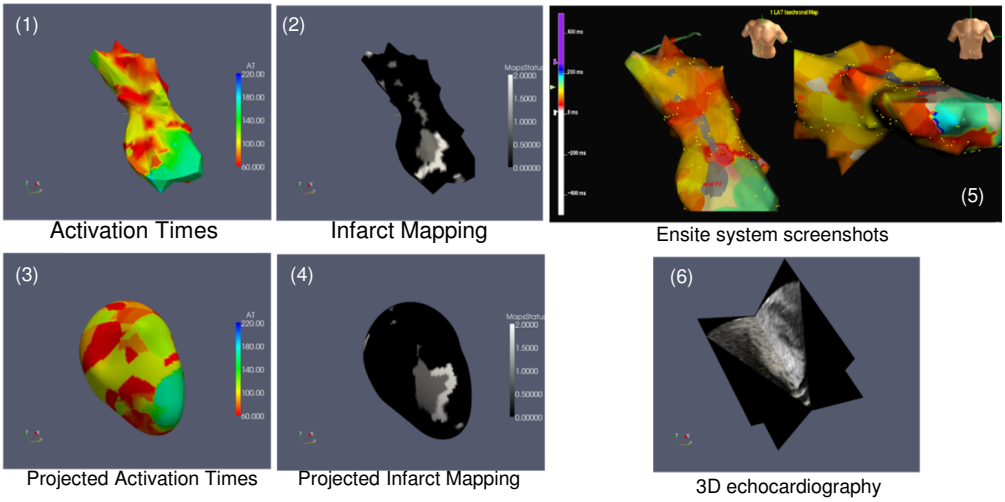

Figure 1.6: Ensite cardiac electrical mapping data is projected to the endocardium surface of the corresponding 3D echocardiography

anomalous motion patterns, for making prognosis by simulating a therapy, and for predicting the results of a therapy. Furthermore, the model can estimate quantities that can be difficult to obtain in a clinical setting. By coping with the limited access to certain clinical data, for example the cardiac electrophysiology mapping, computational cardiac simulation could play an important role in the study of cardiac function.

Furthermore, computational cardiac electromechanical models can be helpful to generate realistic synthetic medical images, i.e. to translate the simulation into an observation comparable to the one usually found at clinics, which are the patient's medical images. This can be done by combining the model with advanced methods in medical imaging and image processing. As a result, it is possible to create a virtual patient or virtual phantom. Examples of virtual phantom are the "voxelized phantom" [Segars 2008] or the "voxelized atlas" where the voxel intensities take into account the motion of the organ or the inter-patient anatomy variability. The "voxelized atlas" has been developed in [Zubal 1994, Xu 2000, Kramer 2003, Kramer 2004, Kramer 2006] where the phantom contains the segmentation of organs from medical images. In our case, a database of realistic synthetic cardiac images were used to study the inverse electro-kinematic relationship since it contains the required ground truth from the model. Since the synthetic image is similar to the real one, the same image processing method can be applied to both of them. The relationship learned using the synthetic dataset can be directly applied to the real dataset in order to predict patient cardiac electrophysiological pattern.

1.2 Context and Motivations

The research work for this thesis were conducted in a collaboration between the Asclepios Research Project - Inria Sophia Antipolis, the Medisys Research Lab - Philips Healthcare Suresnes and the Cardiology Unit - Caen University Hospital. In this collaborative work, a stay (for 6 months) was carried out at the Medisys Research Lab environment under the supervision of Pascal Cathier and Patrick Etyngier. During this stay, a visit to cardiologist Dr. Eric Saloux at the Cardiology Unit of the Caen University Hospital was arranged to study the data acquisition process.

This study focuses on the analysis of the cardiac electrical and kinematic function for patients suffering from heart failure. We aimed at creating computational tools that may help a clinician in better understanding, diagnosing and treating patients suffering from cardiac motion asynchrony, a specific aspect of heart failure. Cardiac motion asynchrony is related to the abnormal cardiac electrophysiology. Currently the analysis of patient cardiac electrophysiological function requires the cardiac electrical mapping information which is usually acquired invasively. Estimating this information from the analysis of the widely available cardiac images acquired non-invasively would give an alternative in the non-invasive cardiac electrical activation pattern estimation. Therefore, understanding the cardiac inverse electro-kinematic coupling relationship is the main task of this study. With this knowledge, the analysis of the motion or the kinematics of the cardiac images sequences can be used to estimate the cardiac electrophysiological activation pattern.

1.3 Objectives and Manuscript Organization

The objective of this thesis led us to consider the following three questions on how we can estimate the electrophysiology of the heart by observing the cardiac motion:

1. The development of non-rigid registration methods for the cardiac motion tracking in the cardiac image analysis allows the quantification of the myocardial deformation. However the evaluation of these methods is still challenging since it requires reference dataset with controlled ground truth. By creating synthetic cardiac sequences, the underlying motion ground truth is provided for each generated sequence. The availability of this dataset then opens a question:
   Can we evaluate objectively cardiac motion algorithms by using controlled synthetic sequences?

2. The generation of synthetic cardiac sequences is important to cope with the limited access to certain clinical information, for example the cardiac electrophysiological information, and also the lack of ground truth, for example the cardiac motion ground truth. However, the created synthetic sequence has often limited realism since it is restricted to a number of simulated objects due to the complexity of the physical models involved. This constraint imposes

to only often simulate an isolated myocardium without much consideration to the blood pool and surrounding structures. Therefore, the second question that we ask is:
How can is it possible to create a realistic synthetic cardiac sequence using a biophysical model?

3. Finally, since electrophysiological activation controls the onset of the mechanical contraction, important information about the electrophysiology could be gathered from the detailed observation of the resulting motion patterns. Indeed the relationship between the mechanical waves and electrical waves is very complex. The availability of the cardiac electromechanical model allows the creation of a cardiac motion database with the underlying cardiac electro-kinematic ground truth. Thus the last question that we tackle is:
How can we estimate the cardiac inverse electro-kinematic relationship using patient-specific databases of synthetic cardiac sequences, in order to estimate the cardiac electrophysiological activation pattern from the analysis of a patient's time series of cardiac images?

This thesis is organized based on our published and submitted studies. It develops from the evaluation of a motion tracking algorithm to the generation of synthetic but visually realistic cardiac sequences and finally to the use of database of synthetic sequences to learn the inverse electro-kinematic study.

Chapter 2 presents a motion tracking algorithm which is largely used in all part of this thesis. As a part of a challenge, the log-domain diffeomorphic demons (LogDemons) and the incompressible LogDemons (iLogDemons) [Mansi 2011] were evaluated on a database of synthetic ultrasound sequences [Prakosa 2012a]. Since these sequences provide the ground truth motion, objective evaluation of the parameters of this non-linear registration algorithm can be done. The iLogDemons had also been applied to a dataset of cine MRI, ultrasound and tagged MRI of healthy volunteers from the previous challenge [McLeod 2012].

In Chapter 3, based on [Prakosa 2012c], a pipeline to generate synthetic but visually realistic cardiac images is presented. This pipeline uses an approach based on stationary velocity field to combine the motion estimated from the real clinical images and the motion simulated using a cardiac electromechanical model. The combined motion is then used to create synthetic cardiac sequences. A method to smooth displacement fields was introduced to maintain the continuity between the simulation and the real image with minimal texture distortion. Using this method a database of synthetic but visually realistic cardiac sequences which contains the underlying ground truth cardiac electrophysiology and motion was created.

The creation of databases of synthetic cardiac sequences using the electromechanical model opens the possibility of the machine learning based approach on the inverse electro-kinematic study. Preliminary studies in the inverse electro-kinematic learning are described in the Appendix B and C. In Appendix B [Prakosa 2010] we attempt to learn this relationship from the displacement and strains estimated directly from the E/M model. More realistic estimation was done in

Appendix C [Prakosa 2011] by first simulating 3D ultrasound images and using an image-based motion tracking algorithm. Chapter 4 [Prakosa 2012b] uses the method developed in Chapter 3 to create patient-specific databases of synthetic MR cardiac sequences. This database is then used as a training set in a machine learning study to find the relationships between the cardiac motion descriptors and the left ventricle (LV) endocardial surface electrical activation time (AT). Using this training set and the learned relationship, patients cardiac LV AT can be estimated from the motion descriptor extracted from this patient's estimated displacement field.

Chapter 2

Evaluation of iLogDemons Algorithm for Cardiac Motion Tracking in Synthetic Ultrasound Sequence

Contents

Based on: [Prakosa 2012a] A. Prakosa, K. McLeod, M. Sermesant and X. Pennec. Evaluation of iLogDemons Algorithm for Cardiac Motion Tracking in Synthetic Ultrasound Sequence. In Proc. MICCAI Workshop on Statistical Atlases and Computational Models of the Heart (STACOM12), LNCS, Nice, France, October 2012. To appear

We evaluate the iLogDemons algorithm for the STACOM 2012 cardiac motion tracking challenge. This algorithm was previously applied to the STACOM 2011 cardiac motion challenge to track the left-ventricle heart tissue in a data-set of volunteers. Even though the previous application showed reasonable results with respect to quality of the registration and computed strain curves; quantitative evaluation of the algorithm in an objective manner is still not trivial. Applying the algorithm to

the STACOM 2012 synthetic ultrasound sequence helps to objectively evaluate the algorithm since the ground truth motion is provided. Different configurations of the iLogDemons parameters are used and the estimated left ventricle motion is compared to the ground truth motion. Using this application, quantitative measurements of the motion error are calculated and optimal parameters of the algorithm can be found.

2.1 Introduction

Understanding cardiac motion dynamics through the heart beat is fundamental for providing useful insights into cardiac diseases. Analyzing medical images is one way to better understand the complex dynamics of the heart and in recent years, cardiac motion tracking algorithms have been developed to attempt to estimate the observed motion. We refer the reader to [Mansi 2011] for the state of the art on cardiac motion tracking. A cardiac motion tracking challenge was introduced in the STACOM 2011 MICCAI workshop which allowed participants to apply algorithms to a given dataset of healthy volunteers with cine-magnetic resonance, ultrasound, and tagged-magnetic resonance image sequences. In this work we describe the application of the incompressible log-domain demons algorithm (iLogDemons for short) to a set of synthetic ultrasound image sequences for which the ground truth deformation is known and provided for training within the STACOM 2012 MICCAI cardiac motion tracking challenge. From this we are able to compute the error between the ground truth and the estimated deformation for the training data.

2.2 Methodology

The iLogDemons algorithm is a consistent and efficient framework for tracking left-ventricle heart tissue through the cardiac cycle using an elastic, incompressible non-linear registration algorithm based on the LogDemons algorithm [McLeod 2012, Mansi 2011]. Applying a non-linear registration to pairs of medical images is a common method to estimate the motion and the deformation of the tissue in the image.

2.2.1 LogDemons

The LogDemons [Vercauteren 2008] non-linear registration aligns a template image $T(\mathbf{x})$ to a reference image $R(\mathbf{x})$ by estimating a dense non-linear transformation $\phi(\mathbf{x})$, where $\mathbf{x} \in \mathbb{R}^3$ is the space coordinate. This transformation $\phi(\mathbf{x})$ is associated with the displacement vector field $\mathbf{u}(\mathbf{x})$ and is parameterized by the stationary velocity vector field $\mathbf{v}(\mathbf{x})$, $\phi(\mathbf{x}) = \mathbf{x} + \mathbf{u}(\mathbf{x}) = \exp(\mathbf{v}(\mathbf{x}))$. This ensures the invertibility of the deformation. The LogDemons algorithm contains two steps, which are the *optimization* and the *regularization* step. The *optimization* step finds the intermediate correspondence transformation $\phi_c(\mathbf{x}) = \exp(\mathbf{v}_c(\mathbf{x})) = \phi(\mathbf{x}) \circ \exp(\delta\mathbf{v}(\mathbf{x})))$ by minimizing the LogDemons energy

$$\varepsilon(\mathbf{v}, \mathbf{v}_c) = \frac{\| R - T \circ \exp(\mathbf{v}_c) \|^2_{L_2}}{\lambda_i^2} + \frac{\| \log(\exp(-\mathbf{v}) \circ \exp(\mathbf{v}_c)) \|^2_{L_2}}{\lambda_x^2} + \frac{\| \nabla \mathbf{v} \|^2}{\lambda_d^2}$$

with respect to $\mathbf{v}_c(\mathbf{x})$, where λ_i^2 is the parameter that estimates the noise in the image $\lambda_i^2(\mathbf{x}) = |R(\mathbf{x}) - T \circ \phi(\mathbf{x})|^2$, λ_x^2 is the parameter that controls the uncertainty of the correspondences and λ_d^2 is the parameter that controls the regularization strength. $\mathbf{v}_c$ parameterizes the intermediate transformation $\phi_c(\mathbf{x})$ which models the voxel correspondences of the two images without considering the regularity of the transformation. The optimal update velocity writes

$$\delta\mathbf{v}(\mathbf{x}) = -\frac{R(\mathbf{x}) - T \circ \phi(\mathbf{x})}{\| J(\mathbf{x}) \|^2 + \lambda_i^2/\lambda_x^2} J(\mathbf{x}),$$

where $J(\mathbf{x})$ is the symmetric gradient $J(\mathbf{x}) = (\nabla R(\mathbf{x}) + \nabla(T \circ \phi(\mathbf{x})))/2$. The correspondence velocity $\mathbf{v}_c$ is updated using the the Baker-Campbell-Hausdorff (BCH) formula $\mathbf{v}_c = Z(\mathbf{v}_c, \delta\mathbf{v})$ [Vercauteren 2008]. Finally, the optimal regularized transformation $\phi(\mathbf{x})$ is estimated in the *regularization step* by minimizing the LogDemons energy with respect to $\mathbf{v}$, which is approximated by smoothing the correspondence velocity $\mathbf{v}_c$ with a Gaussian kernel G_σ.

2.2.2 iLogDemons

iLogDemons adds physiological constraints; *elasticity* and *incompressibility*, to the LogDemons algorithm. It proposes an *elastic* regularizer to filter the correspondence velocities by the elastic-like kernel: $\mathbf{v} = \left(G_\sigma Id + \frac{\sigma^2\kappa}{1+\kappa} HG_\sigma\right) \star \mathbf{v}_c = G_{\sigma,\kappa} \star \mathbf{v}_c$, where HG_σ is the Hessian of the Gaussian kernel G_σ and $G_{\sigma,\kappa}$ is the elastic-like vector filter. *Incompressibility* is achieved by constraining the stationary velocity field $\mathbf{v}(\mathbf{x})$ to be divergence-free. The complete algorithm of the iLogDemons is described in Algorithm 1.

Algorithm 1 iLogDemons: Incompressible Elastic LogDemons Registration

Require: Stationary velocity field $\mathbf{v}^0$. Usually $\mathbf{v}^0 = \mathbf{0}$ i.e. $\phi^0 = Id$.

1: **loop**[*over n until convergence*]
2: Compute the update velocity: $\delta\mathbf{v}^n$ (see [Mansi 2011]).
3: Fluid-like regularization: $\delta\mathbf{v}^n \leftarrow G_{\sigma_f} \star \delta\mathbf{v}^n$, G_{σ_f} is a Gaussian kernel.
4: Update the correspondence velocity using the Baker-Campbell-Hausdorff (BCH) formula: $\mathbf{v}^n \leftarrow Z(\mathbf{v}^{n-1}, \delta\mathbf{v}^n)$ (see [Vercauteren 2008]).
5: Elastic-like regularization: $\mathbf{v}^n \leftarrow G_{\sigma,\kappa} \star \mathbf{v}^n$ (see [Mansi 2011]).
6: Solve: $\Delta p = \nabla \cdot \mathbf{v}^n$ with 0-Dirichlet boundary conditions. This is done in order to achieve the incompressibility.
7: Project the velocity field: $\mathbf{v}^n \leftarrow \mathbf{v}^n - \nabla p$.
8: Update the warped image $T \circ \phi^n = T \circ \exp(\mathbf{v}^n)$.

return $\mathbf{v}$, $\phi = \exp(\mathbf{v})$ and $\phi^{-1} = \exp(-\mathbf{v})$.

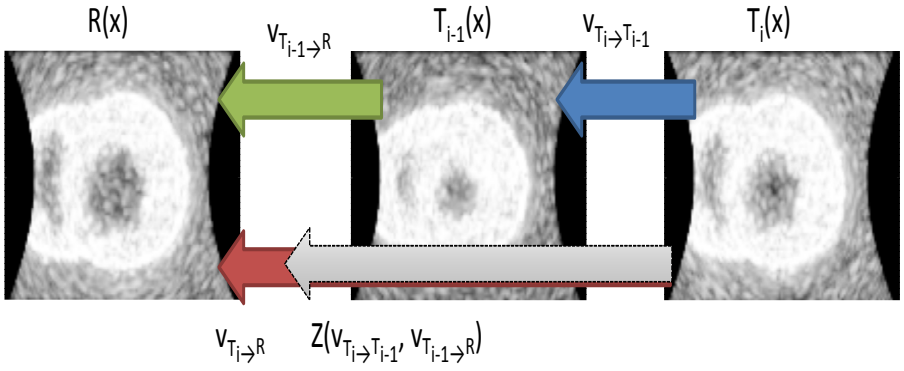

Figure 2.1: The concatenation of the velocity field $\mathbf{v}_{T_i \to T_{i-1}}$ and $\mathbf{v}_{T_{i-1} \to R}$ using the BCH formula is used to initiate the registration of the template image $T_i(\mathbf{x})$ to the reference image $R(\mathbf{x})$.

2.2.3 Cardiac Motion Tracking Strategy

We initialize the registration of the template image $T_i(\mathbf{x})$ at frame i to the reference image $R(\mathbf{x})$ with the concatenation of the previous frame $(i-1)$ to reference velocity field $\mathbf{v}_{T_{i-1} \to R}$ and the current-to-previous frame velocity field $\mathbf{v}_{T_i \to T_{i-1}}$ by $Z(\mathbf{v}_{T_{i-1} \to R}, \mathbf{v}_{T_i \to T_{i-1}})$ with Z is the BCH operation, as a strategy to track the myocardium (cf. Fig. 2.1) [Mansi 2011]. The final registration is always calculated to the same end diastolic reference image $R(x)$.

2.3 Application to Challenge Data

2.3.1 Algorithm Parameter Setting

We used the standard parameters that were used previously in [McLeod 2012]. However, since the ground truth motion is available for the synthetic ultrasound sequence provided, we also tested different parameters of the iLogDemons as described in Table 2.3.1.

iLogDemons non-rigid registration was previously applied to the STACOM 2011 challenge data-set [Tobon-Gomez 2012a, McLeod 2012]. It showed reasonable results in term of the alignment of the registered frames in the cardiac sequence with the reference end diastolic image. Using the estimated transformations, it could also track the myocardium along the cardiac cycle. The calculated strain curve was also comparable to literature for healthy strain values [Moore 2000].

2.3.2 Simulated ultrasound cardiac sequence data

The simulated data-set consisted of 10 synthetic ultrasound sequences with 23 frames per case, with image spatial resolution of 267×355×355, and isotropic voxel size of 0.33 mm. For each sequence, the left ventricle (LV) is almost fully visible while

Input parameters:	Value
Multi-resolution levels (frame-by-frame registration)	3
Multi-resolution levels (refinement step)	2
Number of iterations / level	100
σ_f update field in mm	0.5
κ_f update field in mm	0
σ stationary velocity field in mm	1 or 1.5 or 2
κ stationary velocity field in mm	1
Incompressibility update field (0-Disable,1-Enable)	0
Incompressibility velocity field (0-Disable,1-Enable)	1 or 0

Table 2.1: iLogDemons parameters used in the application

the right ventricle is only partially visible in the ultrasound acquisition cone. To compensate for the part of the LV which is out-of-window region, we artificially expanded the acquisition pyramid. The boundary voxels were copied to fill this region and additional noise was also added. The data-set contains different motion and deformation patterns (normal, LBBB, RBBB, pacing) with the ground truth deformation provided as the deformation of volumetric meshes in a cardiac cycle (See [Craene 2012a] for further details on the synthetic data-set).

2.3.3 Application to the synthetic data

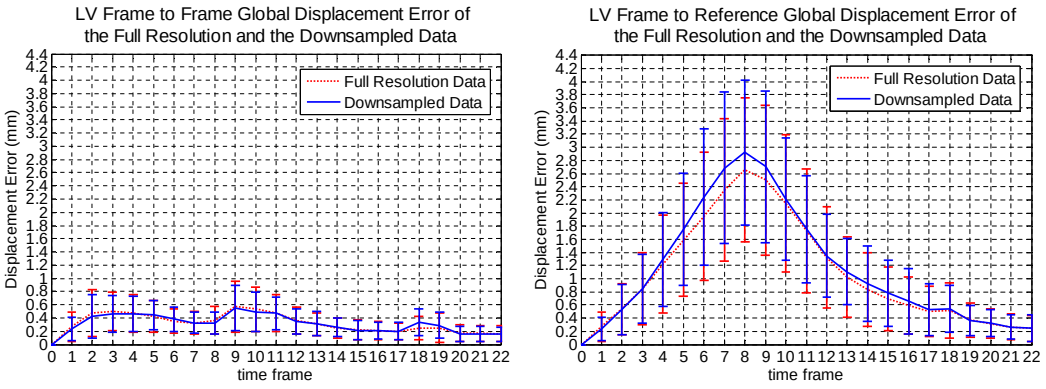

Figure 2.2: The registration error (calculated using the method described in Section. 2.3.4) of the full resolution and down-sampled dataset of the first case are compared. They show relatively small difference. .

In order to find the optimal parameters of the algorithm that are able to handle large deformations, we processed the first case of the ultrasound synthetic data-set since it simulates normal heart motion with large contraction. We launched the parameters that were used previously in [McLeod 2012] to the full resolution data-set. We also applied our algorithm on down-sampled images to reduce the computational

time. We down-sampled the data to a resolution of 88×117×117 with isotropic voxel size of 1.02 mm The computation time of the whole sequence processing was reduced from the order of days to hours. The current implementation can be optimized to handle large volumes by improving the memory access scheme since the addition of computation time of current implementation is not caused by the addition of computational complexity. One configuration of parameters was tested for both the full and down-sampled data to verify the accuracy of the down-sampled registration compared to the full-resolution registration and found very small differences in the results (cf. Fig. 2.2). Other configurations of the key parameters were tested on the down-sampled data.

2.3.4 Quantitative Evaluation

2.3.4.1 Displacement Error

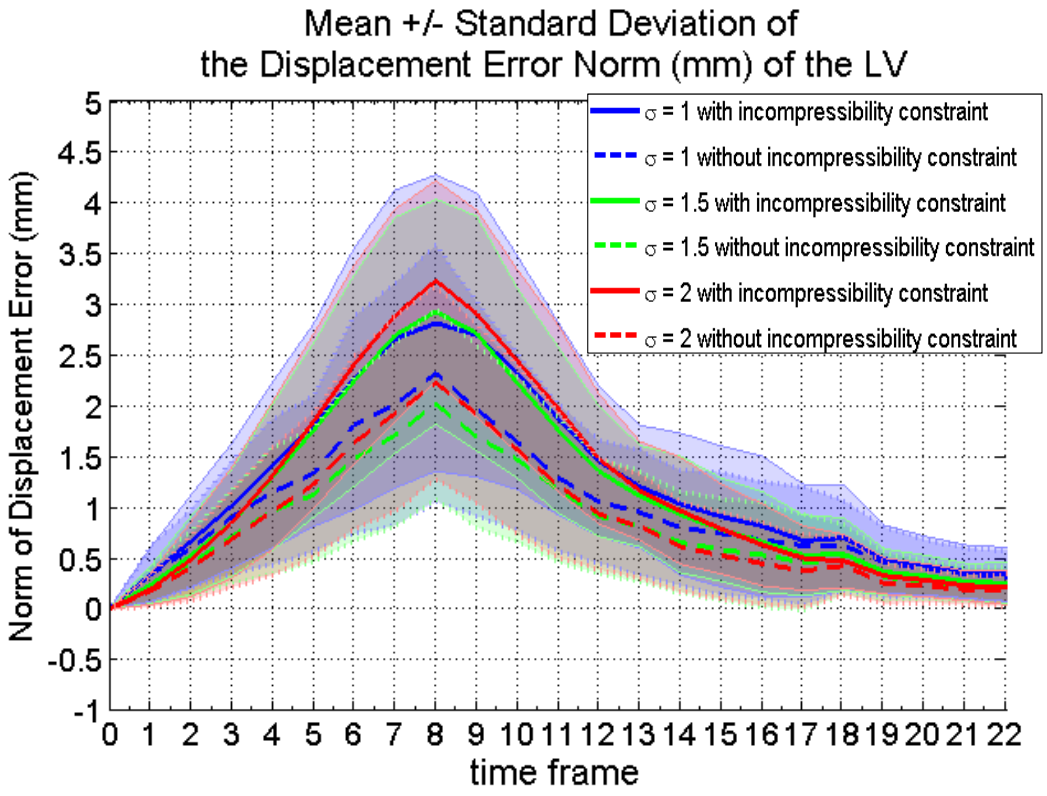

Figure 2.3: The mean and standard deviation of the displacement error calculated on the whole left ventricle for varying values of σ for the first case.

To evaluate quantitatively the performance of each set of the parameters used for the iLogDemons with incompressibility on the velocity field set to 0 or 1, we calculated the ground truth displacement vector field from the deformation of the

provided simulated meshes. We rasterized the displacement vectors to the image $\mathbf{u}_{GT}(\mathbf{x})$ in order to be able to compare them to the iLogDemons estimated displacement field $\mathbf{u}_e(\mathbf{x})$. The norm of the difference of the two vector fields $||\mathbf{u}_{GT}(\mathbf{x}) - \mathbf{u}_e(\mathbf{x})||$ is calculated. The global mean of this values over the whole left ventricle are calculated for each time frame in the cardiac cycle (cf. Fig. 2.3). Based on Fig. 2.3, the parameter $\sigma = 1.5$ without the incompressibility constraint gives the lowest maximum error for the first case. We calculated the LV volume of the ground truth deformed meshes in a cardiac cycle and we observed that the current electromechanical model is not incompressible. Fig. 2.4 shows the mean and standard deviation of the LV myocardium volume change in a cardiac cycle for the whole data-set. There is a 10% change of volume during the maximum contraction. In Fig. 2.5, we compare the ground truth displacement vector for each American Heart Association (AHA) region of the left ventricle. We compare it to the iLogDemons estimated displacement vector and calculated the difference for each AHA segment. Fig. 2.5 also shows the error for the basal (regions 1-6), mid (regions 7-12) and apical (regions 13-17) regions. More error is observed in the apical region since the longitudinal motion of the apex toward the base changes the intensity of the apical region.

The result for the whole data-set processing is shown in Fig. 2.6. As also shown in Fig. 2.5 for the first case, the registration of each frame to its previous frame gives small error which is less than one voxel size. For the frame to reference result, we observe that there is an error accumulation during the maximum contraction.

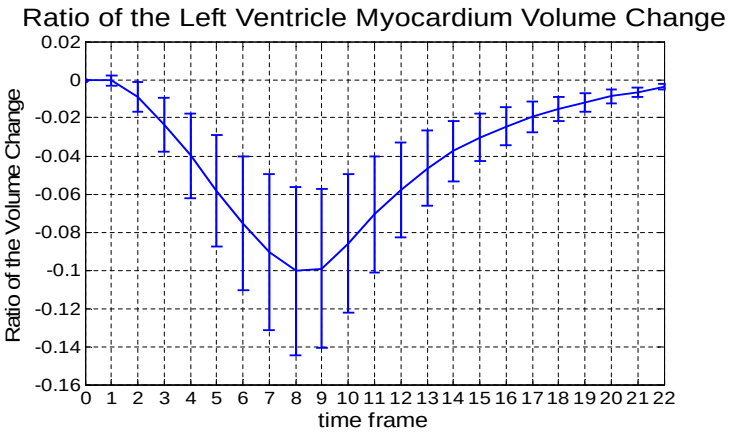

Figure 2.4: The mean and standard deviation of the LV volume change of the ground truth deformed meshes during a cardiac cycle. Current electromechanical model is not incompressible since there is a 10% of volume change during the maximum contraction.

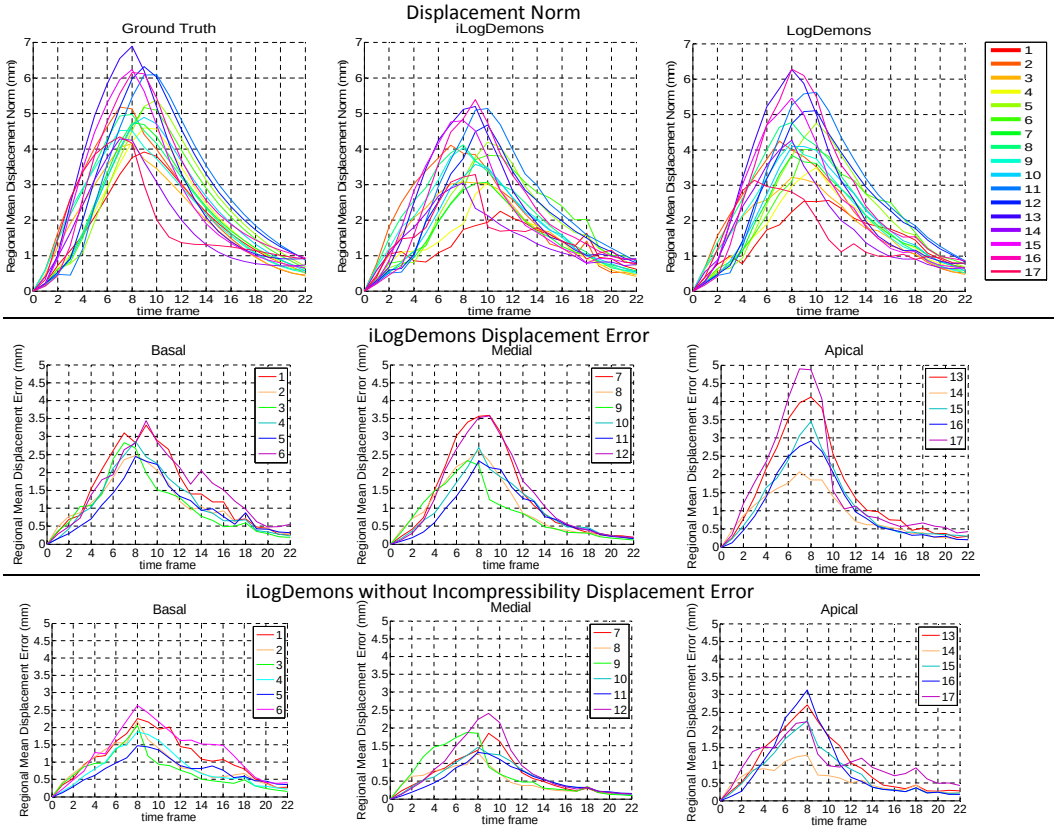

Figure 2.5: The comparison of the ground truth, incompressible and non-incompressible iLogDemons estimated LV displacement norm for the first case on each American Heart Association (AHA) region. In both cases, $\sigma = 1.5$ was used. The mean displacement error is also calculated on each AHA region.

2.3.4.2 Strain Estimation

From the iLogDemons estimated displacement field $\mathbf{u}(x)$, we computed the strain tensor and projected it to the local radial, circumferential and longitudinal directions. The strain tensor was calculated using the 3D Lagrangian finite strain tensor $E(x) = \frac{1}{2}[\nabla\mathbf{u}(x) + \nabla\mathbf{u}^T(x) + \nabla\mathbf{u}^T(x)\nabla\mathbf{u}(x)]$. The mean and standard deviation of the strain estimation of the whole data-set is shown in Fig. 2.7. The result using incompressibility has more realistic range of value (from -15% to 25%) of the estimated strain compared to the one without incompressibility (from 150% to 300%).

2.3.5 Myocardium Tracking

Qualitative evaluation of the algorithm is done by comparing the contour of the simulated mesh at the frame with maximum contraction with the deformation of the end diastolic mesh using the iLogDemons estimated displacement field at the same

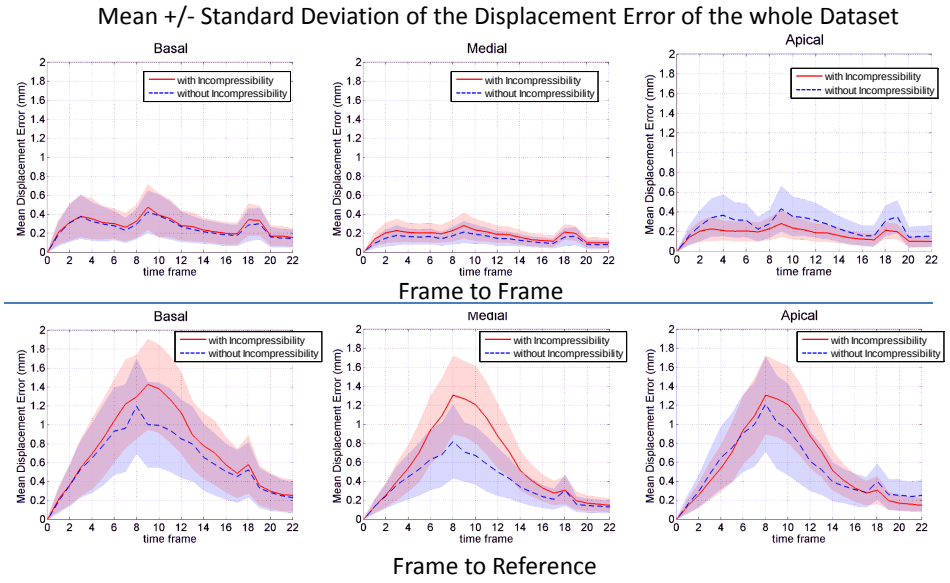

Figure 2.6: The displacement error of the whole training data-set

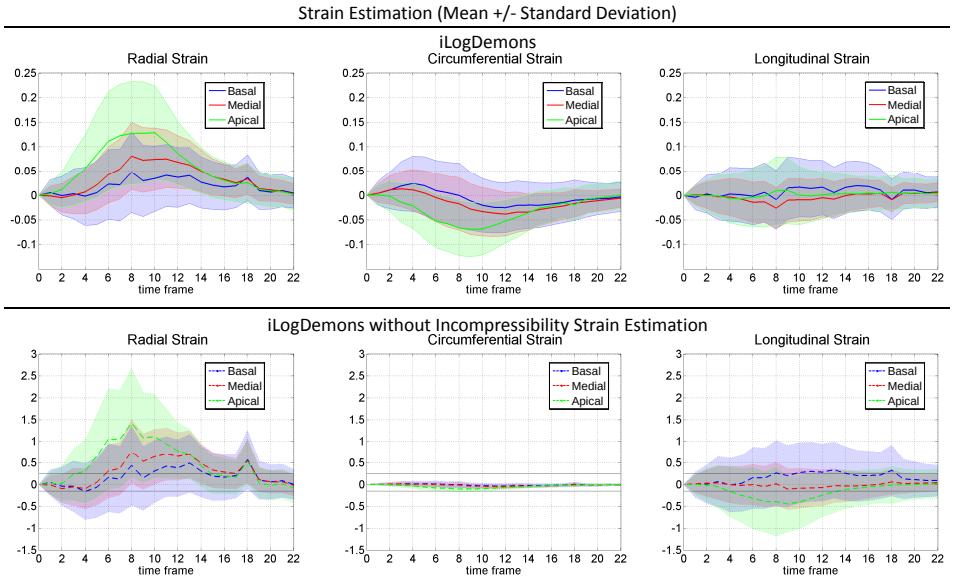

Figure 2.7: The mean and standard deviation of the estimated strain for the whole training data-set with and without incompressibility constrain. Incompressibility constraint gives more realistic range of value of the estimated strain (from -15% to 25%). This range is shown as black horizontal lines on the result without incompressibility.

frame for the first case. Reasonable agreement of the contours can be observed in Fig. 2.8, which indicated that the algorithm is able to capture realistic deformations, even in the case of a synthetically simulated sequence.

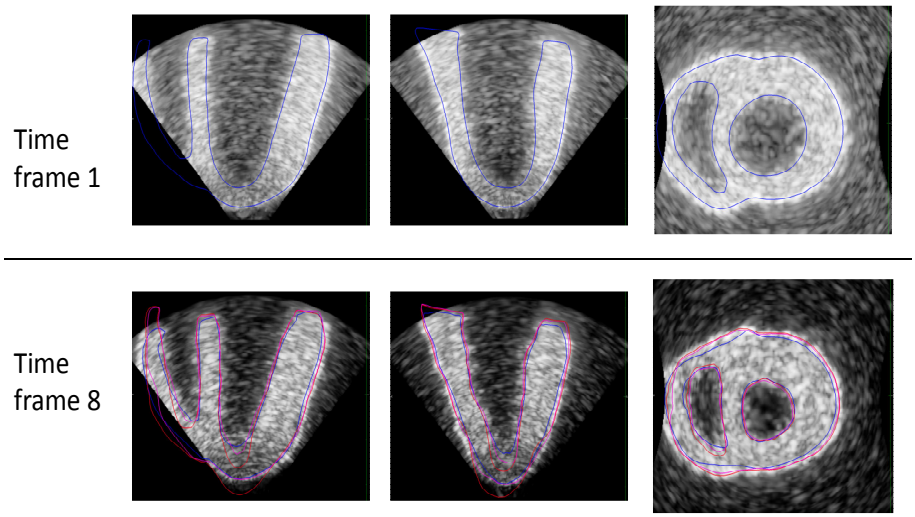

Figure 2.8: Myocardium tracking result for the first case is shown (red for iLogDemons and purple for iLogDemons without incompressibility) and compared to the simulated ground truth (blue) at the time frame 8 which is at the maximum contraction. The tracking result follow the contour of the ground truth, indicating that the algorithm is able to capture reasonably well the dynamics of the motion.

2.4 Discussion

This evaluation shows that the iLogDemons with and without the incompressibility constraint were able to recover the simulated motion in the ultrasound synthetic sequence with reasonable accuracy. It is worth noting that the current electromechanical model is not incompressible, therefore enforcing incompressibility in the registration algorithm naturally does not improve the results, in comparison to the iLogDemons method without the incompressibility constraint. Furthermore, we also found that increasing or decreasing the sigma value does not always improve the result since the best value that we found here is $\sigma_u = 1.5$ while $\sigma_u = 1$ and $\sigma_u = 2$ do not yield significantly better results.

2.5 Conclusion

The iLogDemons algorithm was applied to a data-set of synthetic ultrasound sequence with different motion and deformation pattern. The algorithm was able to reasonably estimate the ground truth deformation of the model. Since the provided

data-set were created using an electromechanical model which is not incompressible, the incompressibility constraint does not improve the result. However, the incompressibility constraint gives more realistic range of estimated strain value. Future work is needed to deal with the error accumulation during the maximum of contraction.

Chapter 3

Generation of Synthetic but Visually Realistic Time Series of Cardiac Images Combining a Biophysical Model and Clinical Images

Contents

Based on: [Prakosa 2012c] A. Prakosa, M. Sermesant, H. Delingette, S. Marchesseau, E. Saloux, P. Allain, N. Villain and N. Ayache. Generation of Synthetic but Visually Realistic Time Series of Cardiac Images Combining a Biophysical Model and Clinical Images. Medical Imaging, IEEE Transactions on, 2012. Note: In press.

The preliminary work in the synthetic sequence generation method for the 3D echocardiography is shown in Appendix C. This work was published in [Prakosa 2011]

We propose a new approach for the generation of synthetic but visually realistic time series of cardiac images based on an electromechanical model of the heart and real clinical 4D image sequences. This is achieved by combining three steps. The first step is the simulation of a cardiac motion using an electromechanical model of the heart and the segmentation of the end diastolic image of a cardiac sequence. We use biophysical parameters related to the desired condition of the simulated subject. The second step extracts the cardiac motion from the real sequence using non-rigid image registration. Finally, a synthetic time series of cardiac images corresponding to the simulated motion is generated in the third step by combining the motion estimated by image registration and the simulated one. With this approach, image processing algorithms can be evaluated as we know the ground-truth motion underlying the image sequence. Moreover, databases of visually realistic images of controls and patients can be generated for which the underlying cardiac motion and some biophysical parameters are known. Such databases can open new avenues for machine learning approaches.

3.1 Introduction

Diagnosis and therapy planning of cardiovascular diseases are often much improved by the analysis of the dynamic cardiac function. The advances in medical imaging offer increasingly detailed visual information on the cardiac motion. However there is a lack of quantification tools and of methods to validate them. The manual ground-truth generated by experts, which is typically used to validate segmentation algorithms, cannot be extended to motion tracking. Experts can only manually track a few landmarks, and doing this in sequences of volumetric images is very tedious, provides very limited accuracy and is prone to inter and intra-expert variabilities. In this article, we propose a framework to generate both cardiac ground-truth motion and corresponding synthetic but visually realistic images in order to enable such validation.

There are three main approaches to obtain quantitative data on cardiac motion. The first one is to use dedicated imaging modalities that directly measure motion information. Echocardiographic Doppler Tissue Imaging [Ho 2006], Magnetic Resonance (MR) tagging [Liu 2010] and several other phase encoding MR sequences [Ozturk 2003] have been developed to directly measure displacement or velocity fields for cardiac motion analysis [Elen 2008, Craene 2010, Mansi 2011]. However, those modalities are not widely used in clinics and give access to limited components of these fields (often one or two dimensional). Even with tridimensional tagging [Rutz 2008], it remains challenging to extract accurately, and to evaluate the quality of the recovered motion from another imaging modality [Mansi 2011] as it requires intermodality temporal and spatial registration.

A second one is to image a physical phantom with known shape and controlled motion [Daisne 2003, Boltz 2010]. However, those phantoms are costly to design and manufacture and often lead to images with a limited realism compared to clinical

images. This is due to the lack of the surrounding structures, and the difficulty to reproduce the complex cardiac motion.

The third method is to completely model the physics of the image acquisition system and of the organ of interest, and compute a numerical simulation of the resulting image. This was applied in the context of MR brain images [Benoit-Cattin 2005, Aubert-Broche 2006], cardiac MR sequences [Tobon-Gomez 2011], tridimensional echocardiographic (US) sequences [Duan 2007, Butakoff 2007, Elen 2008, Kutter 2009] and Computed Tomographic (CT) images [Segars 2008, Veress 2011]. A platform was recently developed to facilitate the access to several medical image simulators [Marion 2011]. This approach has proved to be useful for many validation tasks. For instance, synthetic cardiac SPECT image sequences [Segars 1999] were created for the validation of the developed 4D cardiac image segmentation [Montagnat 2005]. Synthetic 2D ultrasound sequences [Jensen 1996] were also generated for the validation of a non-rigid registration method [Ledesma-Carbayo 2005]. Finally, in order to validate a 3D strain estimation method of ultrasound images [Elen 2008], an adapted convolutional model [Gao 2007] was used to simulate US data sets. However, these approaches are computationally expensive and are restricted to a number of objects in the simulated field of view due to the complexity of the physical models involved. For cardiac sequence simulations, these constraints often impose to only simulate an isolated myocardium without much consideration of the blood pool and surrounding structures even though recently more complex models have been developed [Glatard 2012, Haddad 2007]. Therefore it limits the realism of the created synthetic images.

In this paper, we propose a new approach for creating synthetic and visually realistic cardiac image sequences based on real clinical image sequences, an electromechanical (E/M) model of the heart and an image registration algorithm. The method described below bypasses the simulation of the physics of acquisition by warping an original image sequence and replacing the observed motion of the myocardium by a simulated one. Without mimicking the physics of the acquisition, it uses the existing information in the real sequence to create the synthetic one. A key component to achieve this, is an E/M model of the heart. We use here a simple model [Sermesant 2006a] and an improved one [Sermesant 2012, Chapelle 2012], but the methodology would remain the same with other models (see for instance [Smith 2000, Belik 2004, Sainte-Marie 2006] and references therein). After the geometry and the biophysical parameters are personalised [Shi 2003, Wang 2009, Delingette 2012, Xi 2011, Chabiniok 2012], such a model can beat similarly to the apparent cardiac motion in a given sequence. Therefore we can have a simulated motion that is close to the one observed in the original image. The output of the proposed approach is a synthetic image sequence including the myocardium and its close environment (blood pools, valves...) that looks similar to the original sequence but where the myocardial motion is modified in a controlled manner and results from a simulation with known biophysical parameters. The motion of the structures surrounding the myocardium is slightly modified

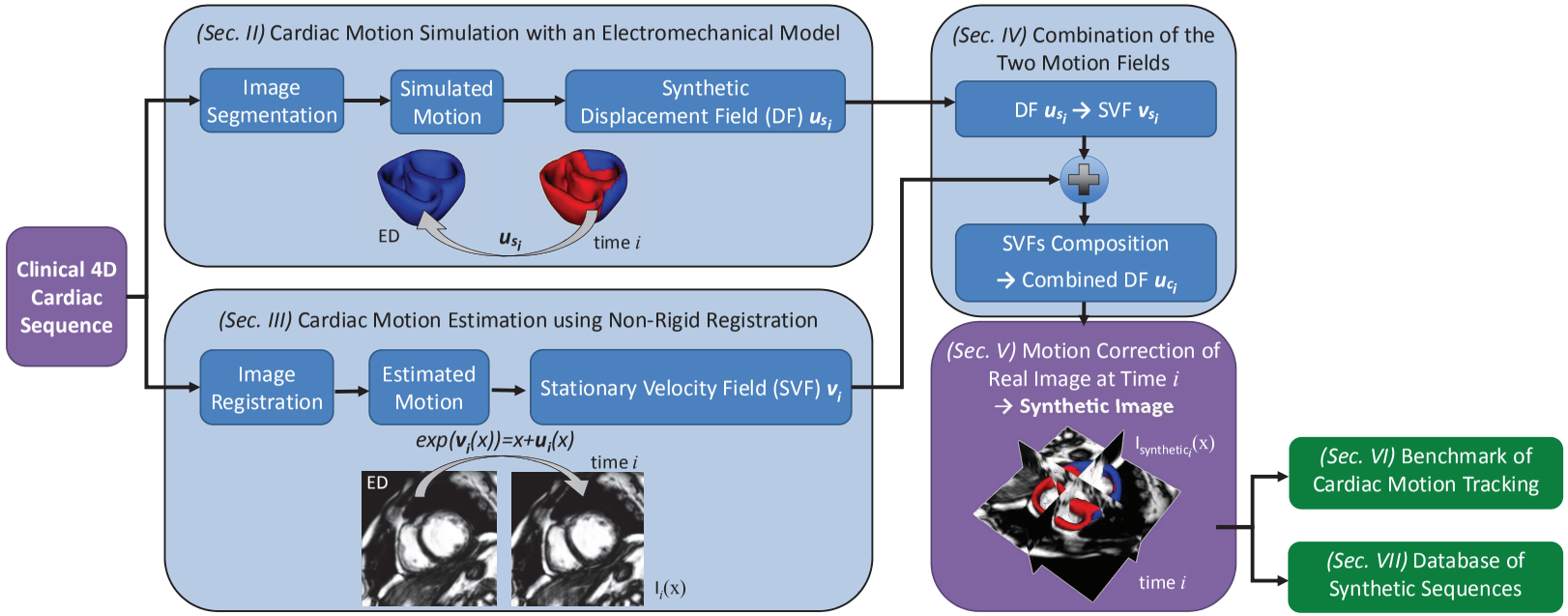

Figure 3.1: **Synthetic 4D Cardiac Sequence Generation Pipeline.** A clinical 4D sequence is used as an input to create a synthetic 4D sequence in which the myocardium motion follows a prescribed simulated displacement field. A cardiac E/M model simulates the cardiac contraction using a cardiac mesh created from the myocardium segmentation at ED. Log Demons registration method is applied to all images in the real clinical sequence to register them to the ED reference image. The combined simulated and registration motion are used to deform the real clinical images in order to create the synthetic cardiac sequence. Two applications are presented: non-rigid registration benchmark and image database generation.

to follow the simulated myocardium motion.

Compared to the previous methods, the proposed approach leads to images that remain very similar to the original clinical images and where the cardiac motion is known everywhere. It does not require complex physical simulations of the acquisition system and may be applied to various modalities as shown in this paper. Synthetic images of brain atrophy were simulated using MR images and generated displacement fields in [Camara 2006] but without taking into account real longitudinal sequences, only from a single time-point. In [Clarysse 2011], simulated sequence is created by using a kinematic model to deform a real tagged-MR image at end diastolic time point. We propose here to use a full time sequence of real data and a biophysical model of the heart, which are two very important points to obtain realistic sequences with large deformations. Using the whole real sequence information would also give better realism in the texture of the created sequence. It will also contain the changes of the surrounding environment such as the motion of the mitral valve.

The overall approach is described in Fig. 3.1 where the simulation of cardiac motion, the clinical cardiac motion estimation and the generation of synthetic sequences are respectively described in Sec. 3.2, Sec. 3.3 and Sec. 3.4. In Sec. 3.5, examples of synthetic sequences for cine MRI, 4D-CT and 4D-US imaging modalities are provided with an evaluation of their realism. Then, two applications are presented. The first one (Sec. 3.6) is the evaluation of a cardiac motion tracking algorithm (iLogDemons). The quantitative analysis of the synthetic images with a non-rigid registration algorithm allows to compare the estimated motion with the ground truth motion. The second application is the creation of a database of synthetic images (Sec. 3.7). It illustrates the application of this framework to help in developing image analysis methods based on machine learning [Tobon-Gomez 2008].

3.2 Cardiac Motion Simulation using an Electromechanical Model of the Heart

The first step in the proposed pipeline consists in simulating a cardiac motion. For this purpose, we used the cardiac E/M model proposed in [Sermesant 2006a]. We personalised the anatomy of the heart with the myocardium segmentation of a real clinical image at a reference time (end diastole / ED). The segmentation was done using an interactive 3D segmentation tool available within the CardioViz3D software [Toussaint 2008] (cf. Fig. 3.2). Using this tool, the 3D left ventricle (LV) and right ventricle (RV) endocardium and epicardium surfaces were segmented. Then a binary mask of the compact biventricular myocardium was created. A computational tetrahedral mesh which is suitable for the simulation was then generated from this myocardium mask using CGAL [Rineau 2009] available within the iso2Mesh tool proposed by [Fang 2009].

From a personalised anatomy, we generated an electrophysiological activation pattern using the dynamic multi-front Eikonal model which calculates the depolar-

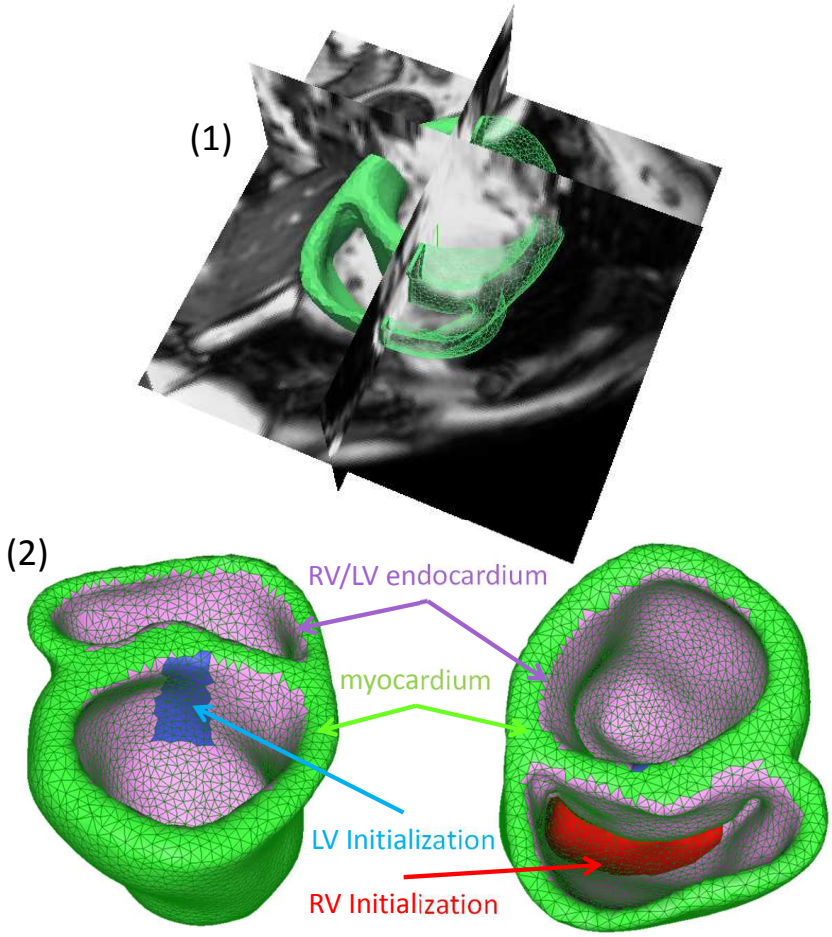

Figure 3.2: **Cardiac Segmentation, Mesh Geometry and Electrophysiological Initialization.** (1) Myocardium segmentation is obtained by using an interactive segmentation tool within the CardioViz3D software. (2) Initial electrical activation area is set for the LV (blue) and RV (red). RV/LV endocardium (purple) is set to have higher conductivity v than the rest of the myocardium (green) to represent the Purkinje network.

ization time T_d at each point of the mesh [Sermesant 2007]. The Eikonal equation $v\sqrt{\nabla T_d^t D \nabla T_d} = 1$ was solved using the multi-front Fast Marching Method which also calculates the repolarization time T_r. In this equation, v is the local conduction velocity and $D = (1-r)f \otimes f + r.I$ is the anisotropic conductivity tensor in Cartesian coordinates as defined in [Sermesant 2006a] where f is the fibre orientation and r is the conductivity anisotropy ratio. Synthetic myocardial fibres were created by varying the elevation angle (w.r.t. the short axis plane) of the fibre from $-80°$ on the epicardium to $0°$ at mid-wall to $+80°$ on the endocardium. The initial electrical activation area was defined on the previously created cardiac mesh (cf. Fig. 3.2). We defined some areas in the LV and the RV which prescribe the His

bundle proximity where the electrical propagation wave starts. We also set the LV and RV endocardium surfaces to have higher conductivity (larger v) compared to the rest of the myocardium, to represent the Purkinje network.

The obtained T_d and T_r were then used in the electromechanical coupling written as

$$\begin{cases} \text{if } T_d \leq t \leq T_r & : \sigma_c(t) = \sigma_0(1 - e^{(\alpha_c(T_d - t))}) \\ \text{if } T_r < t < T_d + HP & : \sigma_c(t) = \sigma_c(T_r)e^{(\alpha_r(T_r - t))} \end{cases}$$

which gives the stress tensor σ_c at time t. HP is the heart period, α_c is the contraction rate, and α_r is the relaxation rate. The force vector F_c was obtained from $F_c = \int_S (\sigma_c f \otimes f) n \, dS$ with n the surface normal and S the element surface. The dynamic equation which governs the displacement vector U was written as $M\ddot{U} + C\dot{U} + KU = F_b + F_c$ where M, C and K are the mass, damping, and stiffness matrices respectively. F_b is the external load from the boundary condition.

We also used an improved E/M model, Bestel-Clément-Sorine (BCS) [Chapelle 2012], which includes a passive non linear elastic part and an active part that describes more accurately the binding and unbinding processes of the actin and myosin filaments in the sarcomere. It also allows *the Starling effect* by which the maximum contraction depends on the fibre strain and includes the dissipation due to friction during the contraction. As a result, the simulated deformation incorporates twisting motion which makes it more realistic. This model was shown to provide realistic simulation of LBBB and heart failure, as well as accurate prediction of ventricular pressure changes with resynchronisation therapy [Sermesant 2012].

For all the parameters of the electromechanical model we took into account the known condition of the heart in the real image we used. We could for instance include a Left Bundle Branch Block (LBBB) or a reduced contractility in an infarcted area. For the LBBB case, a detailed personalisation of the electrophysiology and mechanics models on two patients [Sermesant 2012] has allowed us to characterise the parameter range associated with this pathology. From this experience, LBBB is simulated using a lower electrical conduction velocity (v = 30 cm/s) and a reduced contractility ($\sigma_0 = 50$) compared to the simulation of the normal case with v = 50 cm/s and $\sigma_0 = 90$. The Left Ventricle (LV) initialization (cf. Fig. 3.2) is also blocked to simulate LBBB. This simple personalisation of LBBB leads to reasonable simulated motion which is not too far from the observed one.

We also used a calibration method to assess the mechanical parameters of the BCS model so that the simulation is close to the real clinical sequence in term of ejected blood volume. We used the algorithm derived from the Unscented Transform [Julier 1997], and described in [Marchesseau 2012b]. The algorithm finds a set of parameters that enable the simulation to match observations on the endocardial volume of the LV (the minimum volume, the minimum and maximum of the flow) of the real clinical sequence in one iteration through the analysis of the covariance matrix between the simulated observations and the variation of each parameter independently.

This simulation provides a dense motion field within the myocardium for the

whole cardiac cycle. This motion field can be sampled at the resolution of the original image sequence both in space and time.

3.3 Cardiac Motion Estimation from Images using Non-Rigid Registration

To be able to introduce a given cardiac motion within a clinical 4D image sequence, one has first to estimate the motion visible in this image, in order to replace it. To achieve this, we applied a non-rigid registration algorithm to the clinical 4D cardiac sequence to find the deformation field between each pair of images. We used the symmetric Log-Domain Demons (LogDemons) non-linear registration algorithm proposed in [Vercauteren 2008]. The purpose of applying this non-linear image registration is to find the displacement vector field $\mathbf{u}(\mathbf{x})$ associated with the transformation $\phi(\mathbf{x}) = \mathbf{x} + \mathbf{u}(\mathbf{x})$ which aligns a template image $\mathrm{T}(\mathbf{x})$ to a reference image $\mathrm{R}(\mathbf{x})$, where $\mathbf{x} \in \mathbb{R}^3$ is the space coordinate (voxel (x,y,z)).

Here we took the end diastolic (ED) image as the reference image $\mathrm{R}(\mathbf{x})$. With this non-rigid registration algorithm, the displacement field $\mathbf{u}_i(\mathbf{x})$ between the ED image and each image at frame i of the clinical 4D cardiac sequence was estimated (cf. Fig. 3.1). An accurate registration transforms each image at frame i in the clinical 4D sequence well aligned to the ED reference image. Transformation $\phi_i(\mathbf{x})$ is parameterized by a stationary velocity field $\mathbf{v}_i(\mathbf{x})$ through the exponential map $\phi_i(\mathbf{x}) = \exp(\mathbf{v}_i(\mathbf{x})) = \mathbf{x} + \mathbf{u}_i(\mathbf{x})$. Using this parameterization, we ensure the one-to-one correspondence between all points in the transformation since this is a physical property of the cardiac deformation (no tearing or destruction of tissue). With this method, the clinical image sequence was "stabilised" or "freezed", meaning that the apparent cardiac motion was removed from the sequence. We can then introduce the ground-truth motion generated by the biophysical model. We use the implementation of LogDemons algorithm in ITK [Dru 2009]. For the registration parameters, 1 voxel size of regularization kernel and 3 or 5 multi-resolution levels (depending on the resolution of the image) with 200 iterations for each level usually gives good result.

3.4 Combination of Simulated and Estimated Motions to Create Synthetic Sequences

To combine simulated and estimated motions, we first adjusted temporally the simulated motion and then sampled it in order to match the cycle length and temporal resolution of the clinical 4D sequence. The sampling of the simulated motion consists in computing the displacement field (DF) between the reference configuration (ED) and the deformed position at each time frame of the sequence. This displacement is only known at the vertices of the tetrahedral meshes, but using the linear interpolation inside each tetrahedron, we rasterized the continuous DF into a volumetric image having the same size and spatial resolution as the clinical 4D sequence.

DF	displacement field
SVF	stationary velocity field
ED	end diastolic
$I_i(\mathbf{x})$	real clinical image at time i
$I_{synthetic_i}(\mathbf{x})$	generated synthetic image at time i
$\mathbf{u}_{\mathbf{s}_i}(\mathbf{x})$	simulated DF at time i
$\mathbf{v}_{\mathbf{s}_i}(\mathbf{x})$	simulated SVF at time i
$\mathbf{u}_i(\mathbf{x})$	DF obtained from the registration of $I_i(\mathbf{x})$ to the reference ED real image.
$\mathbf{v}_i(\mathbf{x})$	SVF obtained from the registration of $I_i(\mathbf{x})$ to the reference ED real image.
$\mathbf{v}_{\mathbf{c}_i}(\mathbf{x})$	combined SVF at time i
$\mathbf{u}_{\mathbf{c}_i}(\mathbf{x})$	combined DF at time i
$\phi_{c_i}(\mathbf{x})$	transformation which transform $I_i(\mathbf{x})$ to $I_{synthetic_i}(\mathbf{x})$. $\phi_{c_i}(\mathbf{x}) = \mathbf{x} + \mathbf{u}_{\mathbf{c}_i}(\mathbf{x})$

Table 3.1: **Notations.** Definitions of the notation used in the combination of simulated and estimated motion

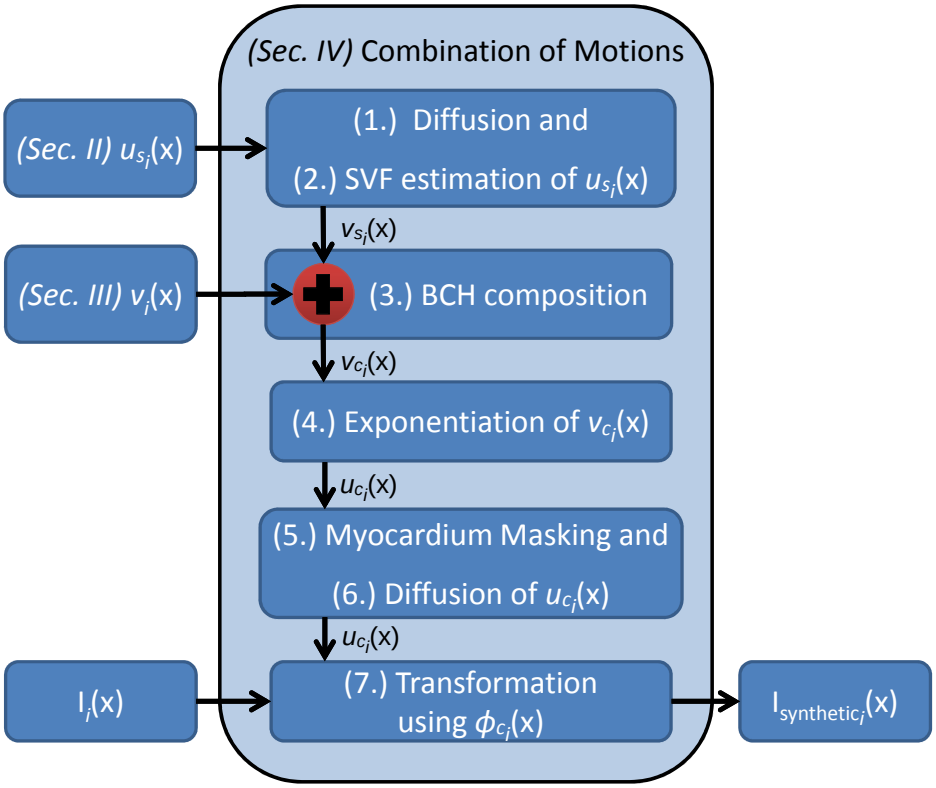

Figure 3.3: **Block Diagram of the Motion Combination Process.** The simulated and the estimated motions are combined to transform the real image.

The steps are summarized in Fig 3.1. They include the warping of clinical image $I_i(\mathbf{x})$ at time i into the synthetic image $I_{synthetic_i}(\mathbf{x})$. This warping mainly occurs around the myocardium, and the amount of deformation depends on how much the simulated cardiac motion differs from the one estimated in the original image sequence.

The transformation $\phi_{c_i}(\mathbf{x})$ of the original image is obtained through several computing stages. However, it can be simply formulated as resulting from the composition of the transformation from time i to ED estimated through the Symmetric Log-Demons algorithm with the transformation from ED to time i which was simulated by the electromechanical model of the heart. The pipeline to create $\phi_{c_i}(\mathbf{x})$ is sketched in Fig. 3.1 and Fig. 3.3 and detailed in Alg. 2.

Algorithm 2 Motion combination and synthetic image generation at time i

Require: Synthetic DF $\mathbf{u}_{\mathbf{s}_i}(\mathbf{x})$, symmetric Log-Domain Demons stationary velocity field (SVF) $\mathbf{v}_i(\mathbf{x})$, real clinical image at time i $I_i(\mathbf{x})$

$\mathbf{u}_{\mathbf{s}_i}(\mathbf{x}) \leftarrow$ diffusion of the synthetic DF $\mathbf{u}_{\mathbf{s}_i}(\mathbf{x})$ (cf. Alg. 3)

$\mathbf{v}_{\mathbf{s}_i}(\mathbf{x}) \leftarrow$ estimation of the SVF from $\mathbf{u}_{\mathbf{s}_i}(\mathbf{x})$ (cf. Alg. 4)

Baker-Campbell-Hausdorff (BCH) (see [Vercauteren 2008]) composition of the SVFs:

$\mathbf{v}_{\mathbf{c}_i}(\mathbf{x}) = \mathbf{v}_i(\mathbf{x}) \circ \mathbf{v}_{\mathbf{s}_i}(\mathbf{x}) = \mathbf{v}_i(\mathbf{x}) + \mathbf{v}_{\mathbf{s}_i}(\mathbf{x}) + 1/2[\mathbf{v}_i(\mathbf{x}), \mathbf{v}_{\mathbf{s}_i}(\mathbf{x})] + ...$

Exponential of the combined SVF:

$\phi_{c_i}(\mathbf{x}) = \exp(\mathbf{v}_{\mathbf{c}_i}(\mathbf{x})) = \mathbf{x} + \mathbf{u}_{\mathbf{c}_i}(\mathbf{x})$

Myocardium masking of the combined DF $\mathbf{u}_{\mathbf{c}_i}(\mathbf{x})$:

$\mathbf{u}_{\mathbf{c}_i}(\mathbf{x}) \leftarrow \mathbf{u}_{\mathbf{c}_i}(\mathbf{x})$ for $\mathbf{x} \in$ simulated myocardium at time i and 0 otherwise

$\mathbf{u}_{\mathbf{c}_i}(\mathbf{x}) \leftarrow$ diffusion of the masked combined DF $\mathbf{u}_{\mathbf{c}_i}(\mathbf{x})$ (cf. Alg. 3)

Transformation of the real clinical image $I_i(\mathbf{x})$:

$I_{synthetic_i}(\mathbf{x}) = I_i(\phi_{c_i}(\mathbf{x})) = I_i(\mathbf{x} + \mathbf{u}_{\mathbf{c}_i}(\mathbf{x}))$ **return** $I_{synthetic_i}(\mathbf{x})$

A first step consists of transforming the simulated DF $\mathbf{u}_{\mathbf{s}_i}(\mathbf{x})$ into a diffeomorphic transformation parameterized by a stationary velocity field $\mathbf{v}_{\mathbf{s}_i}(\mathbf{x})$. Indeed, it is important to handle smooth and diffeomorphic transformations to avoid any tearing or folding of the image textures. To achieve this, we extrapolated the simulated DF outside the myocardium using a diffusion method described in Alg. 3.

The extrapolation is necessary to estimate the velocity field as it is sensitive to discontinuity of displacements. The diffusion of a vector field outside the myocardium is based on the iterative convolution of a Gaussian kernel followed by the reinitialisation of vector values in myocardium and border voxels. We used the recursive Gaussian filter implemented in ITK with 1 voxel size of sigma. The process is iterated until the difference in vectors between two iterations is less than 1% of the smallest voxel size.

We then used the algorithm proposed by [Bossa 2008] as implemented in [Dru 2009] to estimate the synthetic stationary velocity field $\mathbf{v}_{\mathbf{s}_i}(\mathbf{x})$ from the synthetic DF $\mathbf{u}_{\mathbf{s}_i}(\mathbf{x})$, see Alg. 4. The estimation of the velocity field from the displacement field described in Alg. 4 requires the computation of the exponential of

Algorithm 3 Synthetic Displacement Field (DF) Diffusion

Require: Input Synthetic DF $\mathbf{u}_{\mathbf{s}_i}(\mathbf{x})$

Initialize the DF $\mathbf{u}^0_{\mathbf{s}_i}(\mathbf{x}) = 0$, $\mathbf{u}^1_{\mathbf{s}_i}(\mathbf{x}) = \mathbf{u}_{\mathbf{s}_i}(\mathbf{x})$, t=1

while $||\mathbf{u}^t_{\mathbf{s}_i}(\mathbf{x}) - \mathbf{u}^{t-1}_{\mathbf{s}_i}(\mathbf{x})|| >$ threshold **do**

    Smooth the DF:

$\tilde{\mathbf{u}}^t_{\mathbf{s}_i}(\mathbf{x}) \leftarrow G_\sigma * \mathbf{u}^t_{\mathbf{s}_i}(\mathbf{x})$ with G_σ is a Gaussian Kernel

    In the myocardium, replace the smoothed DF with the initial synthetic DF:

$\mathbf{u}^{t+1}_{\mathbf{s}_i}(\mathbf{x}) \leftarrow (1 - w(\mathbf{x}))\tilde{\mathbf{u}}^t_{\mathbf{s}_i}(\mathbf{x}) + w(\mathbf{x})\mathbf{u}^t_{\mathbf{s}_i}(\mathbf{x})$ with $w(\mathbf{x}) = 1$ for $\mathbf{x} \in$ simulated myocardium at time i and 0 otherwise. Set $\mathbf{u}^{t+1}_{\mathbf{i}}(\mathbf{x})$ to 0 on border voxels.

    $t \leftarrow t + 1$

return $\mathbf{u}^t_{\mathbf{s}_i}(\mathbf{x})$

a stationary velocity field. We used here a forward Euler integration scheme as the more standard "Scaling and Squaring" method could have a limited accuracy in large deformation cases.

Algorithm 4 Logarithm $\mathbf{v}_\mathbf{s}(\mathbf{x})$ of the synthetic DF $\mathbf{u}_\mathbf{s}(\mathbf{x})$ s.t. $\phi_\mathbf{s}(\mathbf{x}) = \exp(\mathbf{v}_\mathbf{s}(\mathbf{x}))$

Require: Diffused synthetic DF $\mathbf{u}_\mathbf{s}(\mathbf{x})$

$\mathbf{v}_{\mathbf{s}_0}(\mathbf{x}) = \phi_\mathbf{s}(\mathbf{x}) - \mathbf{x}$ where $\phi_\mathbf{s}(\mathbf{x}) = \mathbf{x} + \mathbf{u}_\mathbf{s}(\mathbf{x})$

for $n = 0 \rightarrow$ max iteration **do**

    $\tilde{\delta}\mathbf{v}_{\mathbf{s}_n}(\mathbf{x}) = \exp(-\mathbf{v}_{\mathbf{s}_n}(\mathbf{x})) \circ \phi_\mathbf{s}(\mathbf{x}) - \mathbf{x}$

    Smooth the stationary velocity fields:

$\tilde{\delta}\mathbf{v}_{\mathbf{s}_n}(\mathbf{x}) \leftarrow G_\sigma * \tilde{\delta}\mathbf{v}_{\mathbf{s}_n}(\mathbf{x})$, $\mathbf{v}_{\mathbf{s}_n}(\mathbf{x}) \leftarrow G_\sigma * \mathbf{v}_{\mathbf{s}_n}(\mathbf{x})$

with G_σ is a Gaussian Kernel

    BCH composition of the stationary velocity fields:

$\mathbf{v}_{\mathbf{s}_{n+1}}(\mathbf{x}) = \mathbf{v}_{\mathbf{s}_n}(\mathbf{x}) + \tilde{\delta}\mathbf{v}_{\mathbf{s}_n}(\mathbf{x}) + 1/2[\mathbf{v}_{\mathbf{s}_n}(\mathbf{x}), \tilde{\delta}\mathbf{v}_{\mathbf{s}_n}(\mathbf{x})] + ...$

return $\mathbf{v}_\mathbf{s}(\mathbf{x}) = \mathbf{v}_{\mathbf{s}_{n+1}}(\mathbf{x})$

In a second step, the symmetric Log Demons registration and the extrapolated diffeomorphic simulated transformation are composed. Since the symmetric Log Demons algorithm also estimates a transformation parameterized by a stationary velocity field $\mathbf{v}_i(\mathbf{x})$, this composition can be done conveniently in the space of velocities using the Baker-Campbell-Hausdorff (BCH) rule (see [Vercauteren 2008]): $\mathbf{v}_{\mathbf{c}_i}(\mathbf{x}) = \mathbf{v}_i(\mathbf{x}) \circ \mathbf{v}_{\mathbf{s}_i}(\mathbf{x})$. This composition is meaningful because velocity field $\mathbf{v}_{\mathbf{s}_i}(\mathbf{x})$ shows the positions at ED for each point in the simulated myocardium at time i and the velocity field $\mathbf{v}_i(\mathbf{x})$ points to the position at time i in the real clinical image for each point at ED. An important fact is that the simulated myocardium at ED is the same as the myocardium segmented in the ED clinical image (cf. Sec. 3.2). Therefore we are filling the simulated myocardium at time i with the myocardium intensity of real image at the same time.

In the last step, we corrected the displacement field $\mathbf{u}_{\mathbf{c}_i}(\mathbf{x}) = \exp(\mathbf{v}_{\mathbf{c}_i}(\mathbf{x})) - Id(\mathbf{x})$ outside the myocardium in order to keep most of the synthetic image similar to

the real clinical image. To this end, we set to zero the DF outside the simulated myocardium by masking $\mathbf{u_{c_i}(x)}$ with the simulated myocardium mask at time i. Then, we applied the same diffusion process as in Alg. 3 to smooth the field and enforce that structures surrounding the myocardium follow the motion of the myocardium. Finally the resulting displacement field is applied to the image $I_i(\mathbf{x})$ to create $I_{synthetic_i}(\mathbf{x})$.

3.5 Producing Synthetic 4D Image Sequences

The processes were performed on a desktop PC with Intel Xeon processor at 3.33 GHz. The computation time is a function of the resolution of the image. The LogDemons registration takes 1 hour for each pair of CT images and 5 minutes for MRI. For the cardiac motion simulation, we used the BCS E/M model which was implemented in the SOFA simulation platform [Faure 2012]. It takes 20 minutes for a cardiac cycle simulation. Without code optimization, the next steps which include the motion combination up to the generation of the synthetic image take 3 hour for a synthetic CT image and 2 minutes for MRI."

3.5.1 Synthetic Cine MRI Sequence

We applied our proposed approach to create a synthetic cine MRI sequence from a clinical cine MRI sequence of an 84 years old male patient with dilated cardiomyopathy and left bundle branch block (LBBB) acquired on Achieva MR Philips Medical System scanner with the following acquistion protocol; Multi-slice steady state free precession (SSFP) sensitivity encoding (SENSE) with 30 views per gating interval, echo time of 1.5071 ms, repetition time of 3.0142 ms and flip angle of 60°. The image size was $171 \times 171 \times 98$ voxels with the resolution of $1.424 \times 1.424 \times 1.424$ mm^3 (the image was isotropically resampled from an image with an original slice thickness of 8 mm). The number of images in the sequence was 30.

In order to be more illustrative, we simulated the resynchronisation of this heart to create the synthetic cine MRI sequence. It allowed to have a correction field of a larger magnitude and therefore to better evaluate the impact on the original image (see Fig. 3.4).

The proposed sequence generation method produced a visually realistic synthetic sequence with a seamless fusion of the simulated myocardial motion and the neighbouring moving structures. The contraction of the created synthetic cine MRI sequence follows the motion of the E/M simulation which is shown by the myocardium contour which corresponds to the contour of the deformed mesh in the E/M simulation (cf. Fig. 3.4).

We also created a personalised synthetic sequence and compared the intensity histograms in the myocardium mask between the original and synthetic images. As expected, we observe that both intensity histograms are similar (cf. Fig. 3.7). It shows that the intensity distribution in the simulated myocardium is not too much distorted.

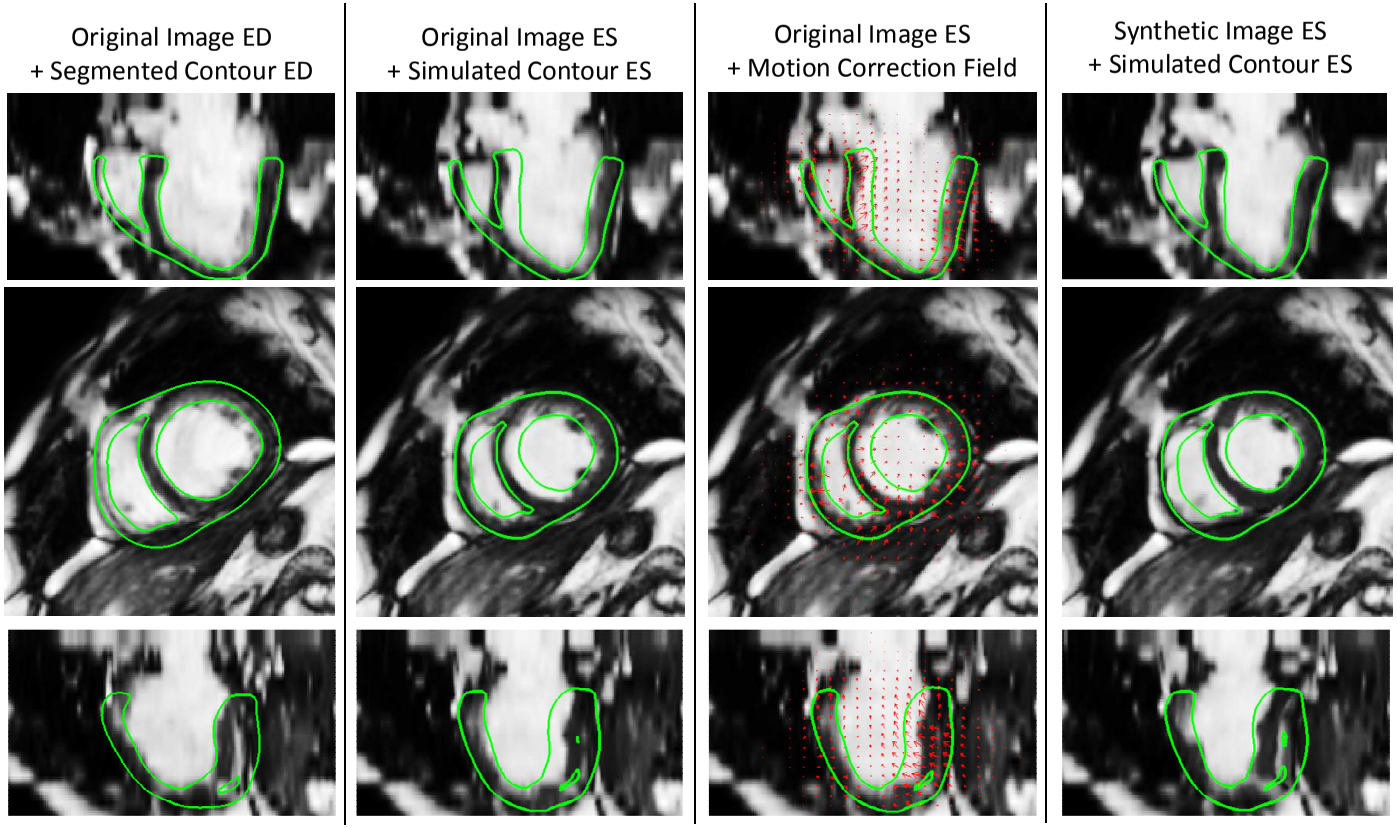

Figure 3.4: **Synchronized Synthetic cine MRI Created from Pathological Sequence.** End diastolic clinical image is shown with its segmentation. The original clinical image at ES is shown with the contour of the simulated mesh at the corresponding time. The synthetic combined displacement field is applied to the original image at ES to correct the motion. The contour of the resulting synthetic image at ES shows a good agreement with the contour of the simulated mesh at ES. Video can be seen in the supplementary material.

3.5.2 Synthetic 4D CT Sequence

A synthetic 4D CT sequence was created from a clinical 4D CT sequence obtained from a public clinical image database [OSIRIX 2012], acquired using a Siemens Sensation 64 CT system. Since the data is anonymized, no patient details are available. The ejection fraction of this patient is 61%, therefore we believe this sequence presents a normal ventricular function. The image size was $512 \times 512 \times 377$ voxels with the resolution of $0.402 \times 0.402 \times 0.402\ mm^3$ (resampled from the original slice thinkness of 2 mm). The number of images in the sequence is 10.

Again, in order to better demonstrate the method, we applied a simulation with a different condition than the original sequence. In this case, we created a left bundle branch block.

The contraction of the synthetic 4D CT also showed a good agreement with the motion of the E/M simulation, as demonstrated by the alignment of the contour of the myocardium with the mesh from the E/M simulation (cf. Fig. 3.5). From the created personalised simulation, the real and the synthetic CT image intensity histograms are very similar (cf. Fig. 3.7)

3.5.3 Synthetic 4D US Sequences

We used a clinical sequence acquired with a iE33 Philips Echocardiography System probe on a healthy 33 years old male volunteer. The image size was $224 \times 208 \times 208$ voxels with the resolution of $0.727 \times 0.716 \times 0.632\ mm^3$. The iE33 system acquired a fully sampled cardiac volume within four cardiac cycles. The number of images in a cardiac cycle was 30.

Generating synthetic US sequences was more challenging than other modalities because of the reduced field of view. The myocardium is not completely visible in the image, thus one has to manage the difference between the myocardial tissue entering the image during contraction in the clinical sequence and in the synthetic one. Additional information might be needed for outside of the ultrasound acquisition cone.

In order to tackle this, different steps were added. First, the field of view was artificially expanded by dilating the acquisition pyramid. We copied the boundary voxels with additional noise to fill this region. It provided an approximation of the image intensity for voxels entering the cone. Then after the synthetic image was generated, the image was cropped at the original size. Finally, the displacement field outside the 3D US acquisition cone was set to be zero during the last diffusion process of the masked displacement field as explained in Sec. 3.4.

We preserved the dynamics of the image, in particular the visible speckle pattern. We also preserved the realism of the ultrasound image quality gradient from base to apex in the synthetic image like in the clinical image where the apical quality is better than the basal quality. The contraction of the synthetic sequence follows the motion of the E/M simulation which was used to create the synthetic sequence. In Fig. 3.6, the contour of the cardiac mesh at end systole was overlaid on the syn-

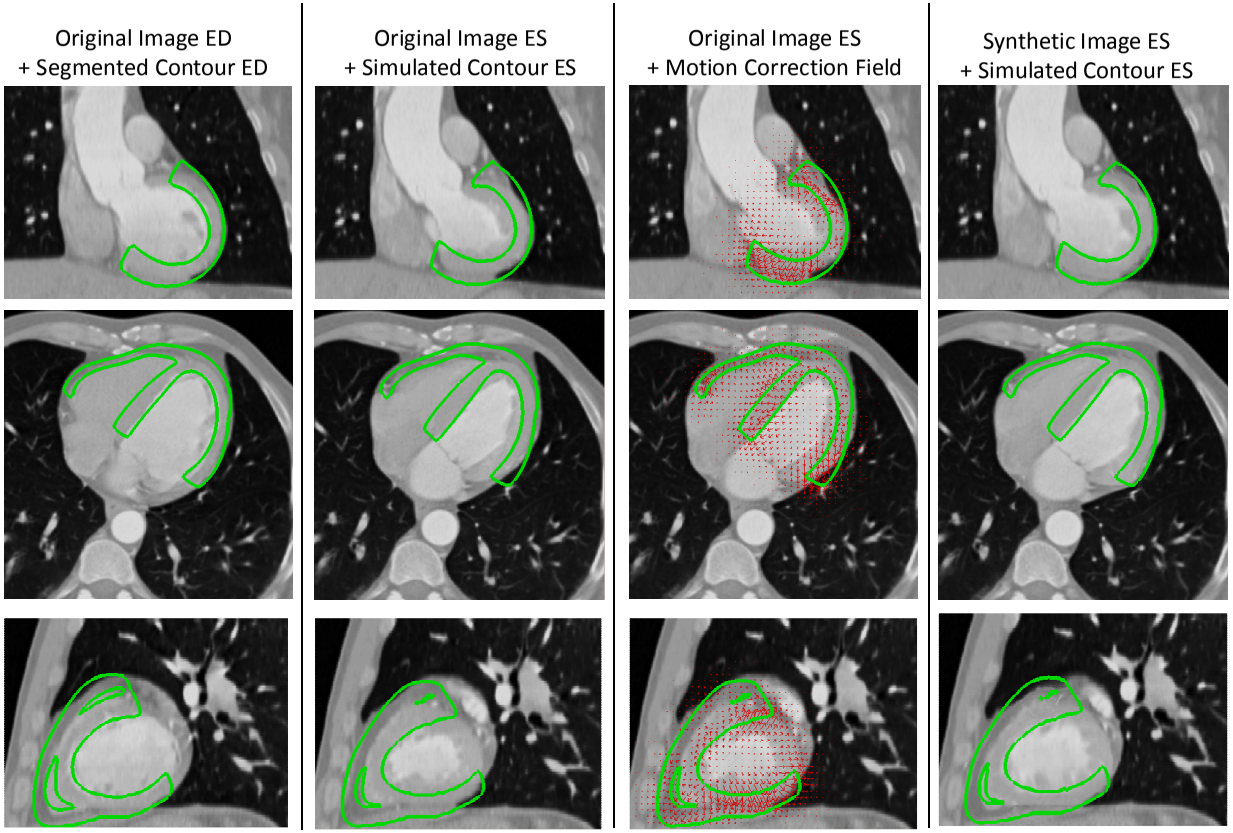

Figure 3.5: **Pathological Synthetic 4D CT Created from a Clinical Sequence.** End diastolic clinical image is shown with its segmentation. The original clinical image at ES is shown with the contour of the simulated mesh at the corresponding time. The synthetic combined displacement field is applied to the original image at ES to correct the motion. The contour of the resulting synthetic image at ES shows a good agreement with the contour of the simulated mesh at ES. Video can be seen in the supplementary material.

Figure 3.6: **Pathological Synthetic 4D US Created from Volunteer Data.** End diastolic clinical image is shown with its segmentation. The original clinical image at ES is shown with the contour of the simulated mesh at the corresponding time. The synthetic combined displacement field is applied to the original image at ES to correct the motion. The contour of the resulting synthetic image at ES shows a good agreement with the contour of the simulated mesh at ES. Video can be seen in the supplementary material.

thetic 3D image at the same time point. The myocardium contour of the synthetic sequences correctly followed the contour of the deformed cardiac mesh from the E/M simulation.

We compared the intensity histograms of the original and the personalised synthetic images (cf. Fig. 3.7); they look similar and tend to follow a typical Rayleigh distribution which is a characteristic of US cardiac tissue images [Gao 2007].

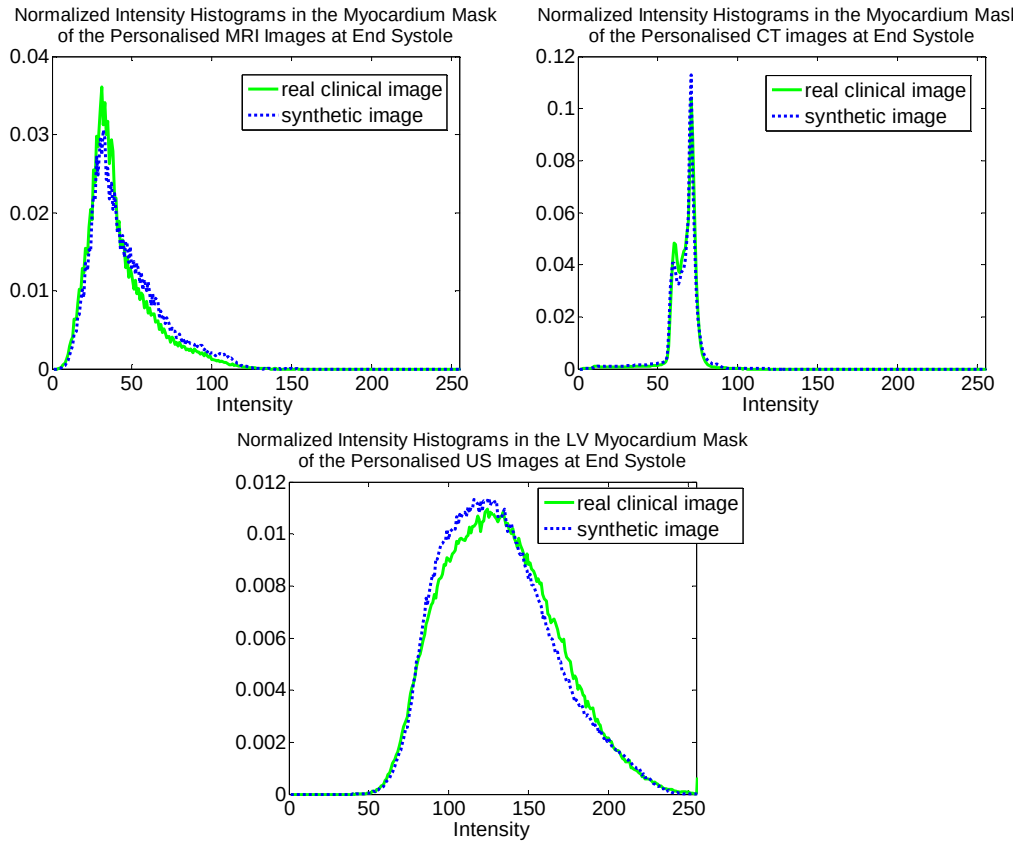

Figure 3.7: **Intensity Histograms Comparison.** Similar intensity histograms are shown from the synthetic and the real clinical image at ES.

3.6 Benchmark of Cardiac Motion Tracking

As an illustrative application we performed cardiac motion tracking on synthetic sequences and compared the results with the ground-truth motion. Compared to the images shown in the previous section, we used here the simple personalised models so that the motion correction is reduced, and therefore the image texture minimally modified.

We tested here the iLogDemons algorithm [Mansi 2011]. Note that this method is different from the one which was used to generate the images, as this method en-

forces the incompressibility of the myocardium during the cardiac motion tracking to regularize the visible motion in the image sequence and better recover the full motion. A binary mask from the ED segmentation is used to apply the incompressibility. The parameters of the tracking algorithm were taken as in [McLeod 2012], where a regularisation kernel of the size of the voxel was used.

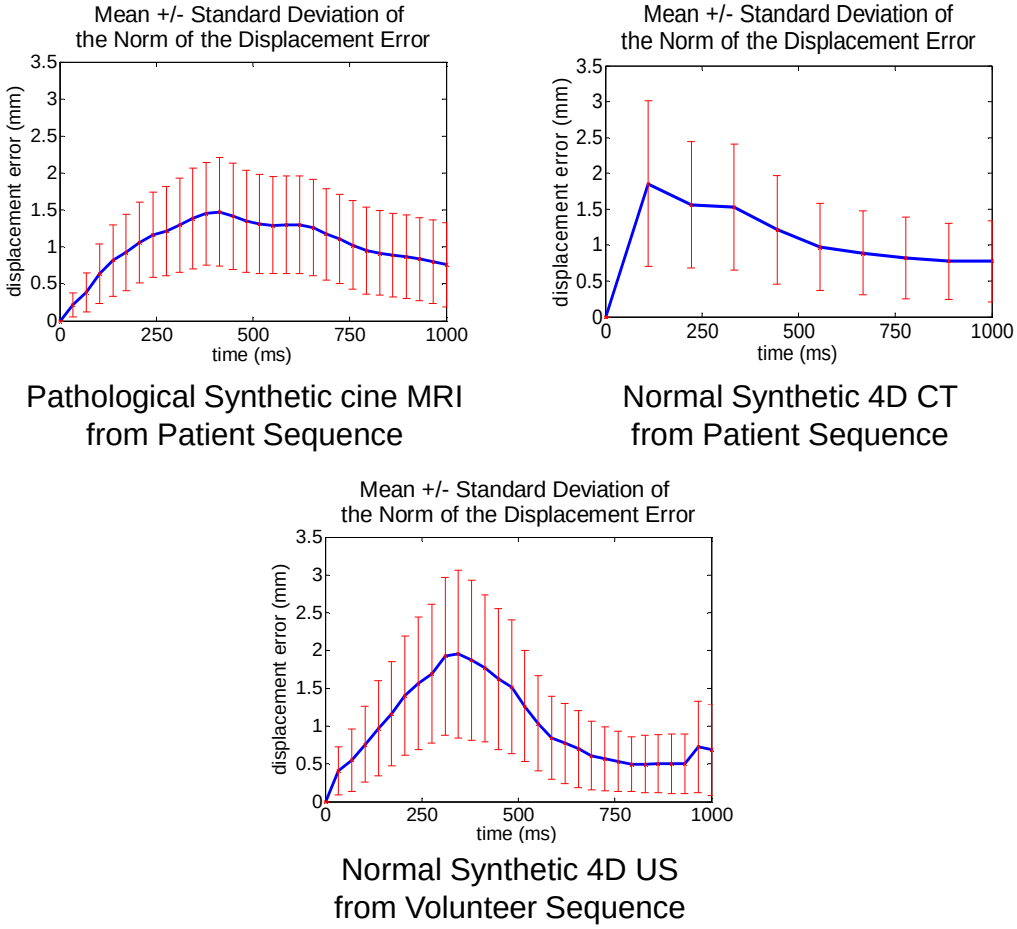

Figure 3.8: **Ground Truth and iLogDemons Estimated Displacement Field Difference.** From the synthetic sequences, the norm of the displacement field differences between the E/M simulated and the iLogDemons estimated motion was computed. The mean and standard deviation during the cardiac cycle are shown.

The motion tracking estimates the DF $\mathbf{u}_{\mathbf{r}_i}(\mathbf{x})$ between each image at time i in the synthetic sequence and the ED reference image. To evaluate the iLogDemons results, we computed the norm of the displacement difference between the ground truth and the iLogDemons motion fields: $||\mathbf{u}_{\mathbf{s}_i}(\mathbf{x})^{-1} - \mathbf{u}_{\mathbf{r}_i}(\mathbf{x})||$. We needed to inverse the ground truth motion that we used previously to generate the synthetic sequence (cf. Sec. 3.4) in order to compute $\mathbf{u}_{\mathbf{s}_i}(\mathbf{x})^{-1}$, but this is easily done as we directly estimate this motion field from meshes. The results are shown in Fig. 3.8. The

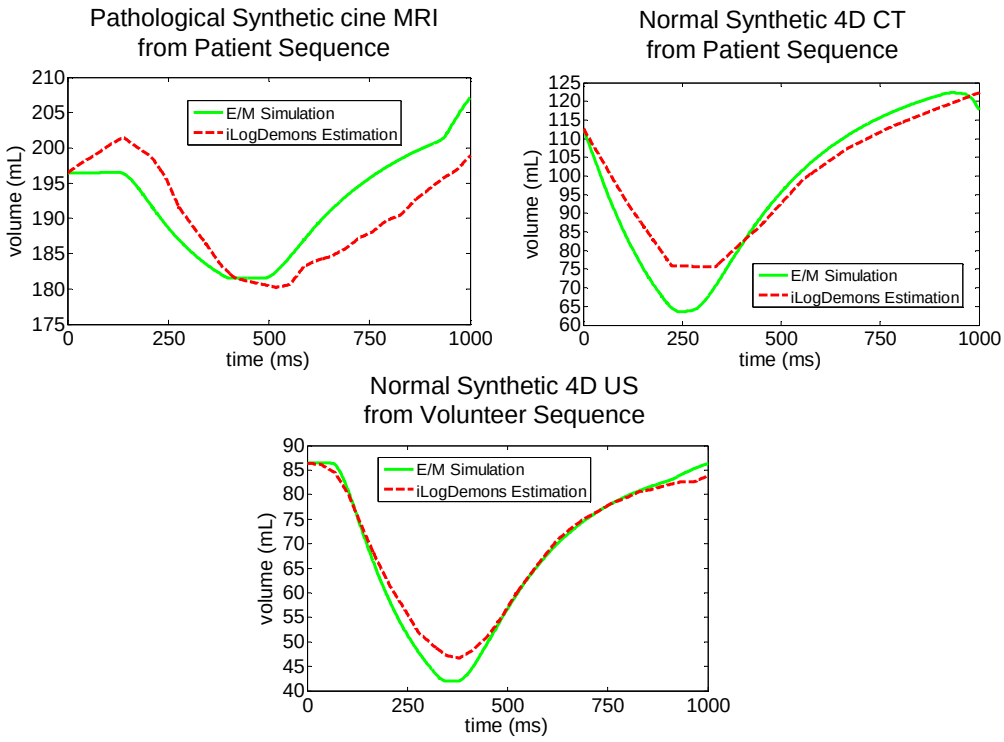

Figure 3.9: **iLogDemons LV Volume Estimation.** The simulation ground truth (green) and the iLogDemons estimation (red) of the LV volume curve along a cardiac cycle are compared. Similar curves and close ejection fraction (EF) values are observed.

maximum value of the mean displacement differences in the sequence are 1.48 mm, 1.86 mm and 1.95 mm for the MRI, CT, and US sequences respectively. While we can see that the iLogDemons achieves reasonable tracking results, it allows to quantify precisely the remaining error and therefore optimise the algorithm to improve the results.

We also measured the estimated LV volumes along the cardiac cycle by deforming the mesh used for the simulation with the deformation field from the iLogDemons, and compared them to the ground truth (Fig. 3.9). Similar curves are observed, the differences of the end systolic volumes are 1.4 mL, -12.0 mL and -4.7 mL for MRI, CT, and US sequences respectively.

As for some therapies, like Cardiac Resynchronisation Therapy (CRT), there is an important interest in knowing regional differences of motion, we analysed in a more detailed way the US sequence (which is the modality typically used in CRT). We extracted a set of kinematic descriptors which describe in a compact way the cardiac motion of each region. To this end, we characterized the motion of each of the 17 LV American Heart Association (AHA) segments by fitting in the least-square way an affine transformation $f(p) = Ap + B$ [Sermesant 2003] to the iLogDemons

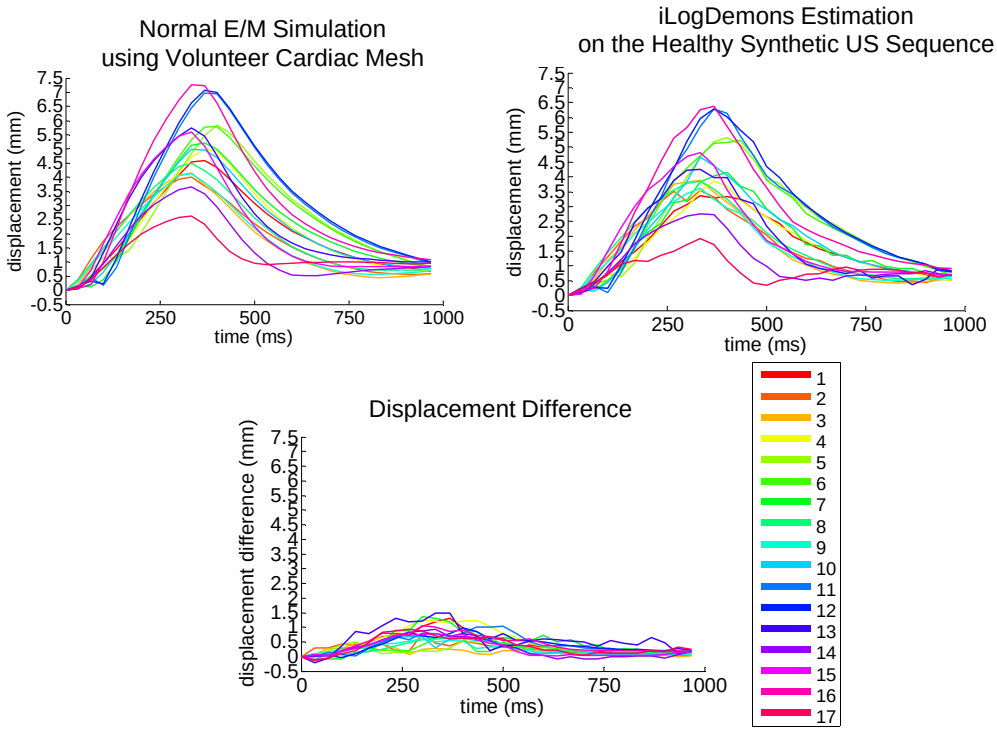

Figure 3.10: **Regional Motion Analysis on the E/M Simulation and the Synthetic US Sequence.** Motion descriptors were extracted from the simulated and from the estimated motion. The last column presents the motion descriptors difference. Different colors show different AHA segments.

estimated displacement field. We then extracted the norm of the displacement of each zone centroid (invariant to any rigid transformation): $\|u\| = \|Ab + B - b\|$, with b the initial position of the centroid. Fig. 3.10 shows the comparison of the kinematic descriptors extracted directly from the motion of the E/M simulation and the ones estimated by the iLogDemons from the synthetic sequence. Similar curves are observed. The calculated Root Mean Squared Error (RMSE) is 0.47 mm.

3.7 Database of Synthetic Sequences

We illustrate here another application of this method: it is possible to multiply the number of images of a small database of typical clinical images, by creating similar but slightly different cases around each original sequence. To achieve this, we used a simple model personalised to a given sequence, and varied the parameters around the personalised values to generate additional cases.

The clinical sequences we used included a healthy volunteer and a heart failure patient, with a Left Bundle Branch Block (LBBB). Therefore different simulation scenarios were performed, including normal and pathological cases. In LBBB, the

Original Image	Simulated Scenario	Clinical Decision
Healthy sequence	Healthy model	Healthy heart
Pathological sequence	Pathological model	Pathological heart
Healthy sequence	Pathological model	Pathological heart
Failing heart sequence	Normal activation pattern	Resynchronised heart

Table 3.2: **Clinical Evaluation.** Clinical diagnosis done on synthetic sequences generated from the given original clinical images and simulated scenarios.

left ventricle (LV) initial electrical activation was blocked (cf. Fig. 3.2). The normal and heart failure cases have also different global contractility (adimensioned) mechanical parameters namely the peak contractility of the E/M coupling σ_0 previously discussed in Sec. 3.2. The heart failure case peak contractility value is set to be lower than the normal case as failing hearts contract less. The global electrical conductivity parameter v (cf. Sec. 3.2), which is the conduction velocity (cm/s) of the electrophysiological model, is also set smaller in this failing heart.

We thus created a synthetic 4D US database containing the previous scenarios. Such database is useful for CRT where the 4D cardiac US is widely used to select the patients and evaluate the treatment. The normal simulation is used to create a healthy synthetic cardiac sequence, with controlled healthy electrical propagation and motion from the E/M simulation, using the volunteer clinical sequence. The LBBB simulation is used to create a pathological synthetic sequence from a pathological clinical sequence.

In order to test the limits of our approach, we also created a heart failure cardiac sequence with LBBB (cf. Fig. 3.6) from the clinical healthy volunteer sequence and a sequence with normal activation from the failing heart clinical image. A cardiologist performed a diagnostic evaluation on the generated synthetic US sequences (cf. Table. 3.2). The simulated conditions were correctly diagnosed in the four cases, the normally activated failing heart being interpreted as a resynchronised heart, which is expected to have the anatomy of a failing heart but a synchronous motion.

Such databases can be used to develop machine-learning approaches as was shown in [Prakosa 2011, Prakosa 2010] with a preliminary version of the approach described in this article.

3.8 Discussion

In this study, we used the information from an existing real image sequence and deformed it using a known displacement field in order to create a synthetic new one. As a result, both of them are similarly looking. However, possible artefacts might occur in the synthetic sequence due to several reason.

First, if the deformation of the original real clinical sequence is too large, the motion tracking may fail to entirely stabilize the clinical data. Therefore the final

motion still contains part of the original motion. As explained in Sec. 3.4, the estimated displacement field of the original sequence is used to construct the combined known displacement field. The variability in clinical image quality could also affect this motion tracking process since LogDemons registration method is based on the intensity of the image.

Second, if the simulated motion is too far from the patient motion, this large difference can warp the texture in an unrealistic way, as the original image has to be resampled with roughly the difference between the two motion fields. This is why the database has to be generated by varying the E/M parameters around the original patient motion.

Third, the resulting synthetic image will have similar quality to the real one. For the MRI case, since we resampled our MR images to be isotropic, the resulting synthetic sequence has similar smooth edge transition in the long axis direction as the real sequence.

Finally, the generation of synthetic 4D US sequences requires delicate interpolations between Polar and Cartesian coordinates, because the registration process is performed in the Cartesian coordinates, as well as the computation of the next steps. Ideally the process should be done in Polar coordinates and only the final data should be re-interpolated in Cartesian coordinates in order to respect the effect of the acquisition on the texture.

Another limitation is related to the heart shape which is related to the original image sequence. Therefore the applied motion must correspond to the condition of the observed heart to be realistic. For instance, if the original sequence is from a patient with a dilated cardiomyopathy, this will appear in the synthetic images, even if we use electromechanical parameters corresponding to a healthy heart. It is better to simulate a closer motion to the original sequence. However, this can still allow the production of a resynchronized heart sequence before remodelling for instance. This could serve in the therapy planning.

Concerning the motion at the heart boundary, continuity is enforced by the diffusion of the motion inside the myocardium. The formulation minimizes the gradient of displacement field in order to avoid deforming as much as possible the texture. Better boundary conditions next to surrounding structures could be used to improve the motion profile in these areas, for instance through a pericardium model. The atria are considered as the surrounding environment since the E/M model does not include them. At the frontiers of the atria, continuity is preserved using the displacement field diffusion method.

The developed software will be available at `http://team.inria.fr/asclepios/software/`. The registration algorithm will be integrated in the medInria software and the cardiac simulation will be available in the SOFA platform.

3.9 Conclusion

We developed a pipeline to create visually realistic synthetic 4D cardiac sequences using the deformation from an electromechanical model simulation. This pipeline combines the simulated myocardium displacement with the estimated myocardium displacement from the original clinical images. This combined displacement field is then used to warp the original images in order to create the synthetic cardiac sequence.

In this pipeline, we proposed a new approach based on Stationary Velocity Fields to combine the motions. We also proposed a new method of motion diffusion in order to maintain the continuity of the simulation and the real image with minimal texture distortion. Thanks to the detailed interplay between image processing and biophysical modeling, we can fully use a complete sequence in order to generate several new ones. This method also gives better realism compared to the traditional method, namely deforming an end-diastolic image, since the generated synthetic sequence will also contain the changes of the surrounding environment such as the motion of the mitral valve.

The new synthetic images are similar to the original ones except for the motion of the heart which is modified to follow the motion provided by a biophysical model. The parameters of the biophysical model can be modified to create variations around this motion. This pipeline has been tested to generate different synthetic sequences from different imaging modalities. It is generic and can be used with a different biophysical model or a different image registration algorithm, and it can be extended to other organs.

As these synthetic 4D cardiac sequences have kinematic ground truth information, those sequences represent in themselves a valuable resource to benchmark motion tracking methods or to train machine-learning algorithms.

Chapter 4

Cardiac Electrophysiological Activation Pattern Estimation from Images using a Patient-Specific Database of Synthetic Image Sequences

Contents

Based on: [Prakosa 2012b] A. Prakosa, M. Sermesant, P. Allain, N. Villain, C. A. Rinaldi, K. Rhode, R. Razavi, H. Delingette and N. Ayache. Cardiac Electrophysiological Activation Pattern Estimation from Images using a Patient-Specific Database of Synthetic Image Sequences. Biomedical Engineering, IEEE Transactions on, 2012. Note: Submitted.
The preliminary studies in the inverse-electro kinematic learning are described in the Appendix B and C. These works were published in [Prakosa 2010] (Appendix B)

and in [Prakosa 2011] (Appendix C)

While abnormal patterns of cardiac electrophysiological activation are at the origin of important cardiovascular diseases (e.g. arrhythmias, asynchrony), the only clinically available method to observe detailed left ventricular endocardial surface activation pattern is through invasive catheter mapping. However this electrophysiological activation controls the onset of the mechanical contraction, therefore important information about the electrophysiology could be deduced from the detailed observation of the resulting motion patterns. In this article, we present the study of this inverse cardiac electro-kinematic relationship. The objective is to predict the activation pattern knowing the cardiac motion from the analysis of cardiac image sequences. To achieve this, we propose to create a rich patient-specific database of synthetic time series of cardiac images using simulations of a personalised cardiac electromechanical model, in order to study this complex relationship between electrical activity and kinematic patterns in the context of this specific patient. We use this database to train a machine learning algorithm which estimates the depolarization times of each cardiac segment from global and regional kinematic descriptors based on displacements or strains and their derivatives. Experiments on the inverse electro-kinematic learning are demonstrated on synthetic sequences and are evaluated on clinical data with promising results.

4.1 Introduction

Since electrophysiological activation controls the onset of the mechanical contraction, important information about the electrophysiology could be gathered from the detailed observation of the resulting motion patterns. Abnormal patterns of this activation are at the origin of important cardiovascular diseases (e.g. arrhythmias, asynchrony). However, only catheter-based intracardiac electrical mappings are available to obtain such information, and these invasive procedures are not classically used for diagnosis but rather for planning and guiding a therapy. Electrocardiographic imaging[Ghanem 2005] (*a.k.a.* body surface potential mapping) is a non-invasive technique for imaging activation times of the myocardium but still remains to be validated thoroughly and is not widely available in clinical centres. Therefore there is a strong need to quantitatively assess a patient electrophysiological condition from non-invasive imaging modalities. Despite advances in both medical image analysis and intracardiac electrophysiological mapping technology, the understanding of the relationship between the cardiac electrophysiology and the cardiac motion visible in images is only partial. Since non-invasive cardiac imaging is readily available, unlike non-invasive detailed electrophysiology maps, it is important to investigate how the cardiac electrophysiology function can be estimated from the analysis of cardiac motion.

This is specifically relevant, for example, in the evaluation of the Cardiac Resynchronization Therapy (CRT) where the placement and tuning of pacemaker leads

play a crucial role in the outcome of the therapy. In this context, cardiologists need to interpret time series of cardiac images in order to detect and characterize kinematic patterns (motion asynchrony, delayed contraction) and then infer possible electrical conduction disorders. However, currently 30% of the patients with CRT show no benefit from this therapy [Helm 2007], which may be caused by the suboptimal implementation of the therapy. Providing activation maps from a time series of cardiac images would be of great interest to better select patients and to optimize the lead placements and delays during and after therapy. For instance, in a recent study, Sohal et al. [Sohal 2012] use time-volume curves of left ventricular segments to identify two classes of contraction patterns, which seem to be correlated with CRT response in patients with left bundle branch block (LBBB). More fundamentally, understanding the relationship between cardiac motion and electrophysiology is essential to improve the diagnosis and therapy of patients suffering from heart failure.

While there is an important literature on the estimation of the cardiac kinematics from cardiac sequences (see for instance [McLeod 2012, Tobon-Gomez 2012a, Mansi 2011, Elen 2008] and references therein), there exists no such tools to estimate the electrical wave propagation from such image sequences. However, the relationship between cardiac motion and electrical activation has been investigated in several studies [Prakosa 2011, Prakosa 2010, Otani 2010, Provost 2010, Sanchez-Ortiz 2004].

Electromechanical Wave Imaging (EWI) modality has been recently introduced to image the Electromechanical Wave (EW) which was shown to correlate with the myocardium electrical wave propagation [Provost 2010, Konofagou 2012]. In [Provost 2011], it was shown that the EW was able to be reproduced by an E/M model. This imaging modality uses high ultrasound frequency to map the small, transient deformation of the EW. However, this method is limited to this specific modality, which has only been demonstrated in 2D (whereas the propagation pattern is 3D) and is not often available clinically.

In this paper, we propose to study the inverse electro-kinematic relationship through the creation of a patient-specific database of synthetic time series of cardiac images based on our previous study in [Prakosa 2011]. Because it is difficult to obtain a large number of cases where both electrophysiological mapping and time series of 3D images are available, we use an electromechanical (E/M) model of the heart to produce synthetic but visually realistic image sequences for which the electrical stimulation is known using our method [Prakosa 2012c]. On this database, invariant kinematic descriptors were extracted from each synthetic sequence and then fed to a machine learning algorithm which estimates the electrical pattern from kinematic descriptors during the cardiac cycle. The creation of this database allows us to develop this machine learning based study. Recently, many medical image analysis studies are motivated by machine learning, for example in [Tobon-Gomez 2008] where a virtual population is created to train an active shape models. As the electro-kinematic relationship is very complex, we prefer here to generate a patient-specific database, so that the learning is done on cases relatively close to the patient condition.

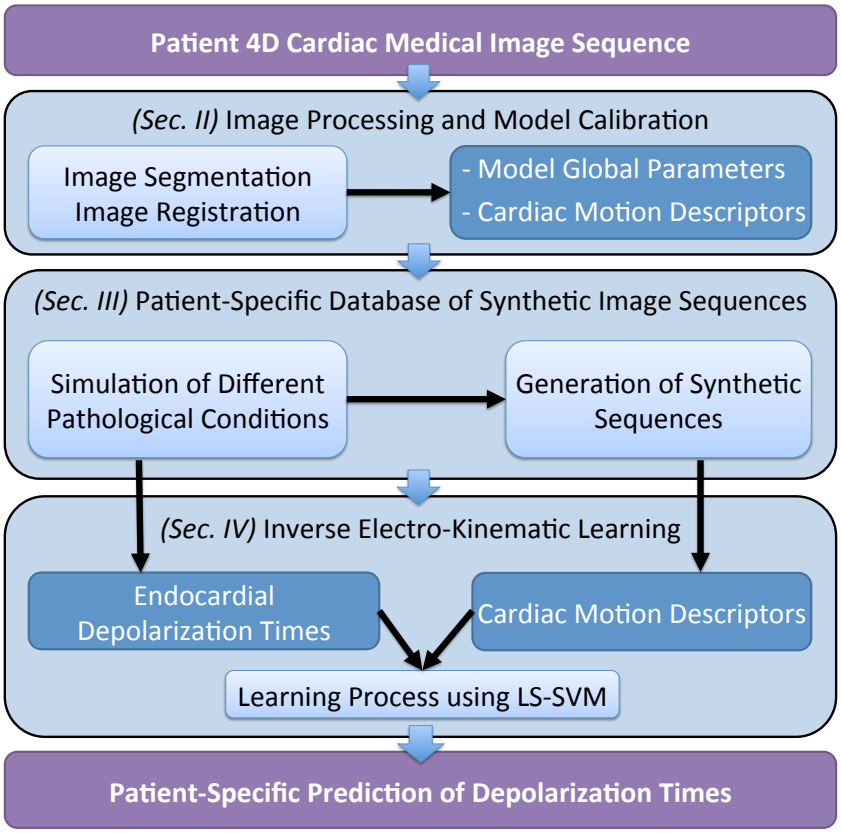

Figure 4.1: **Estimation of Electrophysiological Activation Pattern from Images.** A cardiac mesh is created from image segmentation. Different electromechanical conditions are simulated close to the patient condition to generate the database of electrophysiological patterns and synthetic cardiac sequences.The relationship between the motion descriptors and the activation patterns is learned from this database. The result is used to predict the patient electrophysiological activation pattern.

Previous works [Provost 2010, Sanchez-Ortiz 2004] have mainly focused in detecting E/M wave directly from the displacement and strain patterns estimated from image sequences during the contraction and relaxation of the myocardium. Since the relationship between those mechanical waves and electrical waves is very complex, our approach is to learn it through an E/M model of the heart at a larger spatial and temporal scale. In [Sanchez-Ortiz 2004] the cardiac motion descriptors are combined in order to obtain the electrical activation time, but the weights are assigned manually for the descriptors. Another study by McVeigh et al. [McVeigh 1998] considers only the circumferential strain estimated from tagged MR images as the mechanical activation measure. Another approach has been developed using a mathematical based computational technique to image the active stress from the displacement using an inverse model [Otani 2010]. This method was able to reconstruct travel-

ling plane wave of active stress from a mechanical deformation. The active stress was initially used to generate this deformation using a forward model. However, this method would still need to be evaluated in clinical application. Compared to [Prakosa 2010], instead of estimating displacements and strains directly from the E/M model, we propose a more realistic estimation by first simulating 3D images and then using an image-based motion tracking algorithm. Furthermore, rather than learning the activation forces over time, we have chosen to learn the depolarization times of all American Heart Association (AHA) segments. Finally, our learning approach is optimized in order to detect which kinematic descriptor is most correlated with the electrophysiology waves.

The overall approach is described in Fig. 4.1 and mainly consists in three stages. First, right and left ventricles are segmented from an input cardiac image sequence and the cardiac motion is tracked. An electromechanical model of the heart is mechanically calibrated from this data. In a second stage, a training set, *a.k.a* patient-specific database, is created from this E/M model by changing electrophysiological parameters related to different pathological conditions. For each set of electrophysiology parameters, a different cardiac motion is simulated and a realistic synthetic image sequence is created. In the third stage, motion descriptors are estimated from each sequence. A learning method is then trained to relate those descriptors with the endocardial depolarization times. Finally, the depolarization times of the original sequence are estimated from the knowledge of its motion descriptors. Evaluation of the inverse electro-kinematic learning process on three patients is discussed in Sec. 4.5.

4.2 Image Processing and Parameter Calibration

4.2.1 Image Segmentation and Registration

First we need to apply two image processing steps to the patient clinical image sequence. These steps are the segmentation of the end diastolic (ED) myocardium and the estimation of the myocardium motion. The purpose of the segmentation is to personalize the cardiac mesh geometry required for the cardiac E/M simulation. Furthermore, the estimation of patient cardiac motion allows us to also estimate the patient's endocardial left ventricle (LV) volume curve. Using this information, The E/M simulation can be calibrated with respect to this volume curve so that the simulated ejection fraction as well as the ejection and filling rates are similar to the measured ones [Marchesseau 2012a].

The 3D epicardium and endocardium of the left and the right ventricles of the ED clinical image were delineated using an interactive tool available within the CardioViz3D software [Toussaint 2008]. These delineations were then used to create the myocardium segmentation. Using CGAL software [Rineau 2009], a computational tetrahedral mesh was created from the binary mask of the compact myocardium segmentation (cf. Fig. 4.2). We label the different tetrahedra of the mesh in order to set different electrical conduction parameters for each labelled region (Sec. 4.3.1).

The labels include the scar, the Purkinje network (the tetrahedra next to the endocardial surface), the scarred Purkinje network (the intersection of the scar and the Purkinje network) and the cardiac muscle (the remaining tetrahedra). To create bull-eyes plot, we also label the left ventricle according to the 17 AHA segments.

Applying a non-linear registration to pairs of medical images is a common method to estimate the motion of the tissue in the image. Here we use the symmetric log-domain diffeomorphic demons (LogDemons) [Vercauteren 2008] non-rigid registration method to align the template image $T_i(\mathbf{x})$ to a reference image $R(\mathbf{x})$, which is the ED image of the clinical sequence, by estimating a dense non-linear transformation $\phi_i(\mathbf{x})$, where $\mathbf{x} \in \mathbb{R}^3$ is the space coordinate. $T_i(\mathbf{x})$ is the image at each time frame i in the cardiac sequence. This transformation $\phi_i(\mathbf{x})$ is associated with the displacement vector field $u_i(\mathbf{x})$ and is parameterised by the stationary velocity field $v_i(\mathbf{x})$ which ensures the invertibility of the deformation since we are working in the log-domain. By having this estimated displacement field, we are also able to estimate the patient's endocardial LV volume curve in time. We deformed the ED tetrahedral mesh using the estimated displacement field $u_i(\mathbf{x})$ and then computed the endocardial LV volume of the deformed mesh in time.

4.2.2 Electromechanical Model Calibration

We used the Eikonal model to simulate the electrophysiological activation patterns. This model has the advantage to be fast to compute and involves few parameters. More detailed models[Ten Tusscher 2004, Mitchell 2003] could also have been used however such additional level of complexity is not necessary since we are only interested in providing main patterns of conduction driven by few parameters. The Eikonal equation $v\sqrt{\nabla T_d^t D \nabla T_d} = 1$ was solved using Multi-Front Fast Marching Method [Sermesant 2007] to calculate the depolarization time T_d at each point of the mesh. v is the local conduction velocity and $D = (1-r)f \otimes f + r.I$ is the anisotropic conductivity tensor where f is the fibre orientation, r is the conductivity anisotropy ratio and I is the identity matrix.

We base our approach on the Bestel-Clément-Sorine (BCS) E/M model [Chapelle 2012] composed of a passive non linear elastic part and an active part that describes the binding and unbinding process of the actin and myosin filaments in the sarcomere by a differential equation that controls the active stress τ_c and the sarcomere stiffness k_c:

$$\begin{cases} \dot{k_c} = -(\mid u \mid + \alpha \mid \dot{e_c} \mid)k_c + n_0 k_0 \mid u \mid_+ \\ \dot{\tau_c} = -(\mid u \mid + \alpha \mid \dot{e_c} \mid)\tau_c + \dot{e_c} k_c + n_0 \sigma_0 \mid u \mid_+ \end{cases} \tag{4.1}$$

where α is a constant related to the cross-bridge release due to a high contraction rate, k_0 and σ_0 are respectively the maximum stiffness and contraction. n_0 is a reduction factor that allows to take into account *the Starling effect* by which the maximum contraction depends on the fibre strain e_c. The control variable u is derived from the electrical activation model and is a function of the free calcium concentration only. It is modeled using electrophysiological inputs such as

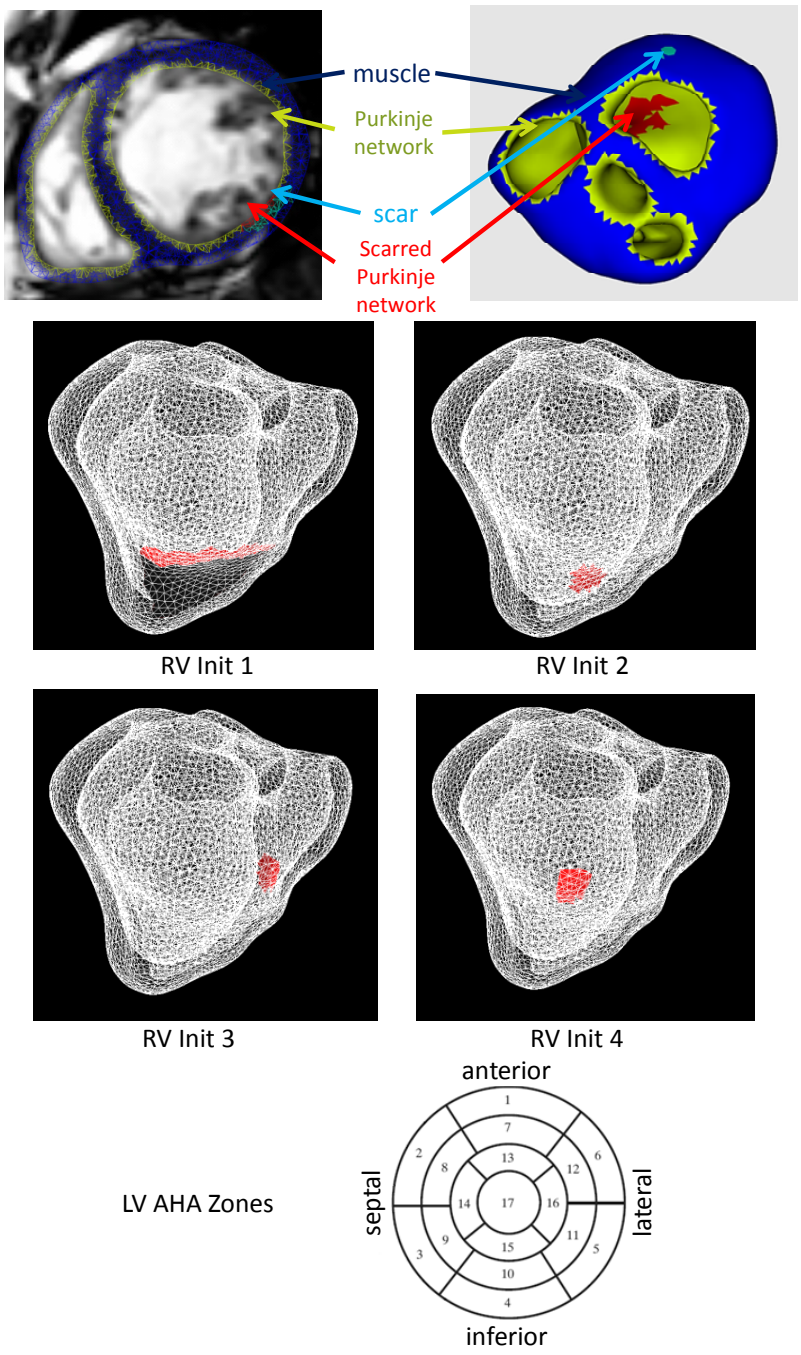

Figure 4.2: **Cardiac Geometry and Electrical Stimulation.** A personalized cardiac mesh is created from the myocardium delineation of the clinical image. The region on the surface of the LV and RV endocardium is set to have higher electrical conduction velocity to simulate the Purkinje network. Different RV initial electrical activation position is set to simulate the extremities of the Bundle of His. These positions are approximately set based on the septal LV AHA Zones.

depolarization times (T_d) and action potential durations (APD). The four-element Windkessel model is used to model the arterial pressure [Marchesseau 2012a].

The BCS E/M model was implemented in the SOFA simulation platform [Faure 2012] and to assess the mechanical parameters of the model, we used the algorithm derived from the Unscented Transform [Julier 1997], and described in [Marchesseau 2012a, Marchesseau 2012b]. The algorithm finds a set of parameters that enable the simulation to match observations on the endocardial LV volume (the minimum volume, the minimum and maximum of the flow) in one iteration through the analysis of the covariance matrix between the simulated observations and the variation of each parameter independently. The assessed calibrated parameters of the BCS E/M model are σ_0, K, μ, APD and Rp. K is the Bulk modulus of the passive part and μ is the viscosity parameter of the active part. APD is the cell excitation duration. Rp is the peripheral resistance, one of the Windkessel parameters.

4.3 Patient-Specific Database of Synthetic Image Sequences

A database of visually realistic synthetic cardiac sequences is created using the method proposed in [Prakosa 2012c]. This database is required to train the machine learning algorithm. This synthetic sequence generation method consists in the combination of the simulated motion and the real motion estimated from the patient image sequence. The database is built using different scenarios which are performed to simulate a variety of conditions close to clinical condition of this patient. Since these datasets are taken from patients with a left bundle branch block (LBBB), the scenarios consist of different variations of electrophysiological and mechanical parameters that simulate this specific pathology.

4.3.1 Simulated Electromechanical Conditions

Electrical Onset Position	Conduction Velocities in cm/s of: Muscle v_m	Purkinje v_p	Scar v_s	Scarred Purkinje v_{sp}
1-2-3-4	40-50-80-110	160-240-350	5-10-20	120

Table 4.1: **Patient-Specific Database of 144 Simulated Cases.** We varied the initial electrical activation position of the LBBB and the conduction velocities of the different components of the electrophysiological model.

An electrophysiological activation pattern which corresponds to each scenario is generated using the Eikonal model in the personalized cardiac mesh geometry. The scenarios are created based on a variation of the parameters of the Eikonal model around the standard values. The varying parameters are the conduction velocity

value of the Purkinje network v_p, the value in the cardiac muscle v_m, and also the initial electrical activation position which simulates the extremities of the Bundle of His. For datasets containing a scar region, a variation of the conduction velocity value for this region v_s and also a value of the scarred Purkinje network v_{sp} are also included in the scenarios (cf. Table 4.1 and Fig. 4.2).

For datasets that do not contain a scar region, we set a low conduction velocity in the anterior lateral region (zone 6, 12, and 16 of the AHA segments) or in the inferior lateral region (zone 5, 11, and 16 of the AHA segments) in order to mimic the occurrence of a functional block in those regions (cf. Table 4.2). The overall conduction velocities are also set lower compared to Table 4.1.

Electrical Onset Position	Conduction Velocities in cm/s of: Muscle v_m	Purkinje v_p	Block v_b	Blocked Purkinje v_{bp}
1-2-3-4	30-50-80	130-210-320	none- 30 (Anterior)- 30 (Posterior)	none- 30-90 (Anterior)- 30-90 (Posterior)

Table 4.2: **Patient-Specific Database of 180 Simulated Cases.** Additional configurations with low conduction velocity in the anterior lateral region or in the inferior lateral region are added to mimic the functional block.

4.3.2 Generation of Synthetic Image Sequences

Visually realistic synthetic time series of MR images were created using the previously simulated deformation which was combined to the real clinical sequence estimated displacement using the method proposed in [Prakosa 2012c]. This method applied non-rigid registration algorithm to extract the motion of the real clinical MRI sequence. This extracted motion was then combined with the E/M simulated motion in the log domain and then used to warp the original images in order to create the synthetic cardiac sequence. With this method, a database of realistic images of the patient was generated for which the underlying cardiac motion and electrophysiological parameters are known. This database served as the training set in our machine learning based study. For each different initial electrical activation position (RV Init 1, 2, 3 and 4) (cf. Fig. 4.2, Table 4.1 and Table 4.2), a mechanical calibration is performed as described in section 4.2.2. Therefore, the variation of the mechanical parameters were included as well in the database.

With the method described previously, a large database of synthetic 3D MR images was created. We then tracked the cardiac motion from those synthetic images by using the symmetric log-domain diffeomorphic demons (LogDemons) registration algorithm [Vercauteren 2008]. More precisely, we registered all the images of the synthetic sequence to its reference ED image as we did to the real clinical sequence.

4.4 Inverse Electro-Kinematic Learning

4.4.1 Cardiac Motion Descriptors

As an input to a machine learning algorithm, we needed to first extract kinematic descriptors which describe in a compact and discriminative way the cardiac motion for each time point in the cardiac cycle. We wanted these descriptors to be regional, as we aim for an activation pattern rather than local activation times, and also intrinsic (frame invariant) as the orientation of the heart in the images varies.

To this end, we first characterized the motion of each AHA segment by fitting in the least-squares sense an affine transformation $f(p) = Ap + B$ to the LogDemons estimated displacement field. The strain tensor E was then computed from the affine matrix A as: $E = (A^T A - I)/2$

We then extracted kinematic descriptors at each time of the cardiac cycle that are invariant to any change of reference frame (or rigid transformation). For the strain matrix E, the three Euclidean invariants are computed as:

$$x_1 = \text{trace}(E),\ x_2 = \text{trace}(E^2),\ x_3 = \det(E)$$

For the displacement vector, we only extracted its norm as invariant:

$$x_4 = \|u\| = \|Ab + B - b\|,$$

where $\|u\|$ is the displacement norm of the zone centroid with b the initial position of the centroid. We also used the strain in the direction of displacement as the invariant:

$$x_5 = (u^T E u)/(2\|u\|^2)$$

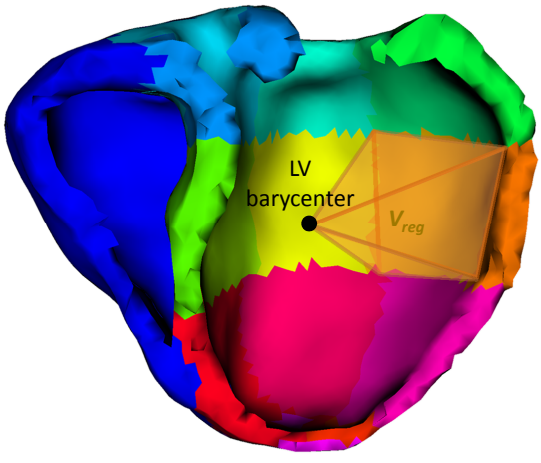

Figure 4.3: **Regional LV Volume.** The V_{reg} is the volume of the region created by the LV AHA segment surface and the LV barycenter.

Compared to our previous study [Prakosa 2011], we added here more descriptors which are usually found in clinical records. We added the QRS duration $x_6 = t_{QRS}$

which is the time needed for the whole myocardium to be activated. We also added the LV volume curve $x_7 = V$ and the regional LV volume curve $x_8 = V_{reg}$ computed for each AHA segment. More precisely, we divided the LV endocardial surface according to the AHA segment surfaces and then computed the volume of the region created by each displaced segment surface and the barycenter of the LV (cf. Fig. 4.3).

Furthermore, in order to learn the influence of the dynamics of some descriptors, we added the derivative of the trace of the strain tensor, of the displacement, and of the global and regional volume curves:

$$x_9 = d\,\mathrm{trace}(E)/dt,\ x_{10} = d\|u\|/dt,$$

$$x_{11} = dV/dt, x_{12} = dV_{reg}/dt$$

These descriptors, except for the volume curve x_7, its derivative x_{11} and the QRS duration x_6, are evaluated regionally for the 17 AHA zones during the n time instances. The value n depends on the temporal resolution of the original clinical sequence, n = number of frames $-$ 1. The volume curve x_7 and its derivative x_{11} are vectors with length of n and the QRS duration x_6 is a single scalar value.

The difficulty in using a simulated database for machine-learning is that there are limitations in both the electromechanical model used to simulate the motion and the image processing methods used to extract the descriptors. Therefore there can be discrepancies between the descriptors used in the learning phase compared to the descriptors extracted from the real images.

In order to cope with this, and also because we are more interested in the relative dynamics of these descriptors which is related to the activation pattern than in their absolute values, we normalized each descriptor. This normalization was done regionally for the descriptors taken from the 17 AHA regions. With this normalization, each descriptor has a range of values from 0 to 1, as we use the relationship $x = (x - x_{min})/(x_{max} - x_{min})$, where x_{max} and x_{min} are the maximum and the minimum values of x respectively. .

These 12 descriptors (cf. Table. 4.3) were used to create a kinematic descriptor vector $\mathbf{x} = (x_i)_{i\in[1,12]} \in \mathbb{R}^d$ for each simulation with

$$\begin{aligned} d &= 9(\mathrm{Descriptors}_{1,2,3,4,5,8,9,10,12}) \times n(\mathrm{Times}) \times 17(\mathrm{Zones}) \\ &\quad + 2(\mathrm{Descriptors}_{7,11}) \times n(\mathrm{Times}) \\ &\quad + 1(\mathrm{Descriptors}_{6}) \\ &= 155n + 1 \end{aligned}$$

For a cardiac image sequence with 30 images, the dimension d of the complete vectorial kinematic descriptor is:

$d = 155 \times (30 - 1) + 1 = 4496$.

4.4.2 Machine Learning Method

In the inverse electro-kinematic learning process, the non-linear relationship between the kinematic descriptors and the electrical propagation was estimated based

Number	Descriptor	Vector Size
x_1	trace(E)	17×n
x_2	trace(E^2)	17×n
x_3	det(E)	17×n
x_4	$\|u\|$	17×n
x_5	$(u^T E u)/(2\|u\|^2)$	17×n
x_6	t_{QRS}	1
x_7	V	n
x_8	V_{reg}	17×n
x_9	dx_1/dt	17×n
x_{10}	dx_4/dt	17×n
x_{11}	dx_7/dt	n
x_{12}	dx_8/dt	17×n

Table 4.3: **List of the Descriptors.** The descriptors are extracted from the estimated cardiac motion, their temporal derivation and also the QRS duration. n = the number of frames in a cardiac cycle - 1.

on a training set extracted from the synthetic database. To represent the cardiac electrophysiology, we considered the activation time when the electrical potential starts to depolarize at a point of the myocardium. The activation time was averaged for all points of the LV endocardial surface in each AHA segment. Therefore, the vector characterizing electrophysiology for each simulation is $\mathbf{y} = (y_i) \in \mathbb{R}^{\mathrm{r}=17\ (\text{AHA Zones})} = log(\text{Activation Times})$.

We modeled the non-linear relationship using Least-Square Support Vector Machine (LS-SVM) for regression [Cawley 2006] which is similar to the Kernel Ridge Regression (KRR).

LS-SVM extends the KRR method by adding a bias term. KRR itself is the non-linear extension of Ridge Regression (RR) which searches a linear function $\mathbf{y} = \mathbf{w}^T\mathbf{x}$ that models the dependencies between the descriptor vectors $\mathbf{x} = \mathbf{x}_i \in \mathbb{R}^d$ and response vectors $\mathbf{y} = \mathrm{y}_i \in \mathbb{R}^r$ (all vectors are column vectors) from a set of N examples $(\mathrm{x}_1, \mathrm{y}_1), (\mathrm{x}_2, \mathrm{y}_2), ..., (\mathrm{x}_N, \mathrm{y}_N)$. Classically, we need to minimize the quadratic cost

$$C(\mathrm{w}) = (1/2)\sum_{i}^{N}(\mathrm{y}_i - \mathrm{w}^T\mathrm{x}_i)^2, \tag{4.2}$$

where w is a $d \times r$ matrix. Regularizing this equation, the total cost function which

needs to be minimized hence becomes

$$C(\mathrm{w}) = (1/2)\sum_{i}^{N}(\mathrm{y}_i - \mathrm{w}^T\mathrm{x}_i)^2 + (1/2)\lambda\left\|\mathrm{w}\right\|^2, \tag{4.3}$$

where $\lambda > 0$ is the regularization parameter. Introducing a $N \times d$ matrix $X = (\mathrm{x}_1, \mathrm{x}_2, ..., \mathrm{x}_N)^T$ and a $N \times r$ matrix $Y = (\mathrm{y}_1, \mathrm{y}_2, ..., \mathrm{y}_N)^T$, the equation can be written as

$$C(\mathrm{w}) = (1/2)\left\|Y - X\mathrm{w}\right\|^2 + (1/2)\lambda\left\|\mathrm{w}\right\|^2. \tag{4.4}$$

Minimizing this function by taking its derivative with respect to w and equating it to zero gives $-X^TY + X^TX\mathrm{w} + \lambda\mathrm{w} = 0 \Rightarrow \mathrm{w} = \left(\lambda\mathrm{I} + X^TX\right)^{-1}X^TY$.

Ridge Regression can be extended to Kernel Ridge Regression by rewriting the solution

$$\begin{aligned}\mathrm{y} &= \mathrm{w}^T\mathrm{x} \\ &= \left(\left(\lambda\mathrm{I} + X^TX\right)^{-1}X^TY\right)^T\mathrm{x} \\ &= Y^T\left(\lambda\mathrm{I} + XX^T\right)^{-1}X\mathrm{x} \\ &= Y^T\left(\lambda\mathrm{I} + K\right)^{-1}\mathrm{k}\end{aligned} \tag{4.5}$$

with $K = XX^T$ and $\mathrm{k} = X\mathrm{x}$. In this form, other type of Kernel function can be used to substitute the linear Kernel function $K = K(\mathrm{x}_i, \mathrm{x}_j) = \mathrm{x}_i^T\mathrm{x}_j$

We modelled the non-linear relationship using Kernel Ridge Regression with a bias term or Least-Square Support Vector Machine (LS-SVM) for regression

$$\mathrm{y} = f(\mathrm{x}) = A\mathrm{k}(\mathrm{x}_i, \mathrm{x}) + \mathrm{b} \tag{4.6}$$

with matrix A is computed as $A = Y^T\left(\lambda\mathrm{I} + K\right)^{-1}$ and $\mathrm{k}(\mathrm{x}_i, \mathrm{x})$ is a kernel vector. We chose the Radial Basis Function (RBF) $K(\mathrm{x}_i, \mathrm{x}_j) = \sum_{k=1}^{D} e^{-z_k}$ as the Kernel function where $z_k = \left(\left|\mathrm{x}_i^k - \mathrm{x}_j^k\right| / (\sigma_k\alpha_k)\right)^2$, $i, j = \{1, ..., N\}$ and $D = 12$ is the number of descriptors. In this kernel function, σ_k is the standard deviation of each descriptor and α_k is a dimensionless coefficient which weights the importance of each descriptor in the learning process, where $\sigma_k^2 = (1/N)\sum_{i=1}^{N}\left\|\mathrm{x}_i^k - \mu\right\|^2$ and $\mu = (1/N)\sum_{i=1}^{N}\mathrm{x}_i^k$.

4.4.3 Parameter Optimization

The chosen λ and α parameters are optimized by using leave-one-out estimates which train the model with all members of the training set but one and test the performance on the singleton. The process is repeated for all the singletons in the training set. We use Allen's PRESS (Predicted Residual Sum of Squares) criterion for the optimization of the λ and α parameters $PRESS = \sum_i^N \mathrm{e}_{(i)}^2$ [Cawley 2006] where $\mathrm{e}_{(i)} = \mathrm{y}_i - \hat{\mathrm{y}}_{(i)}$ is the residual for the ith example with the ith example excluded from the training process and $\hat{\mathrm{y}}_{(i)}$ is the predicted response for the ith example based

on the training process. Fortunately, we have $e_{(i)} = e_i/(1-h_{ii})$ where $e_i = \mathrm{y}_i - \hat{\mathrm{y}}_i$ is the residual for the ith example in the training process which includes all examples and $\hat{\mathrm{y}}_i$ is fitted response based on this training. h_{ii} is the ith element of the leading diagonal of the hat matrix $H = X(\lambda \mathrm{I} + X^T X)^{-1} X^T = XX^T(\lambda \mathrm{I} + XX^T = K(\lambda \mathrm{I} + K)^{-1}$. Therefore, in the end, we can have the PRESS for the chosen parameters λ and α in one iteration without having to do N iterations for the leave-one-out cross validation. We use the Powell's BOBYQA [Powell 2009, Johnson 2012] method to optimize these parameters to have the smallest PRESS.

4.5 Results

4.5.1 Activation Pattern Validation on Synthetic Data

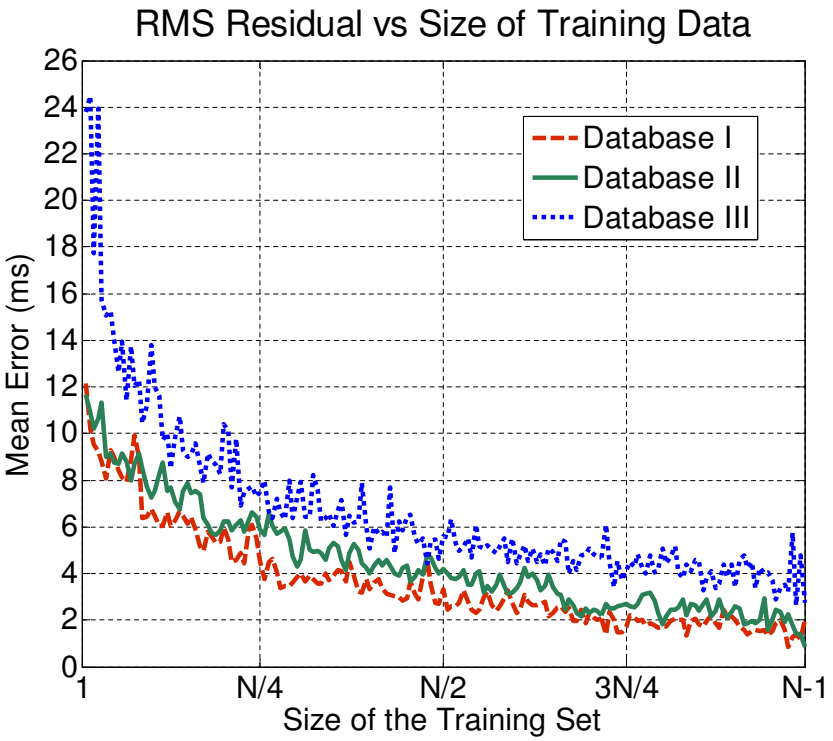

Figure 4.4: **RMS Residual vs Size of Training Data.** Less than 8 ms RMS residual is obtained by using more than 13, 18 and 44 training cases for the Database I, II and III respectively. The Database I, II, and III are the patient-specific databases for patient I, II and III respectively described in Sec. 4.5.2. This means that a good generalization is obtained by using less than 25% of the whole dataset.

First, we evaluated the learning process on the generated synthetic data and estimated the minimum size of the training set to have a small regression error for the remaining entries of the database. Fig. 4.4 shows a good generalization with a root mean square (RMS) error of less than 8 ms of residual by using at least 13, 18

and 44 training datasets for the Database I, II and III respectively. The Database I, II, and III are the patient-specific databases for patient I, II and III respectively described in Sec. 4.5.2. These numbers are less than 25% of the size of datasets of each database.

4.5.2 Activation Pattern Evaluation on Clinical Data

We applied our proposed approach on three clinical cases from patients with different pathologies and etiologies or causes of diseases. However, in all three of them there was a modified activation pattern due to scars or functional blocks, as well as poor ejection fraction, which are the characteristics of the patient groups we are aiming at.

The first patient was a 60 years old woman with heart failure and NYHA class III symptoms. She had subendocardial postero-lateral scar in the left ventricle. Her left ventricular ejection fraction was 25% on maximal tolerated heart failure medication. The surface ECG demonstrated significant conduction disease with left bundle branch block (LBBB) QRS duration of 154 ms (normal QRS is less than 120 ms). Echocardiography, including Tissue Doppler, confirmed significant mechanical dysynchrony in keeping with the ECG findings.

The second patient was a 72 years old male patient with ischemic heart disease. He had a myocardial infarction in the infero-lateral wall. His left ventricular ejection fraction was 35% with the QRS duration of 99 ms.

The third patient was a seventy-seven year old woman with a much more developed dilated cardiomyopathy. She was in NYHA class III heart failure with a LV ejection fraction of 18% and left bundle branch block QRS duration of 200 ms. There was no late gadolinium enhancement images acquired but functional conduction block was observed in the electrophysiological mapping.

For all the cases, the clinical data used to set up the patient-specific models consisted of a cine-MRI for the estimation of ventricular motion and late enhancement images with gadolinium contrast agent for scar anatomy (in case of scars), acquired on an Achieva MR Philips Medical System scanner. A non-contact mapping study was performed using the Ensite 3000 multi-electrode array catheter system (St Jude, Sylmar, CA). The array records intracavity far-field potentials that are sampled at 1.2 kHz and digitally filtered at 0.1-300 Hz. The resulting signals allow the reconstruction of over 3000 virtual unipolar electrograms superimposed on a model of the left ventricle created using a locator signal on a roving endocardial catheter. The XMR fusion provided the location of the Ensite mapping with respect to the MR-derived information.

For each patient, a database of synthetic sequences which contains the scenarios described in Sec. 4.3.1 was built. For the first patient, the total generated synthetic 3D MR images are 144 (scenarios) $\times$ 29 (number of frame -1) = 4176.

We did a first evaluation of this learning process on the clinical 3D MR sequence of the patients. Using the relationship or the optimized parameters previously found, we are able to predict the LV endocardial electrical activation time of the patient.

We apply the same processing to this sequence as we did for the synthetic sequence.

After optimizing the PRESS criterion on the whole synthetic database of each patient, the obtained LS-SVM parameters are shown in Table. 4.4. We listed the descriptors with their $(\alpha_{max} - \alpha_i)/(\alpha_{max} - \alpha_{min})$ value which describes the increasing importance of the descriptor i (cf. Table. 4.4). α_{max} and α_{min} are respectively the maximum and minimum α value of the descriptors for a patient database. Therefore the value range is from 0 for the least important descriptor to 1 for the most important one. Table. 4.4 shows that the kinematic descriptors $x_1 = \text{trace}(E)$ and $x_5 = (u^T E u)/(2\|u\|^2)$ are consistently the most important ones to learn the electro-kinematic relationship from the three databases since they have smaller optimized α_i values compared to the other descriptors.

Descriptor	$\frac{\alpha_{max}-\alpha_i}{\alpha_{max}-\alpha_{min}}$		
	Patient 1	Patient 2	Patient 3
trace(E)	1.000	0.522	0.514
trace(E^2)	0.541	0.431	0.446
det(E)	0.506	0.000	0.464
$\|u\|$	0.428	0.823	1.000
$\frac{1}{2\|u\|^2}(u^T E u)$	0.659	1.000	0.998
t_{QRS}	0.000	0.167	0.040
V	0.046	0.227	0.097
V_{reg}	0.103	0.203	0.053
$\frac{d\,\text{trace}(E)}{dt}$	0.367	0.189	0.171
$\frac{d\,\|u\|}{dt}$	0.597	0.282	0.078
$\frac{d\,V}{dt}$	0.239	0.520	0.232
$\frac{d\,V_{reg}}{dt}$	0.218	0.279	0.000
α_{min}	1.038	1.690	0.985
α_{max}	2.263	2.282	2.583

Table 4.4: **Rank of the Optimized LS-SVM Parameters.** The value of the parameters $(\alpha_{max} - \alpha_i)/(\alpha_{max} - \alpha_{min})$ after optimizing the PRESS criterion gives the importance of each descriptor.

After performing LogDemons non-rigid registration and extracting the vector $\mathbf{x}$ of kinematic descriptors from the estimated displacement field, the electrophysiology vector $\mathbf{y}$ was estimated from the LS-SVM. Since we have the ground truth LV endocardial electrical activation time of the patient acquired using non-contact mapping study, we are able to compare our prediction with this measurement. Similar estimated depolarization times were obtained for this patient (cf. Fig. 4.5) with the root mean square error RMSE = 11.20 ms for the patient I, 13.51 ms for the patient II and 22.42 ms for the patient III.

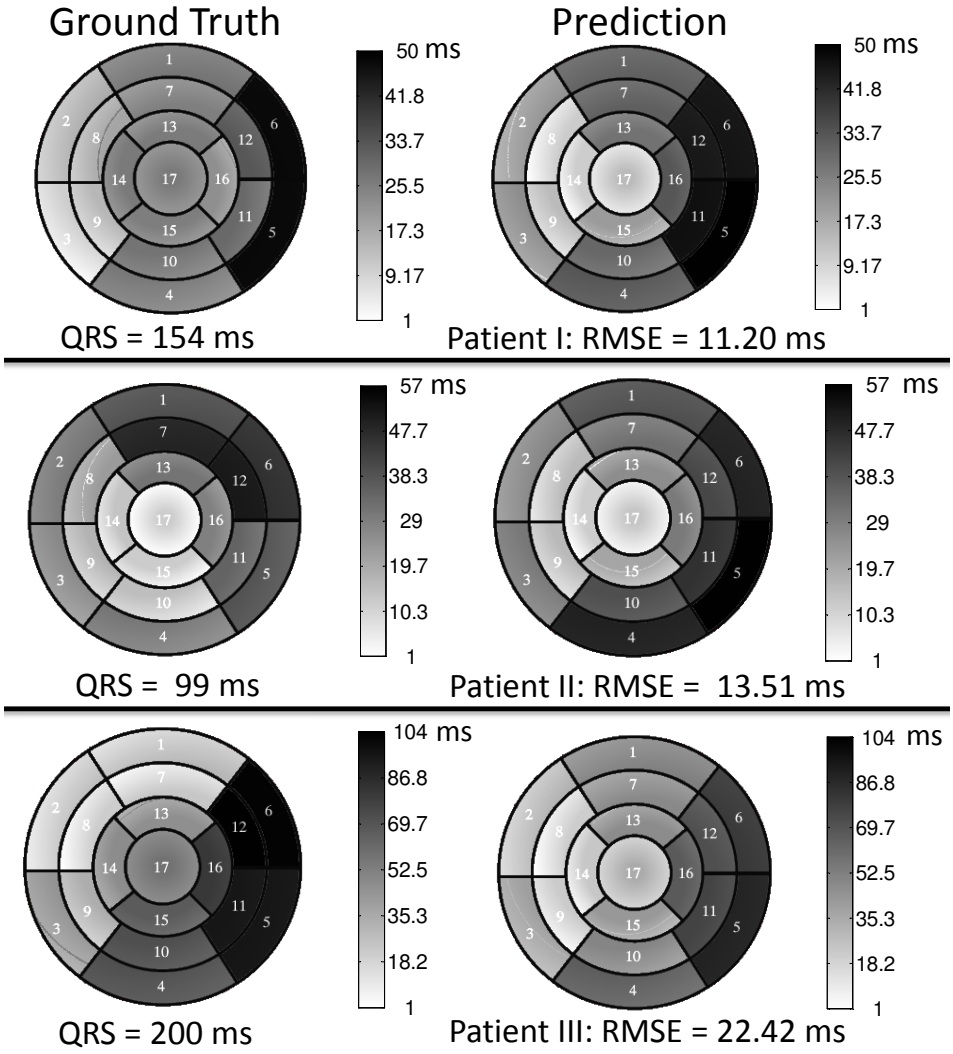

Figure 4.5: **Depolarization Time Estimation from Clinical 3D MR Sequences.** First evaluation of the learning process in the prediction of the LV surface depolarization time on a patient (right) is compared to the ground truth value (left). Similar patterns in the same range are observed on the three of them.

We computed the mean and variance of the electrophysiological database created

previously with the patient's LV endocardial electrical activation time ground truth value. Then, we were able to compare our prediction with these values (cf. Fig. 4.6).

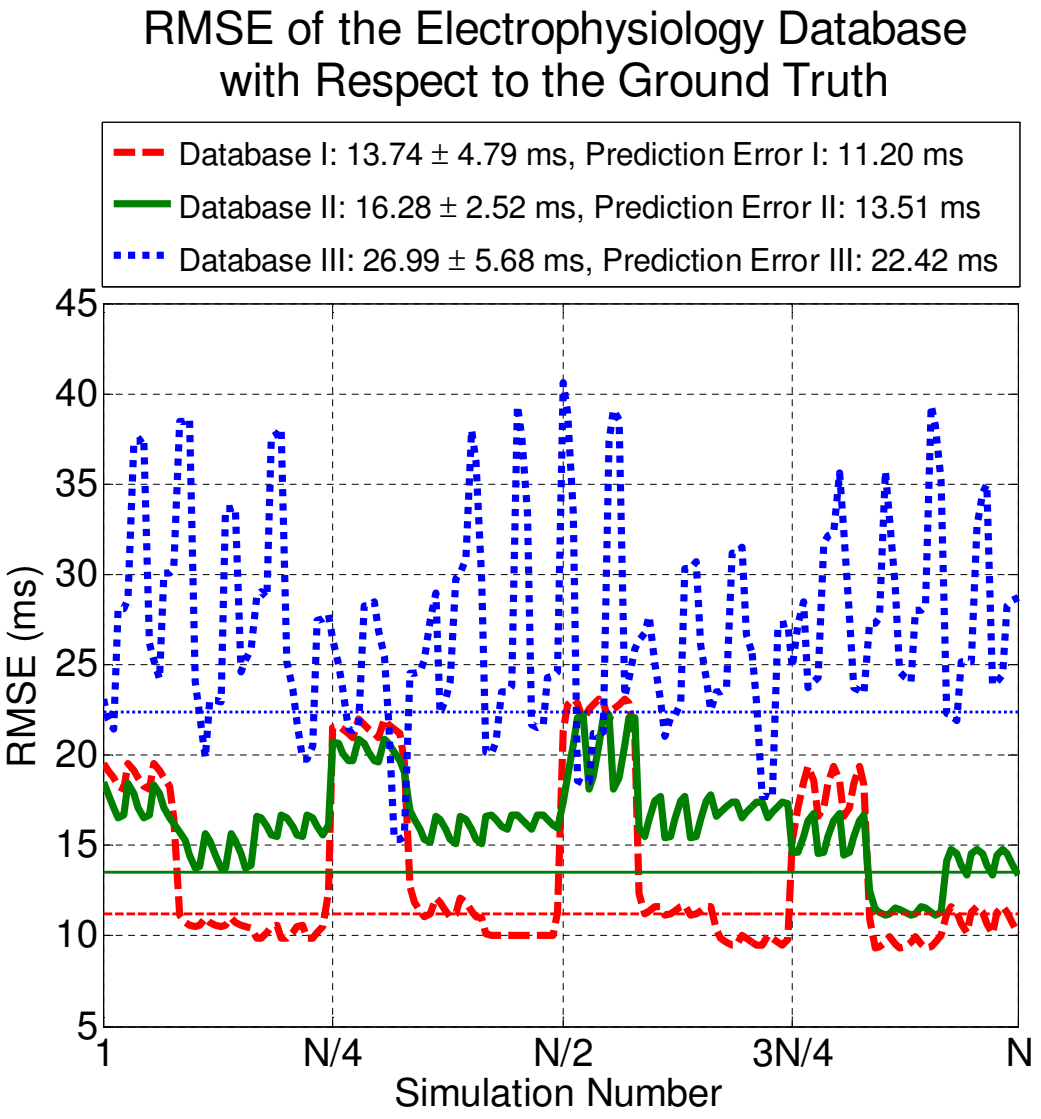

Figure 4.6: **Distance (RMSE) of Each Simulated Electrophysiology with respect to the Patient's Ground Truth.** For each patient's database of simulated electrophysiological patterns, the difference of each pattern with the patient's electrophysiological pattern ground truth is calculated. These differences are shown in a curve which describes the variation of the simulated electrophysiology. The mean and standard deviation of each patient are shown in the legend. The prediction errors in Fig. 4.5 are shown as horizontal lines with the values shown in the legend.

4.6 Discussion

In this study, we created patient-specific database of synthetic sequences in order to learn the cardiac inverse electro-kinematic relationship. In the end, we used the learned relationship to estimate patient's left ventricle endocardium electrical activation time. For each dataset, the prediction error (cf. Fig. 4.5) is in the order of 15 ms which represents typically between 7% and 14% of the QRS duration. This is reasonable given the spatial and temporal accuracy of the invasive intra-cardiac mapping systems and even more compared to the accuracy of non-invasive ECGI systems.

The prediction error is also smaller compared to the average error in the database. Patient I: 11.20 ms $<$ 13.74 ms, Patient II: 13.51 ms $<$ 16.28 ms, Patient III: 22.42 ms $<$ 26.99 ms. This shows the proper behavior of the LS-SVM method since it basically consists in interpolating the depolarization times of the entries in the learning set that are closest to the input kinematics descriptors.

With this learning process, the prediction error combines several types of possible errors: noise in the non-contact mapping acquisition, errors in the learning process, errors in modeling the cardiac electromechanics and discretization errors. Due to the non-contact nature of the mapping, it is often difficult to have an accurate match between the electrophysiology maps and the endocardial surface reconstructed from MR imaging. For example for Patient II, there is an uncertainty in the ground truth data since the latest activated area is not in the region where the scar is. Applying 30° of clockwise rotation to the ground truth data would make the scarred region last activated and reduce the prediction error from 13.51 ms to 8.73 ms. The learning error mostly depends on the size of the electrophysiology scenarios as they should be vast enough to include the actual pathology of the patient. In this paper, we have restricted ourselves to LBBB cases with 5 parameter categories (onset position, conduction velocity...) leading to between 144 and 180 simulated cases. Adding more hypothesis of electrophysiology parameters in the training set would help capturing more complex electrophysiology and kinematics patterns. However, this would also lead to a much increased number of simulations and therefore a trade-off must be found between the range of pathologies and the computational requirements.

Then prediction errors also depend on the accuracy of the electrophysiology model. For instance, applying an automated personalization method [Relan 2011] of an electrophysiology model on the 3 patients' datasets described previously leads to errors of 10.19 ms, 9.19 ms and 16.51 ms respectively. These errors after personalization capture the combined effect of acquisition, discretization and model errors. Given that the prediction errors are respectively 11.20 ms, 13.51 ms and 22.42 ms, it appears that the errors due to the learning process are relatively small. To decrease further those errors may require to use a more complex electrophysiological model or a finer mesh. However, it is probable that improving the acquisition protocol leading to higher spatial resolution would be most beneficial. In practice, obtaining ground truth electrophysiology data is currently difficult due to the invasive nature of the endocardial mapping systems. Using less invasive electrophysiology data from

body surface potential mapping would allow to broaden the number of test cases.

In addition, to decrease the prediction errors, it is important that the cardiac electromechanical model produces realistic simulations of the cardiac motion. This not only implies that the cardiac physiology is well described by the chosen E/M model, but it also means that this model is sufficiently well personalized. In our approach, the chosen E/M has been shown to produce plausible simulations of the cardiac motion and also shown some predictive behavior for the electrophysiology and mechanics [Sermesant 2012]. Furthermore, in this study, we have performed four different mechanical calibrations for each onset position, in order to have similar volume curves between the simulation and the patient data. To improve the prediction, one would probably need to perform a calibration and even a personalisation of the mechanical parameters for each electrophysiology scenario. Indeed, the calibration stage only tries to match the endocardial volume curves whereas the personalisation stage tries to match more regional or local kinematic indices (regional volume curves, estimated displacement...).

One limitation of this study is that the created database is patient-specific. Therefore, numerous simulations need to be performed in order to predict another patient's depolarization time. Currently, predictions from one training set built from one patient does not generalize to another patient because of the difference in their kinematic descriptor. The use of common atlas may overcome this limitation.

4.7 Conclusion

As the generated synthetic cardiac MR sequences have electro-kinematic "ground truth" information, we have performed an inverse electro-kinematic learning on this patient-specific database. Invariant kinematic descriptors were extracted from the displacement field obtained from the sequence registration. The non-linear inverse relationship between the electrical activation times and the kinematic descriptors was modeled using LS-SVM. Evaluation of the learning process for the database of synthetic sequence shows good generalization and a first evaluation on three clinical MR sequences shows encouraging results.

This approach opens the possibility of using non-invasive cardiac motion imaging as a way to estimate electrophysiological patterns. This could provide additional information to the cardiologist during the optimization of the Cardiac Resynchronization Therapy (CRT), for example allowing the placement of the pacemaker leads in the cardiac region which is lately activated. An extension of this work would be the application of this method to different imaging modalities. This can be done since the synthetic sequence generation method is generic and was already demonstrated for different imaging modalities [Prakosa 2012c].

Chapter 5

Conclusion and Perspectives

Contents

In this thesis we presented a novel approach for the generation of realistic synthetic cardiac sequences which were used for the creation of a database for the inverse cardiac electro-kinematic learning. This study aims at answering the following question: can one estimate the electrophysiology characteristics of the heart by observing its motion? The answer to this question is certainly not straightforward but this work aims at providing more hindsight about this issue.

First, we evaluated the non-linear image registration method which is required to analyze cardiac sequences. We then developed a novel method to combine simulated cardiac electromechanical motion with the motion estimated from the real sequence in order to create several synthetic but visually realistic cardiac sequences. This method allowed the creation of large database of synthetic sequences which contains the ground truth electro-kinematic relationship. Since the pairs of real clinical sequence along with the electrical cardiac mapping are still difficult to obtain, the database of synthetic sequence allow us to use a machine learning based approach to learn the inverse electro-kinematic relationship.

5.1 Contributions

This work has led to three main contributions.

Evaluation of iLogDemons Non-Rigid Registration Algorithm

The LogDemons and iLogDemons [Mansi 2011] non-linear registration algorithms were evaluated on a dataset of healthy volunteers and phantoms and also on a dataset of synthetic cardiac ultrasound sequences. The evaluation of the method to the real dataset allowed us to compare the estimated cardiac strain curves with the healthy strain curves from the literature. We observed that the strain estimation showed reasonable result [McLeod 2012]. The strain curves provide some

information about the cardiac motion which can help cardiologist to better analyse the abnormal patterns of the cardiac motion.

In general, objective evaluation of non-linear registration methods is still challenging because of the lack of ground truth. However, with synthetic sequences, it is possible to quantify the performance of these algorithms since the ground truth motion was given. Using this quantification, the best registration parameters can be chosen. Furthermore, the limitations of the registration method during the systolic phase can be quantified and analysed. The evaluation has been performed on a dataset of synthetic ultrasound images generated using the simulated physics of ultrasound acquisition [Prakosa 2012a] and also on a multimodal synthetic dataset (Magnetic Resonance, Computed Tomography and Echocardiography) generated using our proposed method [Prakosa 2012c].

This work was published in [McLeod 2012, Prakosa 2012a].

Generation of Synthetic but Realistic Cardiac Sequences

We developed a pipeline to create visually realistic synthetic 4D cardiac sequences using the cardiac motion simulated by an electromechanical model. This pipeline combines the simulated myocardium displacement field with the estimated myocardium displacement field from a registration method. This combined displacement field is then used to warp the original images in order to create the synthetic cardiac sequence.

In this pipeline, we proposed a new approach based on Stationary Velocity Fields to combine the two motions. We also proposed a new method that diffuses velocity fields in order to maintain the continuity between the simulation and the real image with minimal texture distortion. Thanks to the detailed interplay between image processing and biophysical modeling, we can fully use a complete sequence in order to generate several new ones. This method also gives better realism compared to traditional methods based on the deformation of an end-diastolic image, since the generated synthetic sequence will also contain the motion of surrounding tissues such as the motion of the mitral valve.

The new synthetic images are similar to the original ones except for the motion of the heart which is modified to follow the motion provided by a biophysical model. The parameters of the biophysical model can be modified to create variations around this motion. This pipeline has been applied to generate different synthetic sequences from different imaging modalities. It is generic and can be used with a different biophysical models or a different image registration algorithm, and it can be extended to other organs.

As these synthetic 4D cardiac sequences have kinematic ground truth information, those sequences represent in themselves a valuable resource to benchmark motion tracking methods or to train machine-learning algorithms.

This work was published in [Prakosa 2011, Prakosa 2012c].

Estimation of Cardiac Electrophysiology from Medical Images

As the generated synthetic cardiac sequences have electro-kinematic "ground truth" information, we have performed an inverse electro-kinematic learning on this patient-specific database. Invariant kinematic descriptors were extracted from the displacement field obtained from the sequence registration. The non-linear inverse relationship between the electrical activation times and the kinematic descriptors was modeled using LS-SVM. Evaluation of the learning process for the database of synthetic sequence shows good generalization and a first evaluation on three clinical MR sequences [Prakosa 2012b] and two clinical US sequences [Prakosa 2011] shows encouraging results.

This approach opens the possibility of using non-invasive cardiac motion imaging as a way to estimate electrophysiological patterns. This could provide additional information to cardiologists during the optimization of the Cardiac Resynchronization Therapy (CRT), for example allowing the placement of the pacemaker leads in the cardiac regions that are lately activated.

This work was published in [Prakosa 2010, Prakosa 2011] and it is in preparation for publication in [Prakosa 2012b].

5.2 Perspectives

This work brings the following perspectives both in the short and long term.

5.2.1 Short term perspectives

Evaluation of non-linear registration method on the multimodal synthetic cardiac sequences

The evaluation of the non-linear registration method is still a challenging task. In this thesis the iLogDemons algorithm was applied to a dataset of synthetic ultrasound sequence with different motion and deformation pattern. The algorithm was able to reasonably estimate the ground truth deformation of the model [Craene 2012a, Prakosa 2012a]. The evaluation of the algorithm on the synthetic images of different medical imaging modality will be important to better understand the influence of the different parameter values. An evaluation of the method on synthetic sequences generated by simulating the physics of image acquisition can be compared to the evaluation done in our developed multimodal synthetic sequence [Prakosa 2012c].

Our current implementation could be optimized for instance by improving memory access so that it can handle large volumes faster and it can ease the selection of the best registration parameters.

5.2.2 Long term perspectives

Automatic optimisation and additional constraint to the non-linear registration method

The availability of the synthetic cardiac sequences and the underlying ground truth motion allows the objective evaluation of the non-linear registration method. Using this evaluation, the error given for a choice of registration parameters can be estimated. Therefore, an automatic optimisation method can also be developed to find the best registration parameter for a given objective.

Further improvement of the registration algorithms can be done in order to give better performance. In our evaluation [Prakosa 2012a], *a priori* information on the cardiac cycle could be used as a longitudinal constraint. It would improve the registration result during the maximum contraction where we had the largest error.

Integration of the simulated physics of acquisition to the developed synthetic sequence generation method

The synthetic sequence generation pipeline has been tested to generate different synthetic sequences from different imaging modalities. It is generic and can be used with a different biophysical model or a different image registration algorithm, and it can be extended to other organs. The produced sequence is highly realistic and similar to the one from clinics since the synthetic sequence uses the information from the real one.

Further development in the integration of the simulated physics of acquisition can improve the visible texture information. This can be useful for example in echocardiography when parts of the myocardium is out of the field of view.

The application of the method to other organs should allow the evaluation of different image processing algorithm developed for that organ. For example in the brain tumor growth simulation, combination of the simulated physics of acquisition and the proposed pipeline could yield highly realistic brain image with simulated tumor in the image.

Generalization of the cardiac inverse electro-kinematic learning to the different patient dataset

We developed a method to estimate patient's cardiac electrophysiology pattern from the analysis of sequences of cardiac images. A patient specific database of synthetic cardiac sequences was built as it is required to train a machine learning algorithm. This method opens the possibility of non-invasive cardiac electrical mapping. Clinically, this could give additional information to the cardiologist in the optimization of the Cardiac Resynchronization Therapy (CRT), for example in the placement of the pacemaker leads in the cardiac regions that are lately activated.

The personalization of electromechanical models is one of key tasks to obtain reasonable predictive results. Current personalization is done for one of the kinematic descriptor which is the LV endocardial volume curve. With the advance in the cardiac model personalisation method, personalising each of the kinematic descriptor will make the simulation and also the created database closer to the real observation. Therefore the database will represent better the possible variation of

the real data. It will also yield better prediction since the training set would be closer to the real dataset. After the personalisation, the combination of different datasets from different patients can improve the generalisation of the learning method.

Preliminary evaluation on the echocardiography images was performed in [Prakosa 2011]. Since echocardiography is the most widely used medical imaging modalities in the CRT, it is of great interest to estimate the cardiac electrical mapping from the 4D US images. First evaluation can be done by applying the learning method to different patient images with different pacing mode. However, the real validation can only be done by using the patient cardiac electrical mapping obtained using catheterisation.

Appendix A

List of Publications and Awards

Journal Articles

- [Prakosa 2012c] A. Prakosa, M. Sermesant, H. Delingette, S. Marchesseau, E. Saloux, P. Allain, N. Villain and N. Ayache. Generation of Synthetic but Visually Realistic Time Series of Cardiac Images Combining a Biophysical Model and Clinical Images. Medical Imaging, IEEE Transactions on: Special Issue on Medical Imaging in Computational Physiology, 2012. Note: In press.

- [Prakosa 2012b] A. Prakosa *et al.* Cardiac Electrophysiological Activation Pattern Estimation from Images using a Patient-Specific Database of Synthetic Image Sequences. Biomedical Engineering, IEEE Transactions on, 2012. Note: In preparation for submission.

- [Tobon-Gomez 2012b] C. Tobon-Gomez, M. De Craene, K. McLeod, L. Tautz, W. Shi, A. Hennemuth, A. Prakosa, H. Wang, G. Carr-White, S. Kapetanakis, A. Lutz, V. Rashce, T. Schaeffter, C. Butakoff, O. Friman, T. Mansi, M. Sermesant, X. Zhuang, S. Ourselin, H-O. Peitgen, X. Pennec, R. Razavi, D. Rueckert, A.F. Frangi, and K. S. Rhode. Evaluation of Current Algorithms for Myocardial Tracking and Deformation: Cardiac Motion Analysis Challenge. Medical Image Analysis, 2012. Note: Under review.

Selective Peer-Reviewed Conference Papers

- [Prakosa 2011] A. Prakosa, M. Sermesant, H. Delingette, E. Saloux, P. Allain, P. Cathier, P. Etyngier, N. Villain and N. Ayache. Synthetic Echocardiographic Image Sequences for Cardiac Inverse Electro-Kinematic Learning. In Gabor Fichtinger, Anne Martel and Terry Peters, editors, Medical Image Computing and Computer-Assisted Intervention - MICCAI 2011, volume 6891 of LNCS, pages 500-507, Toronto, Canada, September 2011. Springer, Heidelberg. Note: Oral presentation

Workshop Papers

- [Prakosa 2010] A. Prakosa, M. Sermesant, H. Delingette, E. Saloux, P. Allain, P. Cathier, P. Etyngier, N. Villain and N. Ayache. Non-Invasive Activation Times Estimation using 3D Echocardiography. In Oscar Camara, Mihaela Pop, Kawal Rhode, Maxime Sermesant, Nic Smith and Alistair Young, editors, Statistical Atlases and Computational Models of the Heart, volume 6364 of

LNCS, pages 212-221, Beijing, China, September 2010. Springer, Heidelberg. Note: Oral presentation

- [McLeod 2012] K. McLeod, A. Prakosa, T. Mansi, M. Sermesant and X. Pennec. An Incompressible Log-Domain Demons Algorithm for Tracking Heart Tissue. In Oscar Camara, Ender Konukoglu, Mihaela Pop, Kawal Rhode, Maxime Sermesant and Alistair Young, editors, Statistical Atlases and Computational Models of the Heart: Imaging and Modelling Challenges, volume 7085 of LNCS, pages 55-67, Toronto, Canada, September 2012. Springer, Heidelberg.

- [Prakosa 2012a] A. Prakosa, K. McLeod, M. Sermesant and X. Pennec. Evaluation of iLogDemons Algorithm for Cardiac Motion Tracking in Synthetic Ultrasound Sequence. In Proc. MICCAI Workshop on Statistical Atlases and Computational Models of the Heart (STACOM12), Nice, France, October 2012.

- [Craene 2012b] M. D. Craene, P. Allain, H. Gao, A. Prakosa, S. Marchesseau, L. Hilpert, O. Somphone, H. Delingette, S. Makram-Ebeid, N. Villain, J. D'hooge, M. Sermesant and E. Saloux. Synthetic and Phantom Setups for the Second cardiac Motion Analysis Challenge (cMAC2). In Proc. MICCAI Workshop on Statistical Atlases and Computational Models of the Heart (STACOM12), Nice, France, October 2012.

Awards

- The paper "An Incompressible Log-Domain Demons Algorithm for Tracking Heart Tissue" won the Motion Tracking Challenge organized in the context of the MICCAI satellite workshop Statistical Atlases and Computational Models of the Heart: Imaging and Modelling Challenges 2011 in Toronto, Canada.

- The poster "Analysis and Simulation of Heart Function" won the Best Poster Award in the 9^{th} IEEE EMBS Internatioanl Summer School on Biomedical Imaging 2010 in Berder, France.

Miscellaneous

- A. Prakosa, H. Delingette, M. Sermesant and N. Ayache. Analysis and Simulation of the Heart Function from Multimodal Cardiac Images. Inria-Philips Activity Report, 2010-2011

Appendix B

Non-Invasive Activation Times Estimation using 3D Echocardiography

---

Based on: [Prakosa 2010] A. Prakosa, M. Sermesant, H. Delingette, E. Saloux, P. Allain, P. Cathier, P. Etyngier, N. Villain and N. Ayache. Non-Invasive Activation Times Estimation using 3D Echocardiography. In Oscar Camara, Mihaela Pop, Kawal Rhode, Maxime Sermesant, Nic Smith and Alistair Young, editors, Statistical Atlases and Computational Models of the Heart, volume 6364 of LNCS, pages 212-221, Beijing, 2010. Springer, Heidelberg.
The further development in the estimation of cardiac electrophysiology activation pattern from the analysis of the cardiac image sequence is described in Chapter 4 and in preparation for submission to [Prakosa 2012b].

Despite advances in both medical image analysis and intracardiac electrophysiological mapping technology, the understanding of cardiac mechano-electrical coupling is still incomplete. This knowledge is of high interest since it would help estimating the cardiac electrophysiology function from the analysis of widely available cardiac images, such as 3D echocardiography. This is important, for example, in the evaluation of the cardiac resynchronization therapy (CRT) where the placement and tuning of the pacemaker leads plays a crucial role in the outcome of the therapy. This paper proposes a method to estimate activation times of myocardium using a cardiac electromechanical model. We use Kernel Ridge Regression to find the relationship between the kinematic descriptors (strain and displacement) and the contraction force caused by the action potential propagation. This regression model is then applied to two 3D echocardiographic sequences from a patient, one in sinus rhythm and the other one with left ventricle pacing, for which strains and displacements have been estimated using incompressible diffeomorphic demons for non-rigid registration.

B.1 Introduction

The wide availability of cardiac imaging modalities especially 3D echocardiography allows clinicians to estimate some geometrical characteristics of the myocardium motion such as displacement, strain or strain rate. However, these quantities are only related to the kinematics of the heart whereas in many cases it is important

to also obtain information about the patient's cardiac electrical propagation. Indeed contact or non-contact intracardiac electrical mappings are invasive procedures which are not classically used for diagnosis but rather for applying a therapy. Electrocardiographic imaging[Ghanem 2005] (*a.k.a.* body surface potential mapping) is a non-invasive technique for imaging activation times of the myocardium but still remains to be validated thoroughly and is not widely available in clinical centers. Therefore there is a strong need to quantitatively assess a patient electrophysiological condition from non-invasive imaging modalities such as 3D echocardiography. This is especially valid in the context of cardiac resynchronization therapy (CRT) for which up to 30% of the patients with pacemaker leads show no benefit[Helm 2007]. Providing activation maps from a 3D echocardiography for instance, would be of great interest to select patients responding to the therapy and to optimize the lead placements and delays during and after therapy. More fundamentally, understanding the relationship between cardiac mechanics and electrophysiology is essential to improve the diagnosis and therapy of patients suffering from heart failure.

A study on the relation between cardiac magnetic resonance (MR) motion tracking and the electrical activation pattern has been published by Sanchez-Ortiz *et al.*[Sanchez-Ortiz 2004] which combines some cardiac motion descriptors in order to obtain the electrical activation time. However, in this study, the weights were assigned manually to get an estimation of the activation. McVeigh *et al.*[McVeigh 1998] also consider only the circumferential strain estimated from tagged MR images as the mechanical activation measure. Very high frame rate ultrasound in electromechanical imaging (EWI), which could map the electromechanical wave (EMW) correlated with cardiac electrical activation in 2D echocardiography, has been published by Provost *et al.*[Provost 2010]. However, understanding the 3D cardiac electrical propagation is still very important for clinicians.

In this paper, our main objective is to find a relationship between the different kinematic parameters obtained from cardiac image analysis and the activation times of the myocardium using a machine learning method. The activation times are defined as moments at which the activation forces at a given point sharply increase. Activation times are strongly correlated with the action potential signal through the mechano-electrical coupling.

The training stage is based on motion and contraction forces estimated from an electromechanical model of the heart. This *in silico* cardiac model serves as a reference model in the absence of reliable intracardiac mapping information. Several pathologies and pacing scenarios are considered in this training phase. Based on this learning process, we can predict the cardiac electrical propagation from kinematic parameters estimated from cardiac image analysis. This approach has been evaluated on synthetic cases as well as on one patient. The results are thoroughly discussed and perspectives of this work are provided in a final section.

B.2 3D Echocardiography Image Registration and Motion Estimation

We use 3D echocardiography images provided by the University Hospital of Caen, Normandy - France. This data was acquired from patients under CRT with two implanted electrodes, one in the left ventricle and the other in the right ventricle. Two different pacemaker stimulation modes were imaged and analysed. The first mode corresponds to the sinus rhythm mode when no pacemaker lead is activated. In the second mode, the left ventricle is stimulated. Left ventricle segmentation along whole cardiac sequence was provided by the Medisys Group of Philips Healthcare, Suresnes - France. The 3D echocardiography sequence begins at the end-diastolic phase of the cardiac cycle.

B.2.1 Incompressible Diffeomorphic Demons

Cardiac motion is estimated through a non-linear image registration algorithm applied between consecutive frames of the same cardiac cycle. The purpose of applying this non-linear image registration is to find the displacement vector field $\mathbf{u(x)}$ associated with the transformation $\phi(\mathbf{x}) = \mathbf{x} + \mathbf{u(x)}$ which aligns a template image $\mathrm{T}(\mathbf{x})$ to a reference image $\mathrm{R}(\mathbf{x})$, where $\mathbf{x} \in \mathbb{R}^3$ is the space coordinate (voxel (x,y,z)). This displacement vector field $\mathbf{u(x)}$ is considered as the cardiac displacement field. All images in the cardiac sequence are registered to the same reference image which is the first image of the 3D echocardiography sequence, corresponding to the end-diastolic phase.

We take into account the myocardium near-incompressibility assumption (maximum 5 to 7% of volume variation during the cardiac cycle) by relying on the incompressible demons algorithm proposed by Mansi *et al.*[Mansi 2009] to estimate cardiac motion. This algorithm improves the diffeomorphic demons algorithm[Vercauteren 2007] by adding 2 constraints: the myocardium near-incompressibility and linear elastic regularization of velocity fields. This method has been developed and evaluated for cardiac motion estimation on cine MRI images [Mansi 2009].

A 3D myocardium segmentation for the first frame of the sequence is used as the incompressible region. The 3D echocardiography sequence starts at the end-diastolic phase of a cardiac cycle. All image frames in the 3D echocardiography sequence are being registered to this end-diastolic frame.

The recovered displacement vector field is projected in the radial, circumferential and longitudinal directions using the heart local coordinate system.

B.2.2 Strain Estimation

The displacement vector field $\mathbf{u(x)}$ which recovers the cardiac motion $\phi(\mathbf{x}) = \mathbf{x} + \mathbf{u(x)}$ is then used to compute the Lagrangian finite strain tensor $E = \frac{1}{2}(\nabla\mathbf{u} + \nabla\mathbf{u}^T + \nabla\mathbf{u}^T\nabla\mathbf{u})$. The strain is calculated by using the end-diastolic frame as the

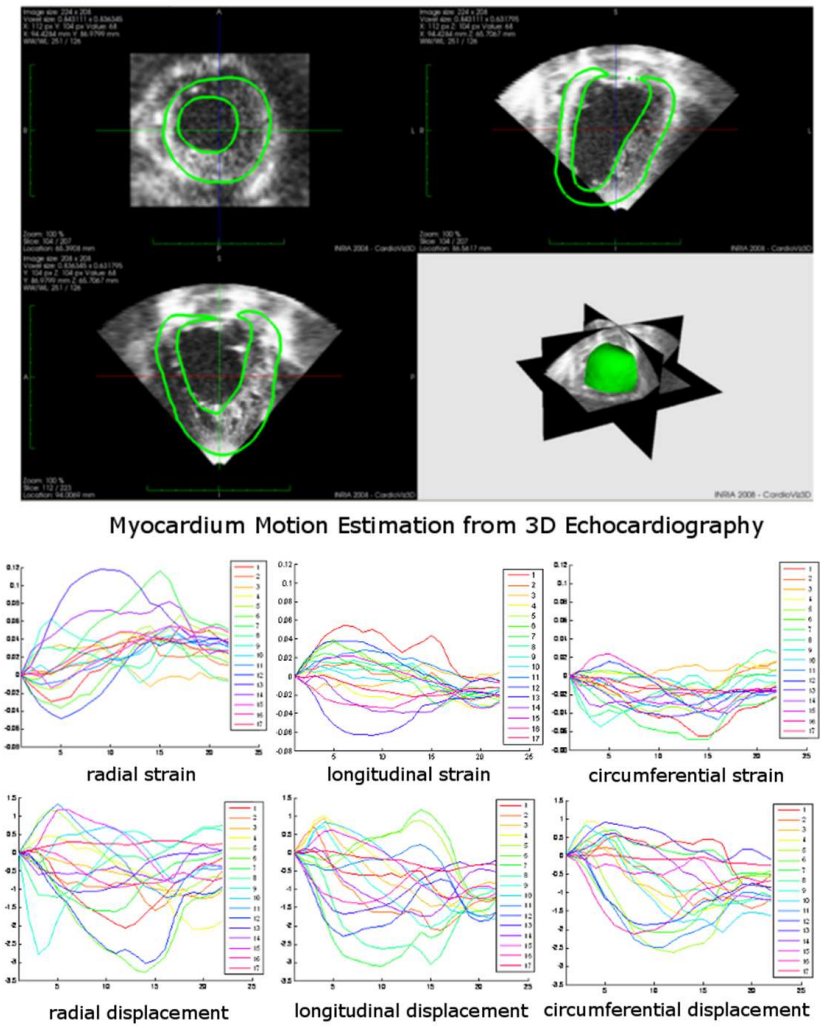

Figure B.1: **3D echocardiography myocardium motion estimation.** Myocardium motion is tracked and then strains and displacements with respect to the first reference image in the cardiac cycle are computed and projected in a local frame representing the radial, longitudinal and circumferential directions. The different colors in the curves show the 17 different AHA zones. The strain and displacement curves shown are from a patient with LBBB and without any pacemaker stimulation. The strain vertical axis is dimensionless while the displacement vertical axis is in millimeters. The horizontal axis shows the image frame number in the cardiac cycle.

reference image $\mathrm{R}(\mathbf{x})$. Similarly for the displacement vector field, the obtained strain is projected in the radial, circumferential and longitudinal directions (cf. Fig. B.1).

B.3 Inverse Mechano-electrical Coupling

B.3.1 Electromechanical Model

In order to learn how the cardiac kinematics are related to the cardiac electrophysiology it is necessary to get for the same patient descriptors of the cardiac motion and electrical wave propagation. This could be provided by 3D echocardiography and intracardiac electrophysiological mapping acquired on the same patient. To merge both information, the patient must be in the same stimulation mode and endocardial surfaces reconstructed from intracardiac mappings must match those segmented in 3D US. However, such joint acquisition was not available in our study. Therefore, we proposed to use an electromechanical model of the heart [Sermesant 2006b] to simulate patient cases. From those simulated cases, we could obtain both electrophysiological and kinematic measurements. To be realistic, this model uses the cardiac anatomy extracted from echocardiography images as a priori information about the shape of the left ventricle (LV). We simulated four cardiac cases using the electromechanical model to create a training database. First, we simulate the cardiac propagation and contraction in normal sinus rhythm where the electrical simulation is coming from the left and right ventricle endocardium. In the second simulation, we simulate a left bundle branch block (LBBB) where the stimulation is coming only from the right ventricle endocardium while the third simulation is the right bundle branch block (RBBB) case where stimulation is coming only from the left ventricle endocardium. The last case is the bi-ventricular pacing case where we initiate the electrical propagation from a zone in the lateral freewall and a zone in the right ventricle apex in order to simulate the pacemaker bi-ventricular pacing (cf. Fig. B.2).

The simulation gives the deformation of the cardiac mesh along with the contraction value and the potential value for each point in the mesh. We perform a thresholding in order to obtain the time at which the contraction value increases. We also compute the displacement vector field which maps the myocardium at a given time point to the end-diastolic image of the sequence. Kinematic descriptors extracted from the obtained displacement vector field are the displacement and the strain projected in the radial, longitudinal and circumferential directions.

B.3.2 Kernel Ridge Regression as a Learning Method

Using an electromechanical model of the heart, we learn the relationship between the kinematic descriptors and the electrical activation. We use Kernel Ridge Regression to find a relationship between these 2 quantities.

Ridge Regression searches a linear function $\mathbf{y} = \mathbf{w}^T\mathbf{x}$ that models the dependencies between the descriptor vectors $\mathbf{x}_i \in \mathbb{R}^d$ and the response vectors $\mathbf{y}_i \in \mathbb{R}^r$ (all vectors are column vectors) from a set of T examples $(\mathbf{x}_1, \mathbf{y}_1), (\mathbf{x}_2, \mathbf{y}_2), ..., (\mathbf{x}_T, \mathbf{y}_T)$. Classically, we need to minimize the quadratic cost $C(\mathbf{w}) = \frac{1}{2}\sum_i^T (\mathbf{y}_i - \mathbf{w}^T\mathbf{x}_i)^2$, where $\mathbf{w}$ is a $d \times r$ matrix. Regularizing this equation, the total cost function which needs to be minimized hence becomes $C(\mathbf{w}) = \frac{1}{2}\sum_i^T (\mathbf{y}_i - \mathbf{w}^T\mathbf{x}_i)^2 + \frac{1}{2}\lambda \|\mathbf{w}\|^2$,

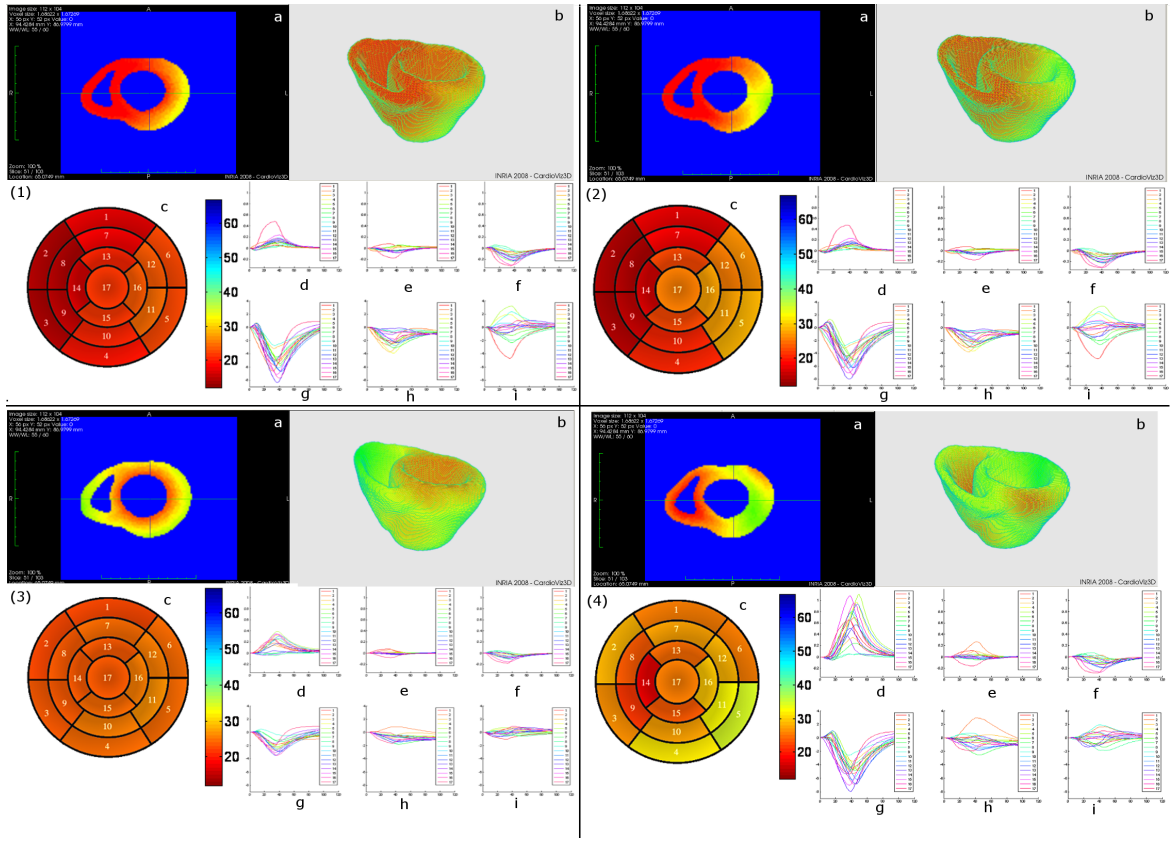

Figure B.2: **Electromechanical simulation.** 4 cardiac cases simulated using the electromechanical model. (1) normal case, (2) LBBB case, (3) RBBB case and (4) bi-ventricular pacing case. (a), (b) and (c) are the contraction force isochrone. (c) is the isochrone for the LV divided to 17 AHA zones. (d), (e), (f) are the radial, longitudinal and circumferential strains respectively and (g), (h), (i) are the radial, longitudinal and circumferential displacements. Axis units are as explained in Fig. B.1. These strains and displacements are extracted from the deformation of the mesh simulated by the electromechanical model.

where $\lambda > 0$ is the regularization parameter. Introducing a $T \times d$ matrix $X = (\mathbf{x}_1, \mathbf{x}_2, ..., \mathbf{x}_T)^T$ which contains the vectors $\mathbf{x}_i$ in its row and a $T \times r$ matrix $Y = (y_1, y_2, ..., y_T)^T$ which contains the vectors $\mathbf{y}_i$ in its row, the equation can be written as $C(\mathbf{w}) = \frac{1}{2}\|Y - X\mathbf{w}\|^2 + \frac{1}{2}\lambda\|\mathbf{w}\|^2$. Minimizing this function by taking its derivative with respect to $\mathbf{w}$ and setting it equal to zero gives $-X^TY + X^TX\mathbf{w} + \lambda\mathbf{w} = 0 \Rightarrow \mathbf{w} = \left(\lambda\mathbf{I} + X^TX\right)^{-1}X^TY$.

Ridge Regression can be extended to Kernel Ridge Regression by rewriting the solution $\mathbf{y} = \mathbf{w}^T\mathbf{x} = \left(\left(\lambda\mathbf{I} + X^TX\right)^{-1}X^TY\right)^T\mathbf{x} = Y^T\left(\lambda\mathbf{I} + XX^T\right)^{-1}X\mathbf{x} = Y^T\left(\lambda\mathbf{I} + K\right)^{-1}\mathbf{k}$ with $K = XX^T$ and $\mathbf{k} = X\mathbf{x}$. We choose to use Radial Basis Function as a Kernel function $K(x_i, x_j) = e^{-\frac{|x_i - x_j|}{\sigma^2}}$ with $i, j = \{1, ..., T\}$.

B.3.2.1 Parameter Optimization

The chosen λ and σ parameters are optimized by using leave-one-out estimates which train the model with all members of the training set but one and test the performance on the singleton. The process is repeated for all the singletons in the training set. We use Allen's PRESS (predicted residual sum of squares) statistic for this process, $PRESS = \sum_i^T \mathbf{e}_{(i)}^2$ [Cawley 2004], where $\mathbf{e}_{(i)} = \mathbf{y}_i - \hat{\mathbf{y}}_{(i)}$ is the residual for the ith example with the ith example excluded from the training process and $\hat{\mathbf{y}}_{(i)}$ is the predicted response for the ith example based on the training process. Fortunately, we have $e_{(i)} = \frac{e_i}{1-h_{ii}}$ where $e_i = \mathbf{y}_i - \hat{\mathbf{y}}_i$ is the residual for the ith example in the training process which includes all examples and $\hat{\mathbf{y}}_i$ is the fitted response based on this training. h_{ii} is the ith element of the leading diagonal of the hat matrix $H = X(\lambda\mathbf{I} + X^TX)^{-1}X^T = XX^T(\lambda\mathbf{I} + XX^T) = K(\lambda\mathbf{I} + K)^{-1}$. Therefore, in the end, we can have the PRESS for the chosen parameters λ and σ in one iteration. We use the downhill simplex search method in MATLAB in order to optimize these parameters to have the smallest PRESS.

With this approach, we learn a non-linear relationship (due to the choice of Radial Basis Function as the Kernel function) between the kinematic descriptors and the activation force caused by the action potential. We take the radial, longitudinal and circumferential strains ($\mathbf{E}_r, \mathbf{E}_l, \mathbf{E}_c \in \mathbb{R}^{t_d}$) and also the radial, longitudinal and circumferential displacements ($\mathbf{u}_r, \mathbf{u}_l, \mathbf{u}_c \in \mathbb{R}^{t_d}$) from points in the myocardium as the components of the kinematic descriptor vector $\mathbf{x}_i \in \mathbb{R}^{d=6\times t_d}$, where t_d is the number of each descriptor sampling time in a cardiac sequence. The contraction force along a cardiac cycle t_r is set as the response vector $\mathbf{y}_i \in \mathbb{R}^{r=t_r}$. The descriptor sampling time t_d is taken for 20 time instances in order to follow the temporal resolution of the real patient data. However, the response vector sampling time t_r is chosen as 100 time instances in order to have high temporal resolution of the contraction force along a cardiac cycle, starting before the beginning of the P wave of the ECG. The examples in the training set consist of the different points in the myocardium. We take 30 points from each of the American Heart Association (AHA) 17 zones so we have 510 learning points along a cardiac cycle. We separate the value σ for the displacement and the strain used in the Kernel $K(x_i, x_j) =$

$e^{-\left(\frac{|u_i-u_j|}{\sigma_u}-\frac{|E_i-E_j|}{\sigma_E^2}\right)}$. Once the learning process is done, we obtain the optimal values for λ, σ_u and σ_E. We use these parameters to predict the other points in the myocardium in order to obtain the cardiac contraction force mapping caused by the potential.

B.4 Results

B.4.1 Evaluation on Simulated Data

First, we tested our machine learning method using the simulated motion from the electromechanical model for which we have a ground truth to compare to. The first 3 cases which have been described in section B.3.1 are included in our training set, whereas the fourth case has not been included. The optimal parameters of the regression have been found as $\lambda = 0.0004$, $\sigma_u = 107.1030$ and $\sigma_E = 9.0276$ which yield the root mean squared error (RMSE) value between the predicted and the ground truth value 0.0016 MPa. This seems to imply that strains are more correlated with activation times than displacements since their variances are smaller (for a similar range of values). We applied the regression method to all points of the first, second and third cases producing quite smooth predicted contraction force curves (see Fig. B.3). Note that the training stage only included a very small subset of those points thus showing that the kernel ridge regression is able to generalize the correlations between strains and forces to the whole myocardium.

In the fourth case, the predicted force values are not as smooth as expected. However the predicted and the ground truth value of the fourth case have the same global bell shape where up and down slopes can be detected using thresholding. The bull's eyes plot computed from the estimated activation times also correspond to their expected value. In the second case (LBBB) we clearly have an early activation from the septal wall whereas in the third case (RBBB) the early activation originated from the endocardial wall of the left ventricle. In the fourth case (bi-ventricular pacing), not included in the training set, the delays between right and left ventricles are slightly decreased. The left ventricle RMSE value between the predicted and the ground truth activation time is 7 ms for the first 3 cases and 37 ms for the fourth case.

B.4.2 Application to Clinical Data

From the time series of 3D echocardiography images, we segmented the myocardium and then estimated the cardiac motion using the incompressible demons algorithm. The myocardium segmentation is used to specify the region where the incompressibility constraint must be satisfied. From the knowledge of the left ventricle axis, we can define the 3 local directions and then project strain tensors and displacements along those three directions (cf. Fig. B.4). These values are then used as input descriptors in the regression method.

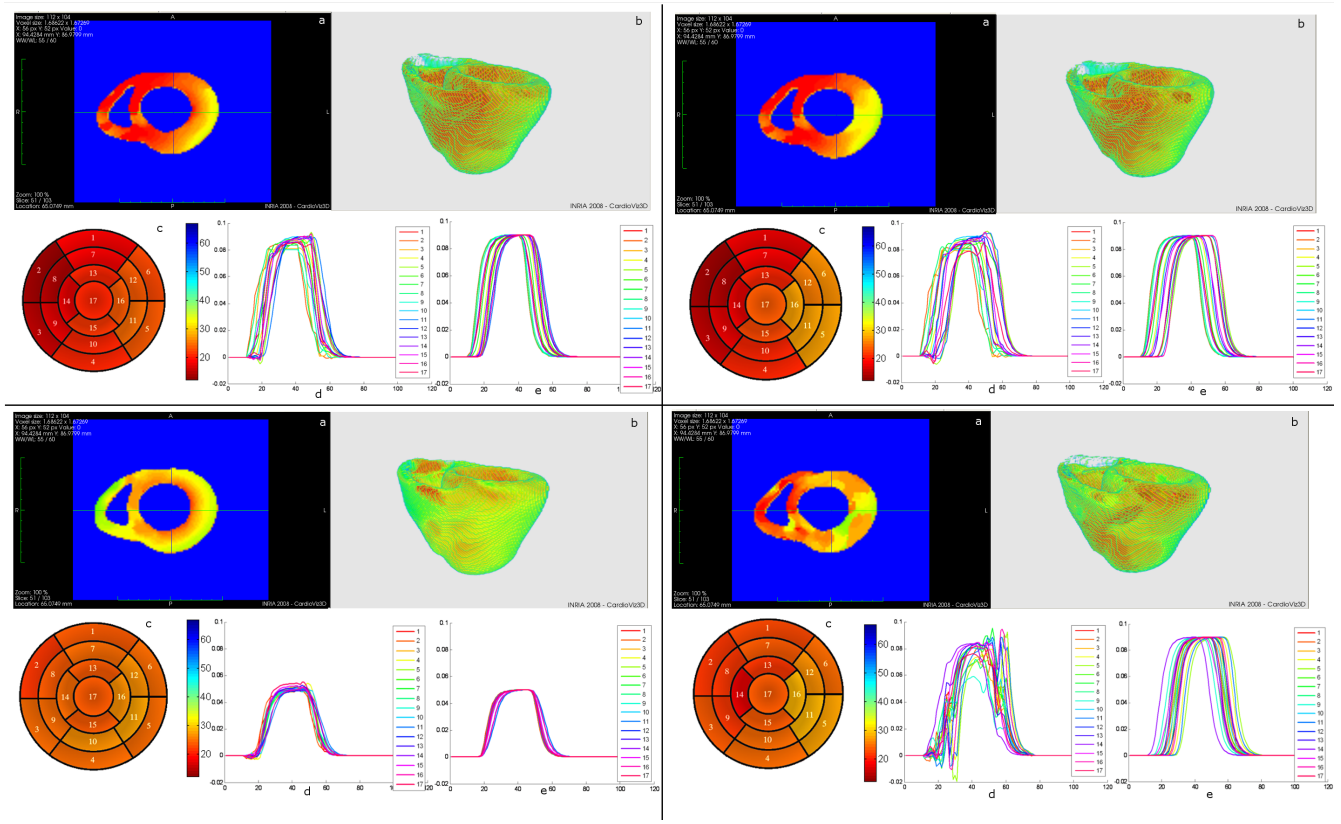

Figure B.3: **Prediction of contraction forces from synthetic data.** (a), (b) are the whole contraction force isochrones (activation times) obtained after applying the learning method on the whole points in the myocardium for case (1) (sinus rhythm), (2) (LBBB), (3) (RBBB) and (4) (bi-ventricular pacing) whereas (c) is the whole contraction force isochrone only for the left ventricle. (d) is the contraction force curve along a cardiac cycle which predicted by the learning method whereas (e) is the ground truth contraction force curve as produced by the electromechanical model. The vertical axis unit is in MPa. The horizontal axis shows the frame number in the cardiac cycle.

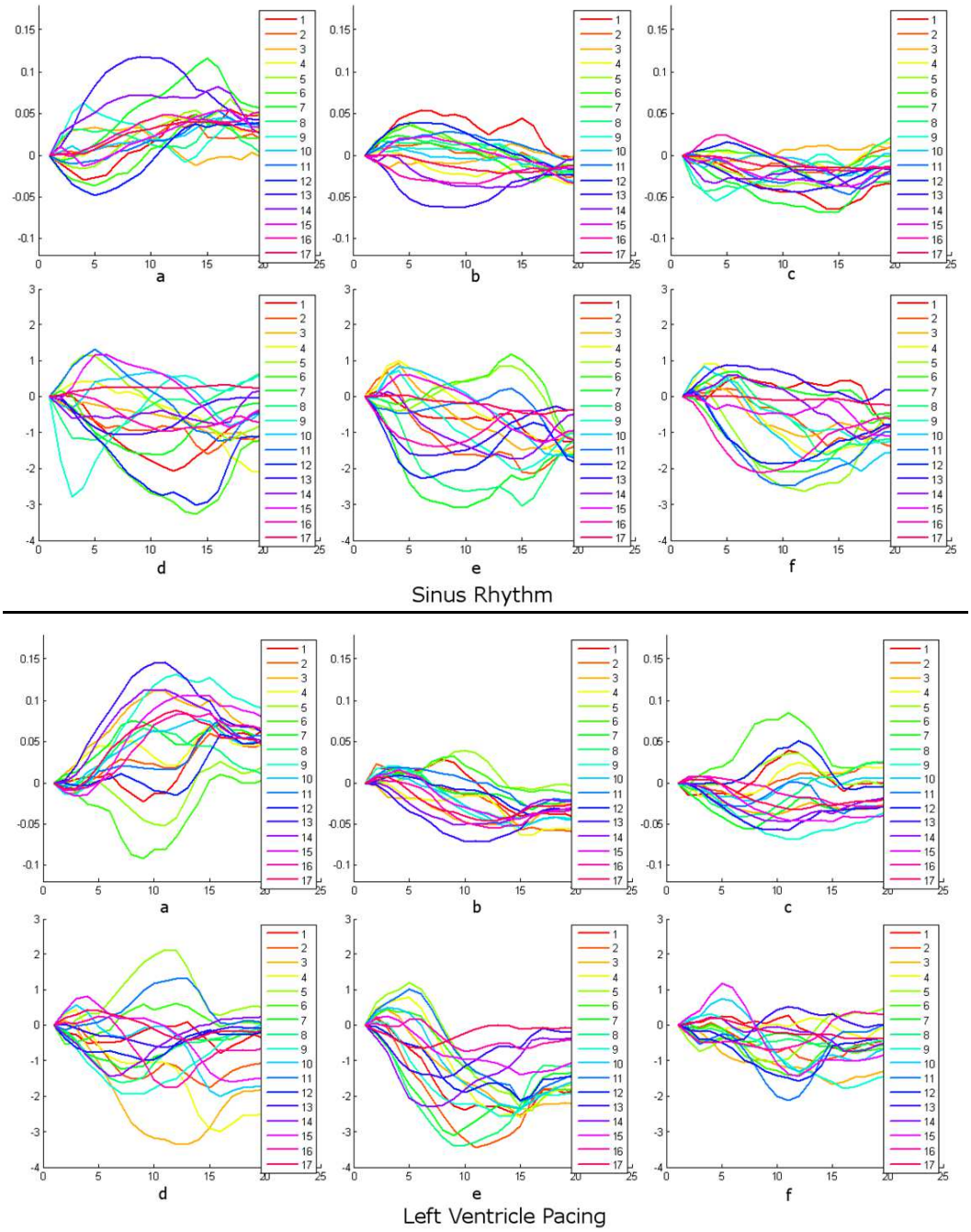

Figure B.4: **Kinematic descriptors extracted from patient's 3D echocardiography.** (a) (b) and (c) are the radial, circumferential and longitudinal strains whereas (d), (e) and (f) are the radial, circumferential and longitudinal displacements. Axis units are as explained in Fig. B.1.

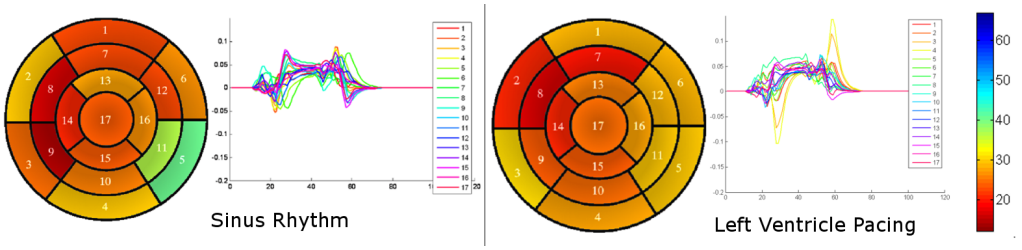

Figure B.5: **Patient contraction force prediction.** Predicted contraction force time and activation time isochrone (bull's eyes) for two different pacemaker stimulation mode from the same patient. Axis units are as explained in Fig. B.3.

B.5 Discussion

The estimation of contraction forces for each AHA segment and for the two simulation modes are shown in Fig. B.5. The estimated curves of contraction forces are noisy as in the case of simulated data but also no longer have a bell shape. In particular, those curves have negative parts at the beginning of systole whereas they have been trained to be positive. Those curves have been thresholded (value chosen as 0.03) to obtain two bull's eyes plot of activation times for the sinus rhythm and left ventricular pacing. It should be noticed that the late activation in green on the lateral wall of the left ventricle at sinus rhythm has been activated much earlier after pacing in the left ventricle which is expected.

From the preliminary results obtained on one patient with 2 stimulation modes, the estimation of activation times seems to correspond to the expected values. However, the shape and negative values of the estimated contraction forces indicate that the regression model does not capture well the observations. This may originate from several factors. First of all, there may be a difference of patterns between the simulated strains and displacement and the ones estimated by the non-linear registration. Second, there is a slight error when choosing the reference end diastolic image which produces significant errors in the estimation of strains. One could cope with those errors by having several regression methods corresponding to several choices of reference images. Finally, it should be noted that the electromechanical model involved for training the method used the anatomy of the left ventricle of the patient (see section B.3.1) on which it was evaluated. Further evaluation on more patient images should indicate whether the learning method is sensitive to the patient anatomy.

B.6 Conclusion

We presented in this paper a method to estimate contraction forces and activation times from echocardiographic images. A supervised learning method has been proposed which relies on synthetic measurements from an electromechanical model of the heart for the training stage. The method has been evaluated on synthetic data

and a patient case. Further work will test the proposed method on a larger sets of patients with various stimulation protocols. Sensitivity of our approach to the estimation of strains and the choice of the reference image will be studied. Learning from intracardiac electrophysiological mapping and 3D echocardiography of the same patient should improve the result and will be done as soon as the data is acquired.

Appendix C

Synthetic Echocardiographic Image Sequences for Cardiac Inverse Electro-Kinematic Learning

---

Based on: [Prakosa 2011] A. Prakosa, M. Sermesant, H. Delingette, E. Saloux, P. Allain, P. Cathier, P. Etyngier, N. Villain and N. Ayache. Synthetic Echocardiographic Image Sequences for Cardiac Inverse Electro-Kinematic Learning. In Gabor Fichtinger, Anne Martel and Terry Peters, editors, Medical Image Computing and Computer-Assisted Intervention - MICCAI 2011, volume 6891 of LNCS, pages 500-507, Toronto, Canada, September 2011. Springer, Heidelberg.
The further development in the generation of synthetic cardiac sequence is described in Chapter 3 which was published in [Prakosa 2012c]. The further development in the estimation of cardiac electrophysiology activation pattern from the analysis of the cardiac image sequence is described in Chapter 4 and in preparation for submission to [Prakosa 2012b].

In this paper, we propose to create a rich database of synthetic time series of 3D echocardiography (US) images using simulations of a cardiac electromechanical model, in order to study the relationship between electrical disorders and kinematic patterns visible in medical images. From a real 4D sequence, a software pipeline is applied to create several synthetic sequences by combining various steps including motion tracking and segmentation. We use here this synthetic database to train a machine learning algorithm which estimates the depolarization times of each cardiac segment from invariant kinematic descriptors such as local displacements or strains. First experiments on the inverse electro-kinematic learning are demonstrated on the synthetic 3D US database and are evaluated on clinical 3D US sequences from two patients with Left Bundle Branch Block.

C.1 Introduction

Despite advances in both medical image analysis and intracardiac electrophysiological mapping technology, the understanding of the relationship between the cardiac electrophysiology and the cardiac motion visible in images is only partial. However

such understanding would be very valuable as it would open possibilities in non-invasive electrophysiological mapping. Since 3D echocardiography (US) is readily available, an important topic of interest for cardiologists would be the estimation of the cardiac electrophysiology function from the analysis of 3D US images. This is specifically important, for example, in the evaluation of the Cardiac Resynchronization Therapy (CRT) where the placement and tuning of pacemaker leads play a crucial role in the outcome of the therapy. In this context, cardiologists need to interpret time series of US images in order to detect and characterize kinematic patterns (motion asynchrony, delayed contraction) and then infer possible electrical conduction disorders.

While there is an important literature on the estimation of the cardiac kinematics from 3D US sequences (see for instance [Elen 2008] and references therein), there exists no such tools to estimate the electrical wave propagation from such image sequences. However, the relationship between cardiac motion and electrical activation has been investigated in several studies [Prakosa 2010, Provost 2010, Sanchez-Ortiz 2004].

In this paper, we propose to study the inverse electro-kinematic relationship through the creation of a large database of synthetic 3D US images. Because it is difficult to obtain a large number of cases where both electrophysiological mapping and 3D US images are available, we use an electromechanical (E/M) model of the heart to produce synthetic but realistic image sequences for which the electrical stimulation is known. Previous work [Provost 2010, Sanchez-Ortiz 2004] has mainly focused in detecting E/M wave directly from the displacement and strain patterns estimated from image sequences during the contraction and relaxation of the myocardium. Since the relationship between those mechanical waves and electrical waves is certainly complex, our approach is to learn it through an E/M model of the heart. Compared to [Prakosa 2010], instead of estimating displacements and strains from the E/M model, we propose a more realistic estimation by first simulating 3D US images and then using an image-based motion tracking algorithm. Furthermore, rather than learning the activation forces over time, we have chosen to learn the depolarization times of all American Heart Association (AHA) segments. Finally, our learning approach is optimized in order to detect which kinematic descriptor is most correlated with the electrophysiology waves.

Different studies have been conducted for the creation of simulated 3D US sequences, e.g. [Duan 2007, Elen 2008]. Instead of simulating the ultrasonic image formation process, in this paper, we propose a new approach to create synthetic 3D US sequences by deforming a real 3D US sequence and combining simulated myocardium displacements with the visible motion of the surrounding environment (blood pool speckle, mitral valve). This approach has the advantage of providing a realistic 3D US sequence at little computational cost and including all neighboring structures. A vast database of electrical propagations along with corresponding synthetic sequences based on the E/M simulation was created. On this database, invariant kinematic descriptors were extracted from each synthetic sequence and then fed to a machine learning algorithm which estimates the electrical pattern from kine-

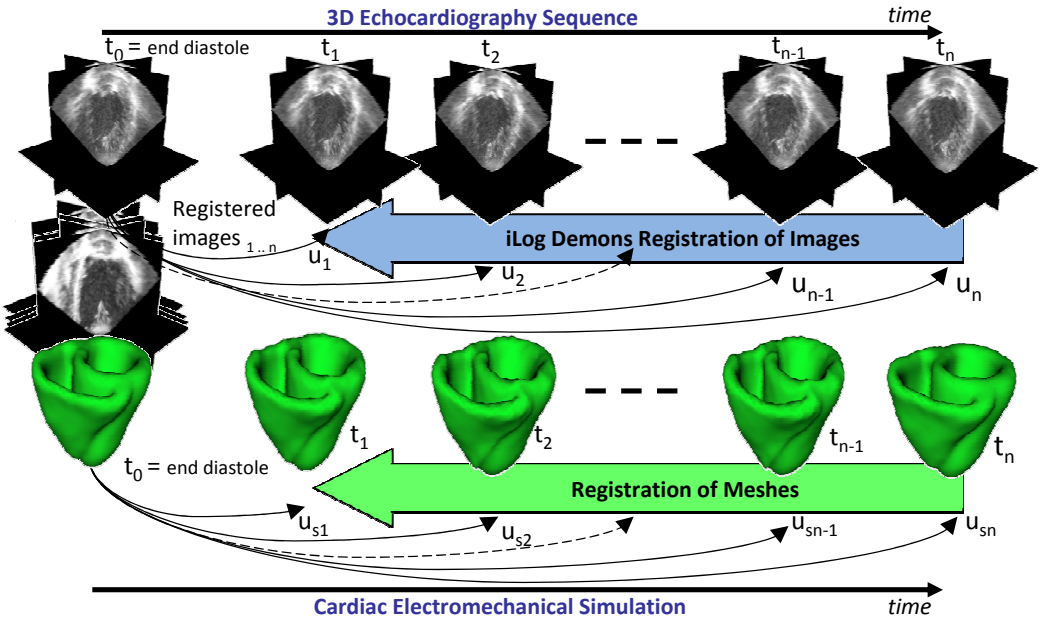

Figure C.1: **Registration of Images and Meshes.** iLog Demons registration method is applied to all images in the sequence to register them to the ED reference image. All meshes in a simulation cycle are also registered to the ED mesh.

matic descriptors during the cardiac cycle. The created synthetic 3D US sequences are of realistic quality and first experiments on the inverse electro-kinematic learning using this database are discussed.

C.2 Creating Synthetic 3D US Sequences

C.2.1 3D US Sequence Non-Rigid Registration

We use as input to our method a real 3D US sequence acquired by the iE33 Philips probe on a patient suffering from heart failure. The first step in the pipeline was to segment semi-interactively or automatically the left ventricle (LV). The binary mask was then used to apply the iLogDemons non-rigid registration algorithm [Mansi 2011] which had been applied in the cardiac cine MR sequence analysis. This motion tracking algorithm enforces the incompressibility of the myocardium during the cardiac motion which provides an additional prior information to regularize the visible motion in the image sequence. With this non-rigid registration algorithm, the displacement field (DF) u between the end diastole (ED) image and each image of the real 3D US sequence was estimated (see Fig. C.1). Thanks to the diffeomorphic nature of u, we computed its inverse and thus resampled each image of the sequence in the ED geometry.

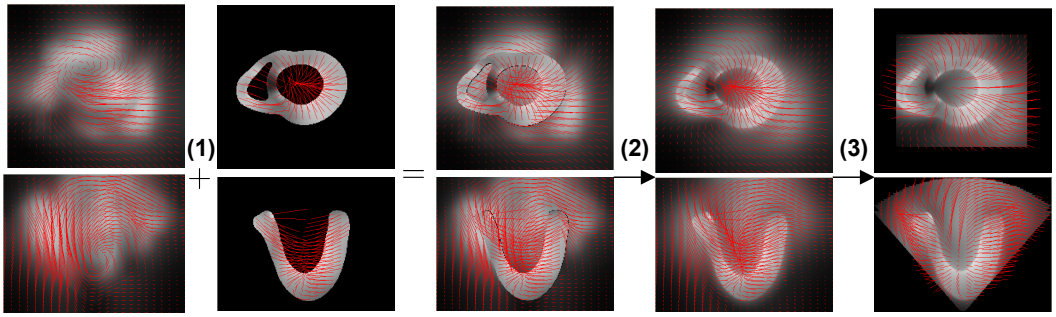

Figure C.2: **Fusion of the Displacement Fields.** (1) The DF estimated from the iLog Demons registration (left) is combined with the myocardium DF from the E/M simulation (second left). The two fields are fused, (2) smoothed, (3) inversed and cropped along the acquisition cone.

C.2.2 Deformation of Registered 3D US Images Using E/M Simulation

From the segmented images of the myocardium at ED, we created a computational tetrahedral mesh which was suitable for the simulation of a cardiac E/M model [Sermesant 2006a] whose myocardium motion is used for the generation of the synthetic sequences. This required additional work since only part of the LV and right ventricle (RV) were visible in the image. Registration of a template mask of the 2 ventricle was used to infer the missing parts.

With this model, we simulated the cardiac motion after specifying an electrophysiological pattern (see Section C.2.3). We sampled the cardiac simulated motion to follow the temporal resolution of the real 3D US sequence and then computed the DF between the reference configuration (ED) and the deformed position at each time of the sequence using the linear interpolation of the displacement of each vertex of the tetrahedral mesh rasterized in a 3D image having the same size and spatial resolution as the real 3D US image (see Fig. C.2). This dense synthetic DF of the myocardium was then merged with the DF estimated from the non-rigid registration. The synthetic DF completely overwrites the registration DF within the myocardium. Additionally, the synthetic DF within the eroded myocardium is diffused by solving the Laplace equation and fused with the registration DF to smooth the transition outside the myocardium. Then, the new DF was inversed and applied to each real image previously resampled in the ED configuration. Finally, a 3D cone mask was applied to remove all the displacements outside the cone, as observed in real acquisitions. With this approach, most of the image will stay unchanged in the synthetic image compared to the original sequence. We preserve the dynamics of the image, in particular the speckle visible in 3D US for most voxels. Only in the myocardium is the image texture slightly warped, the amount of warping depending on the difference between the simulated cardiac motion and the motion in the original images.

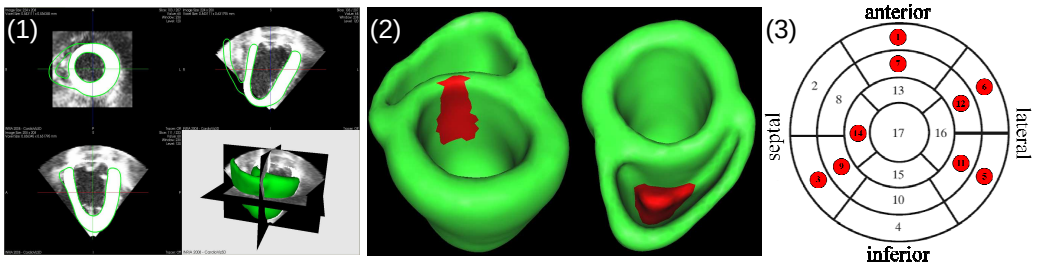

Figure C.3: **Cardiac Geometry and Electrical Stimulation.** (1) LV segmentation (2) Initial electrical activation area for the normal stimulation (3) Positions of the stimulation leads in the LV AHA zones

Simulation Number	Initial Electrical Activation Position	Global Conductivity	Global Contractility
1-4	LVRV (Normal)	50/30	0.09/0.05
5-8	LV (RBBB)	50/30	0.09/0.05
9-12	RV (LBBB)	50/30	0.09/0.05
13-36	RV + AHA 1/5/6/7/11/12 (LV Pacing)	50/30	0.09/0.05
37-48	LV + AHA 3/9/14 (RV Pacing)	50/30	0.09/0.05
49-120	AHA 1/5/6/7/11/12 + AHA 3/9/14 (BV Pacing)	50/30	0.09/0.05

Table C.1: **Simulation Database.** Parameters of the 120 simulations. Global conductivity (cm/s) is the conduction velocity of the electrophysiology model and global contractility (adimensioned) is the peak contractility of the E/M coupling.

C.2.3 Generation of Healthy and Pathological Cardiac Motion

Different simulation scenarios were performed including normal and pathological cases such as left bundle branch block (LBBB) and right bundle branch block (RBBB) by blocking the LV and RV initial electrical activation respectively, LBBB with LV pacing, RBBB with RV pacing and also LBBB and RBBB with biventricular (BV) pacing. The different pacing positions were based on the LV AHA segments (see Fig. C.3). Table C.1 summarizes the electrical and mechanical parameters used for the 120 simulations done from each real 3D US sequences.

C.3 Learning Electro-Kinematic Inverse Relationship

C.3.1 Kinematic Descriptors

With the method described previously, a large database of synthetic 3D US images was created. We then tracked the cardiac motion from those synthetic images by using the iLogDemons registration algorithm [Mansi 2011]. More precisely, we registered all the images of the synthetic sequence to its reference ED image. As an

input to a machine learning algorithm, we needed to first extract kinematic descriptors which describe in a compact and exhaustive way the cardiac motion. To this end, we characterized the motion of each AHA segment by fitting in the least-square sense an affine transformation $f(p) = Ap+B$ to the iLogDemons estimated DF. The strain tensor was computed from the affine matrix $E = \frac{1}{2}(A^T A - I)$. We propose to extract kinematic descriptors that are invariant to any change of reference frame (or rigid transformation). For the strain matrix E, the three Euclidean invariants are written as $x_1 = \text{trace}(E)$, $x_2 = \text{trace}(E^2)$, and $x_3 = \det(E)$. For the displacement vector, we only extracted its norm as invariant: $x_4 = \|u\| = \|Ab + B - b\|$, where $\|u\|$ is the displacement norm of the zone centroid with b the initial position of the centroid. Finally, we also used the strain in the direction of displacement as the last invariant $x_5 = \frac{1}{2\|u\|^2}(u^T E u)$. These 5 descriptors for the 17 AHA zones during the 19 time instances of a cardiac cycle were used to create a vectorial kinematic descriptor for each simulation: $X = x_i \in \mathbb{R}^d$ where d=5 (Descriptors) $\times$ 19 (Times) $\times$ 17 (Zones) = 1615.

C.3.2 Inverse Electro-Kinematic Learning

In the inverse electro-kinematic learning process, the non-linear relationship between the kinematic descriptors and the electrical propagation was estimated based on a training set extracted from the synthetic database. To represent the cardiac electrophysiology, we considered the activation time when the electrical potential starts to depolarize at a point of the myocardium. The activation time was averaged for all points in each AHA segment. Therefore, the vector characterizing electrophysiology for each simulation is $\text{Y} = \text{y}_i \in \mathbb{R}^{\text{r=17 (AHA Zones)}} = log(\text{Activation Times})$.

We modelled the non-linear relationship using Least-Square Support Vector Machine (LS-SVM) $Y = f(X) = Ak(x_i, X) + b$ with the Radial Basis Function (RBF) $K(x_i, x_j) = e^{-z}$ as the Kernel function where $z = \sum_{k=1}^{5} \left(\frac{|x_i^k - x_j^k|}{\sigma_k \alpha_k} \right)^2$. In this kernel function, σ_k is the standard deviation of each descriptor and α_k is a dimensionless coefficient which weights the importance of the descriptor in the learning process. Finally, following the LS-SVM theory, $k(x_i, X)$ is a kernel vector while matrix A is computed as $\text{A} = Y^T (\lambda \text{I} + K)^{-1}$. In order to have a good generalization of the model, the α_k parameters and the regularization parameter λ were optimized with a downhill simplex method using leave-one-out cross-validation based on Allen's predicted residual sum-of-squares (PRESS) statistic [Cawley 2006].

C.4 Results

The proposed synthetic 3D US generation method produces realistic synthetic 3D US sequence (cf. Fig. C.4) with a seamless fusion of simulated myocardium motion with neighboring moving structures. The created synthetic 3D US database contains 120 different cardiac cases consisting of a sequence of 19 3D US images describing

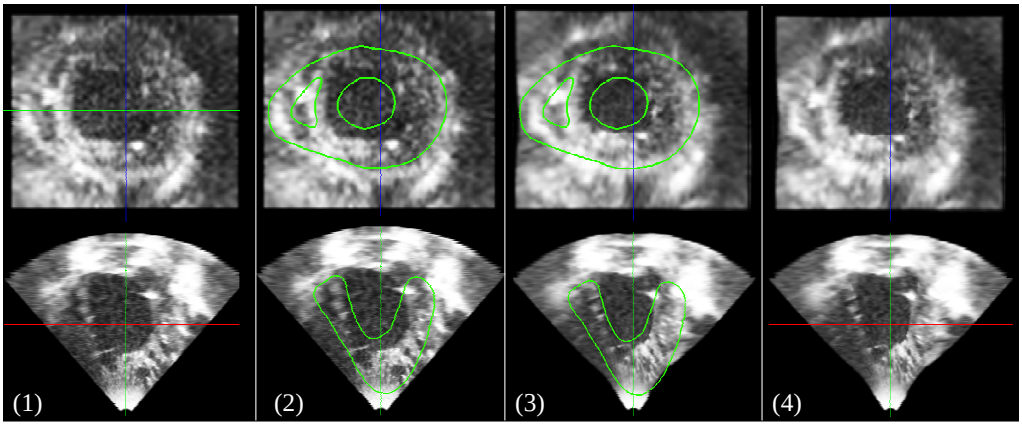

Figure C.4: **Synthetic 3D US.** (1) original real image with (2) contour of the mesh at the corresponding time from the model simulation overlayed, (3) synthetic image generated with the model simulation with model contour overlay, (4) synthetic image.

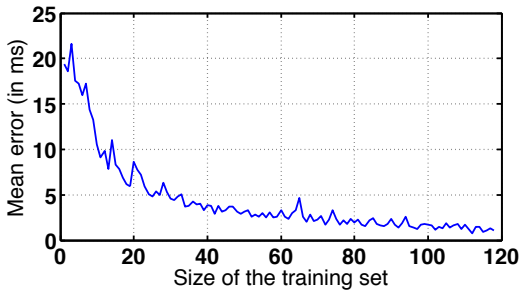

Figure C.5: **RMS Residual vs Size of Training Data.** Less than 10 ms RMS residual is obtained by using more than 15 training cases.

a complete cardiac cycle. In total, $120 \times 19 = 2280$ synthetic 3D US images were generated.

C.4.1 Machine Learning Validation on Synthetic Data

We evaluated the learning process on synthetic data and estimated the minimum size of the training set to have a small regression error for the remaining entries of the database. Fig. C.5 shows a good generalization with a root mean square (RMS) error of less than 10 ms of residual by using at least 15 training datasets.

C.4.2 Machine Learning Evaluation on Real Data

After optimizing the PRESS criterion on the whole synthetic database, we obtained the following LS-SVM parameters : $\lambda = 7.89 \times 10^{-31}$, $\alpha_1 = 463.65$, $\alpha_2 = 2.29 \times 10^{13}$, $\alpha_3 = 8.02 \times 10^{12}$, $\alpha_4 = 14.37$ and $\alpha_5 = 174.51$. This clearly shows that the kinematic

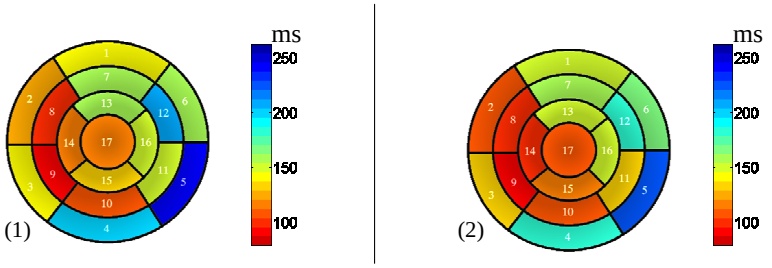

Figure C.6: **Depolarization Time Estimation from Clinical 3D US Sequences.** First evaluation of the learning process on patient (1) and patient (2). Both patients have LBBB.

descriptors x_1, x_4 and x_5 are the only meaningful ones to learn the electro-kinematic relationship. We did a first evaluation of this learning process on clinical 3D US sequences for two patients with LBBB. After performing non-rigid registration and extracting the vector X of kinematic descriptors, the electrophysiology vector Y was estimated from the LS-SVM. Very similar estimated depolarization times were obtained for these two patients (cf. Fig. C.6). Moreover, the activation patterns correspond to what was expected: depolarization starts from the septum towards the lateral wall, and the difference between the first activated zone and the last activated zone, which indicates the QRS duration, is around 150 ms which is also a characteristic of the LBBB.

C.5 Conclusion

We developed a pipeline to create realistic synthetic 3D US sequences using the deformation from an E/M model simulation. Those sequences represent in themselves a valuable result for instance to benchmark motion tracking algorithms. As these synthetic 3D US sequences have electro-kinematic "ground truth" information, we thus performed an inverse electro-kinematic learning on this database. Invariant kinematic descriptors were extracted from the DF obtained from the synthetic 3D US images registration. The non-linear inverse relationship between the electrical activation times and the kinematic descriptors was modelled using LS-SVM. Evaluation of the learning process for the synthetic 3D US sequences database shows good generalization and the first evaluation on clinical 3D US sequences shows encouraging results.

Bibliography

[Aubert-Broche 2006] B. Aubert-Broche, A. C. Evans and L. Collins. *A new improved version of the realistic digital brain phantom.* NeuroImage, vol. 32, pages 138 – 145, 2006. (Cited on page 25.)

[Belik 2004] M. E. Belik, T. P. Usyk and A. D. McCulloch. *Computational Methods for Cardiac Electrophysiology.* In N. Ayache, editeur, Computational Models for the Human Body, volume 12 of *Handbook of Numerical Analysis*, pages 129 – 187. Elsevier, 2004. (Cited on pages 6 and 25.)

[Benoit-Cattin 2005] H. Benoit-Cattin, G. Collewet, B. Belaroussi, H. Saint-Jalmes and C. Odet. *The SIMRI project: a versatile and interactive MRI simulator.* Journal of Magnetic Resonance, vol. 173, pages 97 – 115, 2005. (Cited on page 25.)

[Boltz 2010] T. Boltz, W. Pavlicek, R. Paden, M. Renno, A. Jensen and M. Akay. *An anthropomorphic beating heart phantom for cardiac X-ray CT imaging evaluation.* Journal of Applied Clinical Medical Physics, vol. 11, no. 1, 2010. (Cited on page 24.)

[Bossa 2008] M. Bossa and S. Olmos. *A new algorithm for the computation of the group logarithm of diffeomorphisms.* In X. Pennec, editeur, 2nd MICCAI Workshop on Mathematical Foundations of Computational Anatomy, New-York, October 2008. (Cited on page 32.)

[Butakoff 2007] C. Butakoff, S. Balocco, S. Ordas and A. F. Frangi. *Simulated 3D Ultrasound LV Cardiac Images for Active Shape Model Training.* In J. P. W. Pluim and J. M. Reinhardt, editeurs, Medical Imaging 2007: Image Processing, volume 6512 of *SPIE*, page 65123U, 2007. (Cited on page 25.)

[Camara 2006] O. Camara, M. Schweiger, R. I. Scahill, W. R. Crum, B. I. Sneller, J. A. Schnabel, G. R. Ridgway, D. M. Cash, D. L. G. Hill and N. C. Fox. *Phenomenological Model of Diffuse Global and Regional Atrophy Using Finite-Element Methods.* Medical Imaging, IEEE Transactions on, vol. 25, no. 11, pages 1417 –1430, November 2006. (Cited on page 27.)

[Cawley 2004] G. C. Cawley and N. L. C. Talbot. *Fast exact leave-one-out cross-validation of sparse least-squares support vector machines.* Neural Networks, vol. 17, no. 10, pages 1467–1475, 2004. (Cited on page 81.)

[Cawley 2006] G. C. Cawley. *Leave-One-Out Cross-Validation Based Model Selection Criteria for Weighted LS-SVMs.* In IJCNN'06, pages 1661–1668, Vancouver, 2006. IEEE. (Cited on pages 58, 59 and 92.)

[Chabiniok 2012] R. Chabiniok, P. Moireau, P.-F. Lesault, A. Rahmouni, J.-F. Deux and D. Chapelle. *Estimation of tissue contractility from cardiac cine-MRI using a biomechanical heart model.* Biomechanics and Modeling in Mechanobiology, vol. 11, pages 609–630, 2012. (Cited on page 25.)

[Chapelle 2012] D. Chapelle, P. Le Tallec, P. Moireau and M. Sorine. *An energy-preserving muscle tissue model: formulation and compatible discretizations.* International Journal for Multiscale Computational Engineering, vol. 10, no. 2, pages 189–211, 2012. (Cited on pages 6, 25, 29 and 52.)

[Clarysse 2011] P. Clarysse, J. Tafazzoli, P. Delachartre and P. Croisille. *Simulation based evaluation of cardiac motion estimation methods in tagged-MR Image sequences.* Journal of Cardiovascular Magnetic Resonance, vol. 13, no. Suppl 1, page P360, 2011. (Cited on page 27.)

[Craene 2010] M. D. Craene, G. Piella, N. Duchateau, E. Silva, A. Doltra, H. Gao, J. D'hooge, O. Camara, J. Brugada and M. Sitges. *Temporal Diffeomorphic Free-Form Deformation for Strain Quantification in 3D-US Images.* In T. Jiang, N. Navab, J. Pluim and M. Viergever, editeurs, Medical Image Computing and Computer-Assisted Intervention - MICCAI 2010, volume 6362 of *LNCS*, pages 1–8. Springer Heidelberg, 2010. (Cited on page 24.)

[Craene 2012a] M. D. Craene. *Statistical Atlases and Computational Models of the Heart (STACOM) 2012 cardiac Motion Analysis Challenge (cMAC2)*, 2012. http://www.physense.org/stacom2012/. (Cited on pages 15 and 69.)

[Craene 2012b] M. D. Craene, P. Allain, H. Gao, A. Prakosa, S. Marchesseau, L. Hilpert, O. Somphone, H. Delingette, S. Makram-Ebeid, N. Villain, J. D'hooge, M. Sermesant and E. Saloux. *Synthetic and Phantom Setups for the Second cardiac Motion Analysis Challenge (cMAC2).* In Proc. MICCAI Workshop on Statistical Atlases and Computational Models of the Heart (STACOM12), LNCS, Nice, October 2012. To appear. (Cited on page 74.)

[Daisne 2003] J.-F. Daisne, M. Sibomana, A. Bol, G. Cosnard, M. Lonneux and V. Grégoire. *Evaluation of a multimodality image (CT, MRI and PET) coregistration procedure on phantom and head and neck cancer patients: accuracy, reproducibility and consistency.* Radiotherapy and Oncology, vol. 69, no. 3, pages 237 – 245, 2003. (Cited on page 24.)

[Delingette 2012] H. Delingette, F. Billet, K. C. L. Wong, M. Sermesant, K. Rhode, M. Ginks, C. A. Rinaldi, R. Razavi and N. Ayache. *Personalization of Cardiac Motion and Contractility from Images using Variational Data Assimilation.* Biomedical Engineering, IEEE Transactions on, vol. 59, no. 1, pages 20 –24, January 2012. (Cited on page 25.)

[Dru 2009] F. Dru and T. Vercauteren. *An ITK Implementation of the Symmetric Log-Domain Diffeomorphic Demons Algorithm.* Insight Journal – 2009, May 2009. (Cited on pages 30 and 32.)

[Duan 2007] Q. Duan, P. Moireau, E. D. Angelini, D. Chapelle and A. F. Laine. *Simulation of 3D ultrasound with a realistic electro-mechanical model of the heart.* In F. B. Sachse and G. Seemann, editeurs, FIMH'07, volume 4466 of *LNCS*, pages 463–473, Berlin, 2007. Springer. (Cited on pages 25 and 88.)

[Elen 2008] A. Elen, H. F. Choi, D. Loeckx, H. Gao, P. Claus, P. Suetens, F. Maes and J. D'hooge. *Three-Dimensional Cardiac Strain Estimation Using Spatio-Temporal Elastic Registration of Ultrasound Images: A Feasibility Study.* Medical Imaging, IEEE Transactions on, vol. 27, pages 1580–1591, 2008. (Cited on pages 24, 25, 49 and 88.)

[Fang 2009] Q. Fang and D. A. Boas. *Tetrahedral mesh generation from volumetric binary and gray-scale images.* In IEEE International Symposium on Biomedical Imaging (ISBI), pages 1142–1145, 2009. (Cited on page 27.)

[Faure 2012] F. Faure, C. Duriez, H. Delingette, J. Allard, B. Gilles, S. Marchesseau, H. Talbot, H. Courtecuisse, G. Bousquet, I. Peterlik and S. Cotin. *SOFA: A Multi-Model Framework for Interactive Physical Simulation.* In Y. Payan, editeur, Soft Tissue Biomechanical Modeling for Computer Assisted Surgery, volume 11 of *Studies in Mechanobiology, Tissue Engineering and Biomaterials*, pages 283–321. Springer Heidelberg, 2012. (Cited on pages 34 and 54.)

[Gao 2007] H. Gao, H. F. Choi, P. Claus, S. Boonen, G. Van der Perre, W. Lauriks and J. D'hooge. *A New Convolution-Based Methodology to Simulate Ultrasound Images in a 2D / 3D Sector Format.* In Ultrasonics Symposium, 2007. IEEE, pages 2243 –2246, 2007. (Cited on pages 25 and 39.)

[Ghanem 2005] R. N. Ghanem, P. Jia, C. Ramanathan, K. Ryu, A. Markowitz and Y. Rudy. *Noninvasive electrocardiographic imaging (ECGI): comparison to intraoperative mapping in patients.* Heart Rhythm, vol. 2, pages 339–354, Apr 2005. (Cited on pages 48 and 76.)

[Glatard 2012] T. Glatard, A. Marion, H. Benoit-Cattin, S. Camarasu-Pop, P. Clarysse, R. Ferreira da Silva, G. Forestier, B. Gibaud, C. Lartizien, H. Liebgott, K. Moulin and D. Friboulet. *Multi-modality image simulation with the virtual imaging platform: Illustration on cardiac MRI and echography.* In IEEE International Symposium on Biomedical Imaging (ISBI), pages 98–101, Barcelona, Spain, 2012. (Cited on page 25.)

[Haddad 2007] R. Haddad, I. E. Magnin and P. Clarysse. *A new fully-digital anthropomorphic and dynamic thorax/heart model.* In Engineering in Medicine and Biology Society, 2007. EMBS 2007. 29th Annual International Conference of the IEEE, pages 5999 –6002, August 2007. (Cited on page 25.)

[Helm 2007] R. H. Helm, M. Byrne, P. A. Helm, S. K. Daya, N. F. Osman, R. Tunin, H. R. Halperin, R. D. Berger, D. A. Kass and A. C. Lardo. *Three-dimensional mapping of optimal left ventricular pacing site for cardiac resynchronization.*

Circulation, vol. 115, pages 953–961, February 2007. (Cited on pages 49 and 76.)

[Ho 2006] C. Y. Ho and S. D. Solomon. *A clinician's guide to tissue Doppler imaging.* Circulation, vol. 113, no. 10, pages e396–8, March 2006. (Cited on page 24.)

[Jensen 1996] J. A. Jensen. *FIELD: A Program for Simulating Ultrasound Systems.* In 10th Nordic-Baltic Conference on Biomedical Imaging Published in Medical and Biological Engineering and Computing, volume 34, pages 351–353, 1996. (Cited on page 25.)

[Johnson 2012] S. G. Johnson. *The NLopt nonlinear-optimization package.* Online, 2012. http://ab-initio.mit.edu/nlopt. (Cited on page 60.)

[Julier 1997] S. J. Julier and J. K. Uhlmann. *A new extension of the Kalman filter to nonlinear systems.* In International Symposium on Aerospace/Defense Sensing, Simulation and Controls, volume 3, page 26, 1997. (Cited on pages 29 and 54.)

[Konofagou 2012] E. E. Konofagou and J. Provost. *Electromechanical wave imaging for noninvasive mapping of the 3D electrical activation sequence in canines and humans in vivo.* Journal of Biomechanics, vol. 45, no. 5, pages 856 – 864, 2012. Special Issue on Cardiovascular Solid Mechanics. (Cited on page 49.)

[Kramer 2003] R. Kramer, J. W. Vieira, H. J. Khoury, F. R. A. Lima and D. Fuelle. *All about MAX: a male adult voxel phantom for Monte Carlo calculations in radiation protection dosimetry.* Physics in Medicine and Biology, vol. 48, no. 10, page 1239, 2003. (Cited on page 7.)

[Kramer 2004] R. Kramer, H. J. Khoury, J. W. Vieira, E. C. M. Loureiro, V. J. M. Lima, F. R. A. Lima and G. Hoff. *All about FAX: a Female Adult voXel phantom for Monte Carlo calculation in radiation protection dosimetry.* Physics in Medicine and Biology, vol. 49, no. 23, page 5203, 2004. (Cited on page 7.)

[Kramer 2006] R. Kramer, H. J. Khoury, J. W. Vieira and V. J. M. Lima. *MAX06 and FAX06: update of two adult human phantoms for radiation protection dosimetry.* Physics in Medicine and Biology, vol. 51, no. 14, page 3331, 2006. (Cited on page 7.)

[Kuijpers 2011] N. H. L. Kuijpers, E. Hermeling, T. Delhaas and F. W. Prinzen. *Mechano-electrical coupling explains worsening of cardiac function in the asynchronous heart.* In Computing in Cardiology, 2011, pages 161 –164, September 2011. (Cited on page 3.)

[Kutter 2009] O. Kutter, R. Shams and N. Navab. *Visualization and GPU-accelerated simulation of medical ultrasound from CT images.* Computer

Methods and Programs in Biomedicine, vol. 94, pages 250–266, June 2009. (Cited on page 25.)

[Lebenberg 2012] J. Lebenberg, I. Buvat, A. Lalande, P. Clarysse, C. Casta, A. Cochet, C. Constantinides, J. Cousty, A. de Cesare, S. Jehan-Besson, M. Lefort, L. Najman, E. Roullot, L. Sarry, C. Tilmant, M. Garreau and F. Frouin. *Non-supervised Ranking of Different Segmentation Approaches: Application to the Estimation of the Left Ventricular Ejection Fraction From Cardiac Cine MRI Sequences*. Medical Imaging, IEEE Transactions on, vol. 31, no. 8, pages 1651 –1660, August 2012. (Cited on page 5.)

[Leclercq 2004] C. Leclercq and J. M. Hare. *Ventricular Resynchronization*. Circulation, vol. 109, no. 3, pages 296–299, 2004. (Cited on page 3.)

[Ledesma-Carbayo 2005] M. J. Ledesma-Carbayo, J. Kybic, M. Desco, A. Santos, M. Sühling, P. Hunziker and M. Unser. *Spatio-temporal nonrigid registration for ultrasound cardiac motion estimation*. Medical Imaging, IEEE Transactions on, vol. 24, no. 9, pages 1113–26, September 2005. (Cited on page 25.)

[Liu 2010] X. Liu and J. L. Prince. *Shortest Path Refinement for Motion Estimation From Tagged MR Images*. Medical Imaging, IEEE Transactions on, vol. 29, no. 8, pages 1560 –1572, August 2010. (Cited on page 24.)

[Mansi 2009] T. Mansi, J.-M. Peyrat, M. Sermesant, H. Delingette, J. Blanc, Y. Boudjemline and N. Ayache. *Physically-Constrained Diffeomorphic Demons for the Estimation of 3D Myocardium Strain from Cine-MRI*. In Proceedings of Functional Imaging and Modeling of the Heart 2009 (FIMH'09), volume 5528 of *LNCS*, pages 201–210, June 2009. (Cited on page 77.)

[Mansi 2011] T. Mansi, X. Pennec, M. Sermesant, H. Delingette and N. Ayache. *iLogDemons: A Demons-Based Registration Algorithm for Tracking Incompressible Elastic Biological Tissues*. International Journal of Computer Vision, vol. 92, pages 92–111, 2011. (Cited on pages 5, 9, 12, 13, 14, 24, 39, 49, 67, 89 and 91.)

[Marchesseau 2012a] S. Marchesseau, H. Delingette, M. Sermesant and N. Ayache. *Fast Parameter Calibration of a Cardiac Electromechanical Model from Medical Images based on the Unscented Transform*. Biomechanics and Modeling in Mechanobiology, 2012. (Cited on pages 6, 51 and 54.)

[Marchesseau 2012b] S. Marchesseau, H. Delingette, M. Sermesant, K. Rhode, S. G. Duckett, C. A. Rinaldi, R. Razavi and N. Ayache. *Cardiac Mechanical Parameter Calibration based on the Unscented Transform*. In N. Ayache, H. Delingette, P. Golland and K. Mori, editeurs, Medical Image Computing and Computer-Assisted Intervention - MICCAI 2012, volume 7511 of *LNCS*, pages 41–48. Springer, Heidelberg, October 2012. (Cited on pages 29 and 54.)

[Marion 2011] A. Marion, G. Forestier, H. Benoit-Cattin, S. Camarasu-Pop, P. Clarysse, R.F. da Silva, B. Gibaud, T. Glatard, P. Hugonnard, C. Lartizien, H. Liebgott, S. Specovius, J. Tabary, S. Valette and D. Friboulet. *Multi-modality medical image simulation of biological models with the Virtual Imaging Platform (VIP).* In Computer-Based Medical Systems (CBMS), 2011 24th International Symposium on, pages 1 –6, June 2011. (Cited on page 25.)

[McLeod 2012] K. McLeod, A. Prakosa, T. Mansi, M. Sermesant and X. Pennec. *An Incompressible Log-Domain Demons Algorithm for Tracking Heart Tissue.* In O. Camara, E. Konukoglu, M. Pop, K. Rhode, M. Sermesant and A. Young, editeurs, Statistical Atlases and Computational Models of the Heart: Imaging and Modelling Challenges, numéro 7085 de LNCS, pages 55–67, Toronto, Canada, September 2012. Springer, Heidelberg. (Cited on pages 5, 9, 12, 14, 15, 40, 49, 67, 68 and 74.)

[McVeigh 1998] E. R. McVeigh, F. W. Prinzen, B. T. Wyman, J. E. Tsitlik, H. R. Halperin and W. C. Hunter. *Imaging asynchronous mechanical activation of the paced heart with tagged MRI.* Magnetic Resonance in Medicine, vol. 39, pages 507–513, April 1998. (Cited on pages 50 and 76.)

[Mitchell 2003] C. C. Mitchell and D. G. Schaeffer. *A two current model for the dynamics of cardiac membrane.* Bulletin of Mathematical Biology, vol. 65, no. 5, pages 767–793, 2003. (Cited on page 52.)

[Montagnat 2005] J. Montagnat and H. Delingette. *4D Deformable Models with temporal constraints: application to 4D cardiac image segmentation.* Medical Image Analysis, vol. 9, no. 1, pages 87–100, February 2005. (Cited on page 25.)

[Moore 2000] C. Moore, C. Lugo-Olivieri, E. McVeigh and E. Zerhouni. *Three-dimensional systolic strain patterns in the normal human left ventricle: Characterization with tagged MR imaging.* Radiology, vol. 214, pages 453–466, February 2000. (Cited on page 14.)

[OSIRIX 2012] OSIRIX. *DICOM sample image sets.* Online, 2012. http://pubimage.hcuge.ch:8080/DATA/MAGIX.zip. (Cited on page 36.)

[Otani 2010] N. Otani, S. Luther, R. Singh and R. Gilmour. *Transmural Ultrasound-based Visualization of Patterns of Action Potential Wave Propagation in Cardiac Tissue.* Annals of Biomedical Engineering, vol. 38, pages 3112–3123, 2010. (Cited on pages 49 and 50.)

[Ozturk 2003] C. Ozturk, J. A. Derbyshire and E. R. M. McVeigh. *Estimating motion from MRI data.* Proceedings of the IEEE, vol. 91, no. 10, pages 1627 – 1648, October 2003. (Cited on page 24.)

[Powell 2009] M. J. D. Powell. *The BOBYQA algorithm for bound constrained optimization without derivatives.* DAMTP 2009/NA06, August 2009. (Cited on page 60.)

[Prakosa 2010] A. Prakosa, M. Sermesant, H. Delingette, E. Saloux, P. Allain, P. Cathier, P. Etyngier, N. Villain and N. Ayache. *Non-Invasive Activation Times Estimation using 3D Echocardiography.* In O. Camara, M. Pop, K. Rhode, M. Sermesant, N. Smith and A. Young, editeurs, Statistical Atlases and Computational Models of the Heart, volume 6364 of *LNCS*, pages 212–221, Beijing, China, 2010. Springer, Heidelberg. (Cited on pages 9, 43, 47, 49, 51, 69, 73, 75 and 88.)

[Prakosa 2011] A. Prakosa, M. Sermesant, H. Delingette, E. Saloux, P. Allain, P. Cathier, P. Etyngier, N. Villain and N. Ayache. *Synthetic Echocardiographic Image Sequences for Cardiac Inverse Electro-Kinematic Learning.* In G. Fichtinger, A. Martel and T. Peters, editeurs, Medical Image Computing and Computer-Assisted Intervention - MICCAI 2011, volume 6891 of *LNCS*, pages 500–507, Toronto, Canada, September 2011. Springer, Heidelberg. (Cited on pages 10, 23, 43, 48, 49, 56, 68, 69, 71, 73 and 87.)

[Prakosa 2012a] A. Prakosa, K. McLeod, M. Sermesant and X. Pennec. *Evaluation of iLogDemons Algorithm for Cardiac Motion Tracking in Synthetic Ultrasound Sequence.* In Proc. MICCAI Workshop on Statistical Atlases and Computational Models of the Heart (STACOM12), LNCS, Nice, October 2012. To appear. (Cited on pages 5, 9, 11, 68, 69, 70 and 74.)

[Prakosa 2012b] A. Prakosa, M. Sermesant, P. Allain, N. Villain, C. A. Rinaldi, K. Rhode, R. Razavi, H. Delingette and N. Ayache. *Cardiac Electrophysiological Activation Pattern Estimation from Images using a Patient-Specific Database of Synthetic Image Sequences.* Biomedical Engineering, IEEE Transactions on, 2012. Submitted. (Cited on pages 10, 47, 69, 73, 75 and 87.)

[Prakosa 2012c] A. Prakosa, M. Sermesant, H. Delingette, S. Marchesseau, E. Saloux, P. Allain, N. Villain and N. Ayache. *Generation of Synthetic but Visually Realistic Time Series of Cardiac Images Combining a Biophysical Model and Clinical Images.* Medical Imaging, IEEE Transactions on, 2012. In press. (Cited on pages 9, 23, 49, 54, 55, 66, 68, 69, 73 and 87.)

[Provost 2010] J. Provost, W. Lee, K. Fujikura and E. Konofagou. *Electromechanical wave imaging of normal and ischemic hearts in vivo.* Medical Imaging, IEEE Transactions on, vol. 29, pages 625–635, March 2010. (Cited on pages 49, 50, 76 and 88.)

[Provost 2011] J. Provost, V. Gurev, N. Trayanova and E. E. Konofagou. *Mapping of cardiac electrical activation with electromechanical wave imaging: An in silico-in vivo reciprocity study.* Heart Rhythm, vol. 8, no. 5, pages 752 – 759, 2011. (Cited on page 49.)

[Relan 2011] J. Relan, M. Pop, H. Delingette, G. Wright, N. Ayache and M. Sermesant. *Personalisation of a Cardiac Electrophysiology Model using Optical Mapping and MRI for Prediction of Changes with Pacing.* Bio-Medical Engineering, IEEE Transactions on, vol. 58, no. 12, pages 3339–3349, 2011. (Cited on page 65.)

[Rineau 2009] L. Rineau, S. Tayeb and M. Yvinec. *3D Mesh Generation.* In CGAL Editorial Board, editeur, CGAL User and Reference Manual. 3.5 édition, 2009. (Cited on pages 27 and 51.)

[Rutz 2008] A. K. Rutz, S. Ryf, S. Plein, P. Boesiger and S. Kozerke. *Accelerated whole-heart 3D CSPAMM for myocardial motion quantification.* Magnetic Resonance in Medicine, vol. 59, no. 4, pages 755–63, 2008. (Cited on page 24.)

[Sainte-Marie 2006] J. Sainte-Marie, D. Chapelle, R. Cimrman and M. Sorine. *Modeling and estimation of the cardiac electromechanical activity.* Computers and Structures, vol. 84, pages 1743 – 1759, 2006. (Cited on pages 6 and 25.)

[Sanchez-Ortiz 2004] G. I. Sanchez-Ortiz, M. Sermesant, R. Chandrashekara, K. S. Rhode, R. Razavi, D. L. G. Hill and D. Rueckert. *Detecting the onset of myocardial contraction for establishing inverse electro-mechanical coupling in XMR guided RF ablation.* In Proceedings of International Symposium on Biomedical Imaging, pages 1055–1058, Arlington, 2004. IEEE. (Cited on pages 49, 50, 76 and 88.)

[Schaerer 2010] J. Schaerer, C. Casta, J. Pousin and P. Clarysse. *A dynamic elastic model for segmentation and tracking of the heart in MR image sequences.* Medical Image Analysis, vol. 14, no. 6, pages 738–749, 2010. (Cited on page 5.)

[Segars 1999] W. P. Segars, D. S. Lalush and B. M. W. Tsui. *A realistic spline-based dynamic heart phantom.* Nuclear Science, IEEE Transactions on, vol. 46, no. 3, pages 503 –506, June 1999. (Cited on page 25.)

[Segars 2008] W. P. Segars, M. Mahesh, T. J. Beck, E. C. Frey and B. M. W. Tsui. *Realistic CT simulation using the 4D XCAT phantom.* Medical Physics, vol. 35, no. 8, pages 3800–3808, 2008. (Cited on pages 7 and 25.)

[Sermesant 2003] M. Sermesant, C. Forest, X. Pennec, H. Delingette and N. Ayache. *Deformable biomechanical models: Application to 4D cardiac image analysis.* Medical Image Analysis, vol. 7, no. 4, pages 475–488, 2003. (Cited on page 41.)

[Sermesant 2006a] M. Sermesant, H. Delingette and N. Ayache. *An Electromechanical Model of the Heart for Image Analysis and Simulation.* Medical Imaging, IEEE Transactions on, vol. 25, pages 612–625, 2006. (Cited on pages 25, 27, 28 and 90.)

[Sermesant 2006b] M. Sermesant, P. Moireau, O. Camara, J. Sainte-Marie, R. Andriantsimiavona, R. Cimrman, D. L. Hill, D. Chapelle and R. Razavi. *Cardiac function estimation from MRI using a heart model and data assimilation: Advances and difficulties.* Medical Image Analysis, vol. 10, no. 4, pages 642–656, 2006. (Cited on page 79.)

[Sermesant 2007] M. Sermesant, E. Konukoglu, H. Delingette, Y. Coudiere, P. Chinchaptanam, K. S. Rhode, R. Razavi and N. Ayache. *An anisotropic multi-front fast marching method for real-time simulation of cardiac electrophysiology.* In Proceedings of Functional Imaging and Modeling of the Heart 2007 (FIMH'07), volume 4466 of *LNCS*, pages 160–169, 7-9 June 2007. (Cited on pages 28 and 52.)

[Sermesant 2012] M. Sermesant, R. Chabiniok, P. Chinchapatnam, T. Mansi, F. Billet, P. Moireau, J.M. Peyrat, K. Wong, J. Relan, K. Rhode, M. Ginks, P. Lambiase, H. Delingette, M. Sorine, C. A. Rinaldi, D. Chapelle, R. Razavi and N. Ayache. *Patient-specific electromechanical models of the heart for the prediction of pacing acute effects in CRT: A preliminary clinical validation.* Medical Image Analysis, vol. 16, no. 1, pages 201–215, 2012. (Cited on pages 6, 25, 29 and 66.)

[Shi 2003] P. Shi and H. Liu. *Stochastic finite element framework for simultaneous estimation of cardiac kinematic functions and material parameters.* Medical Image Analysis, vol. 7, no. 4, pages 445–464, 2003. (Cited on page 25.)

[Smith 2000] N. P. Smith, D. P. Nickerson, E. J. Crampin and P. J. Hunter. *Computational mechanics of the heart. From tissue structure to ventricular function.* Journal of Elasticity, vol. 61, no. 1, pages 113–141, 2000. (Cited on pages 6 and 25.)

[Sohal 2012] Manav Sohal, Anoop Shetty, Simon Duckett, Zhong Chen, Eva Sammut, Sana Amraoui, Gerry Carr-White, Reza Razavi and Christopher Aldo Rinaldi. *Non-Invasive Assessment of Left Ventricular Contraction Patterns Using Cardiac Magnetic Resonance Imaging to Identify Responders to Cardiac Resynchronization Therapy.* Journal of the American College of Cardiology Cardiovascular Imaging, 2012. Accepted for publication. (Cited on page 49.)

[Ten Tusscher 2004] K. H. Ten Tusscher, D. Noble, P. J. Noble and A. V. Panfilov. *A model for human ventricular tissue.* American Journal of Physiology, vol. 286, pages H1573–H1589, 2004. (Cited on page 52.)

[Tobon-Gomez 2008] C. Tobon-Gomez, C. Butakoff, S. Aguade, F. Sukno, G. Moragas and A. F. Frangi. *Automatic Construction of 3D-ASM Intensity Models by Simulating Image Acquisition: Application to Myocardial Gated SPECT Studies.* Medical Imaging, IEEE Transactions on, vol. 27, no. 11, pages 1655 –1667, November 2008. (Cited on pages 27 and 49.)

[Tobon-Gomez 2011] C. Tobon-Gomez, F. M. Sukno, B. H. Bijnens, M. Huguet and A. F. Frangi. *Realistic simulation of cardiac magnetic resonance studies modeling anatomical variability, trabeculae, and papillary muscles.* Magnetic Resonance in Medicine, vol. 65, no. 1, pages 280–288, 2011. (Cited on page 25.)

[Tobon-Gomez 2012a] C. Tobon-Gomez, M. D. Craene, A. Dahl, S. Kapetanakis, G. Carr-White, A. Lutz, V. Rasche, P. Etyngier, S. Kozerke, T. Schaeffter, C. Riccobene, Y. Martelli, O. Camara, A. F. Frangi and K. S. Rhode. *A Multimodal Database for the 1 st Cardiac Motion Analysis Challenge.* In O. Camara, E. Konukoglu, M. Pop, K. Rhode, M. Sermesant and A. Young, editeurs, Statistical Atlases and Computational Models of the Heart: Imaging and Modelling Challenges, volume 7085 of *Lecture Notes in Computer Science*, pages 33–44, Toronto, Canada, 2012. Springer. (Cited on pages 14 and 49.)

[Tobon-Gomez 2012b] C. Tobon-Gomez, M. D. Craene, K. McLeod, L. Tautz, W. Shi, A. Hennemuth, A. Prakosa, H. Wang, G. Carr-White, S. Kapetanakis, A. Lutz, V. Rashce, T. Schaeffter, C. Butakoff, O. Friman, T. Mansi, M. Sermesant, X. Zhuang, S. Ourselin, H.-O. Peitgen, X. Pennec, R. Razavi, D. Rueckert, A. F. Frangi and K. S. Rhode. *Evaluation of Current Algorithms for Myocardial Tracking and Deformation: Cardiac Motion Analysis Challenge.* Medical Image Analysis, 2012. Under review. (Cited on page 73.)

[Toussaint 2008] N. Toussaint, T. Mansi, H. Delingette, N. Ayache and M. Sermesant. *An Integrated Platform for Dynamic Cardiac Simulation and Image Processing: Application to Personalised Tetralogy of Fallot Simulation.* In Proc. Eurographics Workshop on Visual Computing for Biomedicine (VCBM), Delft, The Netherlands, 2008. (Cited on pages 27 and 51.)

[Vercauteren 2007] T. Vercauteren, X. Pennec, A. Perchant and N. Ayache. *Non-parametric Diffeomorphic Image Registration with the Demons Algorithm.* In N. Ayache, S. Ourselin and A. J. Maeder, editeurs, Medical Image Computing and Computer-Assisted Intervention - MICCAI 2007, volume 4792 of *LNCS*, pages 319–326, Brisbane, Australia, October 2007. Springer, Heidelberg. (Cited on page 77.)

[Vercauteren 2008] T. Vercauteren, X. Pennec, A. Perchant and N. Ayache. *Symmetric Log-Domain Diffeomorphic Registration: A Demons-based Approach.* In D. Metaxas, L. Axel, G. Fichtinger and G. Székely, editeurs, Medical Image Computing and Computer-Assisted Intervention - MICCAI 2008, volume 5241 of *LNCS*, pages 754–761, New York, USA, September 2008. Springer, Heidelberg. (Cited on pages 12, 13, 30, 32, 33, 52 and 55.)

[Veress 2011] A. I. Veress, W. P. Segars, B. M. W. Tsui and G. T. Gullberg. *Incorporation of a Left Ventricle Finite Element Model Defining Infarction Into the*

XCAT Imaging Phantom. Medical Imaging, IEEE Transactions on, vol. 30, no. 4, pages 915 –927, April 2011. (Cited on page 25.)

[Wang 2009] V. Y. Wang, H. I. Lam, D. B. Ennis, B. R. Cowan, A. A. Young and M. P. Nash. *Modelling passive diastolic mechanics with quantitative MRI of cardiac structure and function.* Medical Image Analysis, vol. 13, no. 5, pages 773–784, October 2009. (Cited on page 25.)

[WHO 2012] WHO. *Cardiovascular diseases (CVDs).* Online, 2012. http://www.who.int/mediacentre/factsheets/fs317/en/index.html. (Cited on page 3.)

[Xi 2011] J. Xi, P. Lamata, J. Lee, P. Moireau, D. Chapelle and N. Smith. *Myocardial transversely isotropic material parameter estimation from in-silico measurements based on reduced-order unscented Kalman filter.* Journal of the Mechanical Behavior of Biomedical Materials, vol. 4, no. 7, pages 1090–1102, 2011. (Cited on page 25.)

[Xu 2000] X. G. Xu, T. C. Chao and A. Bozkurt. *VIP-Man: an image-based whole-body adult male model constructed from color photographs of the Visible Human Project for multi-particle Monte Carlo calculations.* Health Physics, vol. 78, no. 5, pages 476–86, 2000. (Cited on page 7.)

[Zubal 1994] I. G. Zubal, C. R. Harrell, E. O. Smith, Z. Rattner, G. Gindi and P. B. Hoffer. *Computerized three-dimensional segmented human anatomy.* Medical Physics, vol. 21, no. 2, pages 299–302+, 1994. (Cited on page 7.)